Univerzita Karlova
Přírodovědecká fakulta

Studijní program: Geologie
Studijní obor: NGEOL

Bc. Tadeáš Hájek

Petrogeneze a vmístění postkolizních granitoidů jihovýchodní části Moldanubického batolitu

Petrogenesis and emplacement of post-collisional granitoids of southeastern Moldanubian Batholith

Diplomová práce

Školitel: doc. RNDr. Kryštof Verner, PhD.

Praha, 2019

Prohlašuji, že jsem závěrečnou práci zpracoval samostatně a že jsem uvedl všechny použité informační zdroje a literaturu. Tato práce ani její podstatná část nebyla předložena k získání jiného, nebo stejného akademického titulu.

V Praze, 22.8 2019 Podpis:

Poděkování

V první řadě bych chtěl poděkovat svému školiteli doc. RNDr. Kryštofu Vernerovi, Ph.D, pro jeho podporu, cenné rady a také čas věnovaný terénnímu výzkumu. Dále bych chtěl poděkovat celému kolektivu z Oddělení pro Chemii a Fyziku materiálů na Univerzitě v Salzburgu, kde jsem měl to potěšení po tři měsíce studovat a provádět výzkum. Jmenovitě bych chtěl poděkovat Univ.-Prof. Dr. Friedrichu Fingerovi za jeho pomoc a skvělé vedení a Martinu Lindnerovi a Davidu Schillerovi za jejich neocenitelnou pomoc. Cítím se velice vděčný za finanční pomoc poskytnutou institucí OeAD-GmbH na můj stipendijní pobyt v rámci programu "AKTION Česká republika – Rakousko, spolupráce ve vědě a vzdělávání". V neposlední řadě patří velké poděkování mé rodině a přátelům, jejichž podpora mi velmi pomohla při psaní této diplomové práce.

Abstrakt

Weinsbergský kompozitní pluton, situovaný v jižní části moldanubického batolitu, je rozsáhlé intruzivní těleso s komplexní stavbou a procesy vmístění a petrogeneze. Na základě geochemických analýz a zirkonové morfologie lze konstatovat, že dominantní litologií v severovýchodní části tohoto plutonu je druhý typ granitoidů typu weinsberg (WbG II). Na základě aplikování strukturních, petrologických a geochemických dat získaných ze zájmové oblasti může být předložena interpretace geodynamického vývoje a procesů vmístění východní části weinsbergského kompozitního plutonu. Tato interpretace zahrnuje: (a) podsouvání kontinentální mikrodesky Brunie ve východní oblasti v časovém rozmezí kolem 340–330 Ma mělo za následek delaminaci a následný nárůst teploty a anatexi metapelitických hornin spodní kontinentální kůry, ze kterých se stává heterogenní zdroj pro vznik granitoidních magmat typu weinsberg a eisgarn; (b) následný růst rozsáhlého metamorfního dómu na rozhraní okraje brunijské mikrodesky, následovaný multifázovým vmístěním celé východní části moldanubického batolitu včetně weinsbergského kompozitního plutonu v intervalu mezi 330 a 325 Ma; (c) rostoucí vliv zkrácení v severojižním směru a s ním spojený pravostranný střih podél lokalizovaných střižných zón měl za následek vznik převládající ZSZ–VJV orientované magmatické stavby v granitoidech weinsbergského plutonu; (d) mírné subvertikální zkrácení jako následek pozdějších etap exhumace a následné nízkoteplotní deformace a mylonitizace podél východního okraje SSV–JJZ orientované Vitiz-Přibyslavské mylonitové zóny.

Abstract

The Weinsberg Composite Pluton, located in the southern part of the Moldanubian Batholith is a large intrusive body with complex internal fabrics, petrogenesis and emplacement processes. On the basis of geochemistry and zircon morphology classification the dominating lithology in the northeastern part of the pluton seems to be the second type of the Weinsberg granitoids (WbG II). Based on the integration of the structural, petrological and geochemical data set acquired from the investigated area, the interpretation of geodynamic evolution and emplacement of the eastern part of the Weinsberg Pluton could be proposed. This interpretation invokes: (a) indentation and underthrusting of a continental microplate (Brunia) in the east at around ~340–330 Ma, driving mantle delamination and subsequent heating and anatexis in the metapelitic lower crust as the heterogeneous source for Weinsberg- and Eisgarn-types of granitoids; (b) subsequent growth of a large metamorphic dome along the edge of the Brunia indentor followed by polyphase emplacement of entire eastern part of the Moldanubian Batholith around ~330–325 Ma including the Weinsberg Composite Pluton in the south; (c) increasing role of the N–S shortening and associated NW–SE dextral shearing along localized shear zones which caused the prevailing WNW–ESE trending magmatic fabrics in Weinsberg Pluton; (d) minor subvertical shortening as the result of later stages of domal exhumation and subsequent low-temperature localized deformation and mylonitization along the eastern edge of NNE–SSW trending domal structure (polyphase Vitiz-Přibyslav Mylonite Zone).

Obsah

1. Introduction

The post-collisional voluminous granitic plutonism and widespread LP–HT crustal anatexis in the Moldanubian Zone active between ca. 330 to 300 Ma represent the latest Variscan tectonothermal events in the Bohemian Massif (e. g. Žák et al., 2014). Though research into tectonomagmatic evolution of one of the most outstanding plutonic complex – the Moldanubian Batholith is still in progress and many issues are unresolved, the two batholith branches with contrasting pluton geometry, volume, orientation, and composition clearly reflect different emplacement processes. The eastern branch of the batholith was interpreted as having resulted from large-scale gravity-driven diapiric upwelling along margin of the underthrust Brunia microplate (Žák et al., 2011; Verner et al., 2014). In contrast, its western branch was built in close relation to the right-lateral transpression (N-S compression) continuously changing to dextral strike-slip shearing at the later stages of magma crystallization (U/Pb zircon ages of plutons ranging between 324 and 327 Ma).

This diploma thesis includes processing of available multiple field structural data (field fabric pattern and magnetic anisotropy – AMS) and mainly the application of new laboratory methods (optical microscopy, whole-rock chemical analysis) allowing to determine shapes and internal fabric of intrusive bodies, magma emplacement mechanisms, relations and thermal interactions between granitic magmas and host migmatite complexes, geochemical features of magmas and their sources in the crucial part of the Moldanubian Batholith (its southeastern part) between cities Nové Hrady (Czech Republic) and Zwettl (Austria).

Based on comprehensive field structural data, analysis of anisotropy of magnetic susceptibility (AMS), petrological and geochemical data including zircon morphology classification from the northeastern part of the Weinsberg Pluton dated at 325 to 330 Ma (Finger et al., in prep.) tectonic aspects and mechanisms of granite emplacement in close relation to late-Variscan tectonothermal event are considered.

2. Geological Settings

2.1 The Variscan Orogenenesis

The Variscan Orogeny was a geological process which took place at the time from the Devonian to the lower Permian. This orogeny was very important for the Bohemian Massif because major lithologies and rocks in this area have their origin in Variscan geodynamic and kinematic processes. It is generally agreed that the Variscan Orogenesis was caused by the convergence and collision of Gondwana, Laurussia and other adjacent microcontinents. Late Devonian and Carboniferous subduction developed a massive and heterogenous orogen with two zones of subductions. A northern, southward-dipping system that probably led to the closing of Saxothuringian and Rhenohercynian basins, and a southern, northward-dipping system that led to the closure of south Variscan oceanic domains (Finger et al., 2007; Franke, 1989; Franke, 2000; Von Raumer et al. 2012).

The Variscan Orogenic belt in the area of Mid-Europe can be divided into units with different lithologies, degree of metamorphosis and geodynamical process (Franke, 2000). Locations of structural subdivision can be observed in Figure 1.

Rheno-Hercynian Belt. This unit can be further divided into Parautochthon, Allochthon and Northern Phyllite Zone and is dominated by weakly metamorphosed Devonian clastic shelf sediments.

Mid German Crystalline High. This unit represents the south-eastern margin of the Rheno-Hercynian Belt and is characterized by arc-related plutonism (340–325 Ma) (Franke, 2000).

Saxo-Thuringian Belt. The parautochthon of this unit consists of the Cadomian basement and the Cambro-Ordivician rift sequence, overlain by pelagic and flysch sediments. The upper allochthon contains MORB mafic rocks metamorphosed into eclogite facies and a variety of MP metamorphic rocks with metamorphic age between 380 and 365 Ma (Franke et al., 1995b).

Teplá-Barrandian. This unit is one of the best preserved Cadomian Orogens in central Europe. Its basement is composed of late Proterozoic sediments and arc-related volcanics

rocks metamorphed into amphibolite facies at 550–540 Ma (Franke, 2000; Zulauf et al., 1999). Cambrian to Devonian sedimentary and volcanics rocks are overlying this Cadomian basement (Chlupáč et al., 1998). The northwestern and southeastern margins of Teplá-Barrandian are lined by eclogite facies and mantle rocks, which probably represent former sutures. Variscan deformation and low-grade metamorphism probably affected the Teplá-Barrandian between 385 and 365 Ma (Dallmeyer and Urban, 1998; Franke, 2000; Zulauf et al., 1998).

Moldanubian of the Bohemian Massif. This unit consists of high-grade metamorphosed rocks representing lower and middle continental crust. Protoliths are mostly volcanosedimentary and magmatic rocks of Neoproterozoic and Lower-Paleozoic age. It is the root zone of Variscan Orogen (Schulmann, 2008; Vrána et al., 1995).

The Moldanubian Zone has been subdivided into two lithotectonic units: the Gföhl and Drosendorf units (Franke, 2000). The Gföhl Unit consists mostly of granulites, orthogneisses and migmatites which were affected by HP–HT metamorphism and subsequently exhumed into middle continental crustal levels (Franke, 2000). The Drosendorf Unit is composed of paragneisses, migmatites, marbles and amphibolites. It is further divided into the Variegated Series and the Monotonous Series. The Gföhl Unit was metamorphosed under HP–HT conditions (900-1050 °C and 16-18 kbar (Schulmann et al., 2008). Conditions for metamorphism of the Drosendorf Unit were around 650-750 °C and 6-10 kbar (Racek et al., 2006; Lindner and Finger, 2018).

Variscan Orogenesis of Moldanubian Unit of the Bohemian Massif took place in two subsequent tectono-metamorphic phases: the Moravo-Moldanubian phase (345-335 Ma) and the Bavarian phase (335-315 Ma) (Finger et al., 2007). In the course of the Moravo-Moldanubian phase thickening of the crust occurred, HT-HP metamorphic rocks exhumed into middle crustal levels. During the Bavarian phase the heat flow from the Asthenosphere through the continental crust was significantly increased. This led to LP-HT metamorphism and abundant granitoid magmatism (Finger et al., 2009).

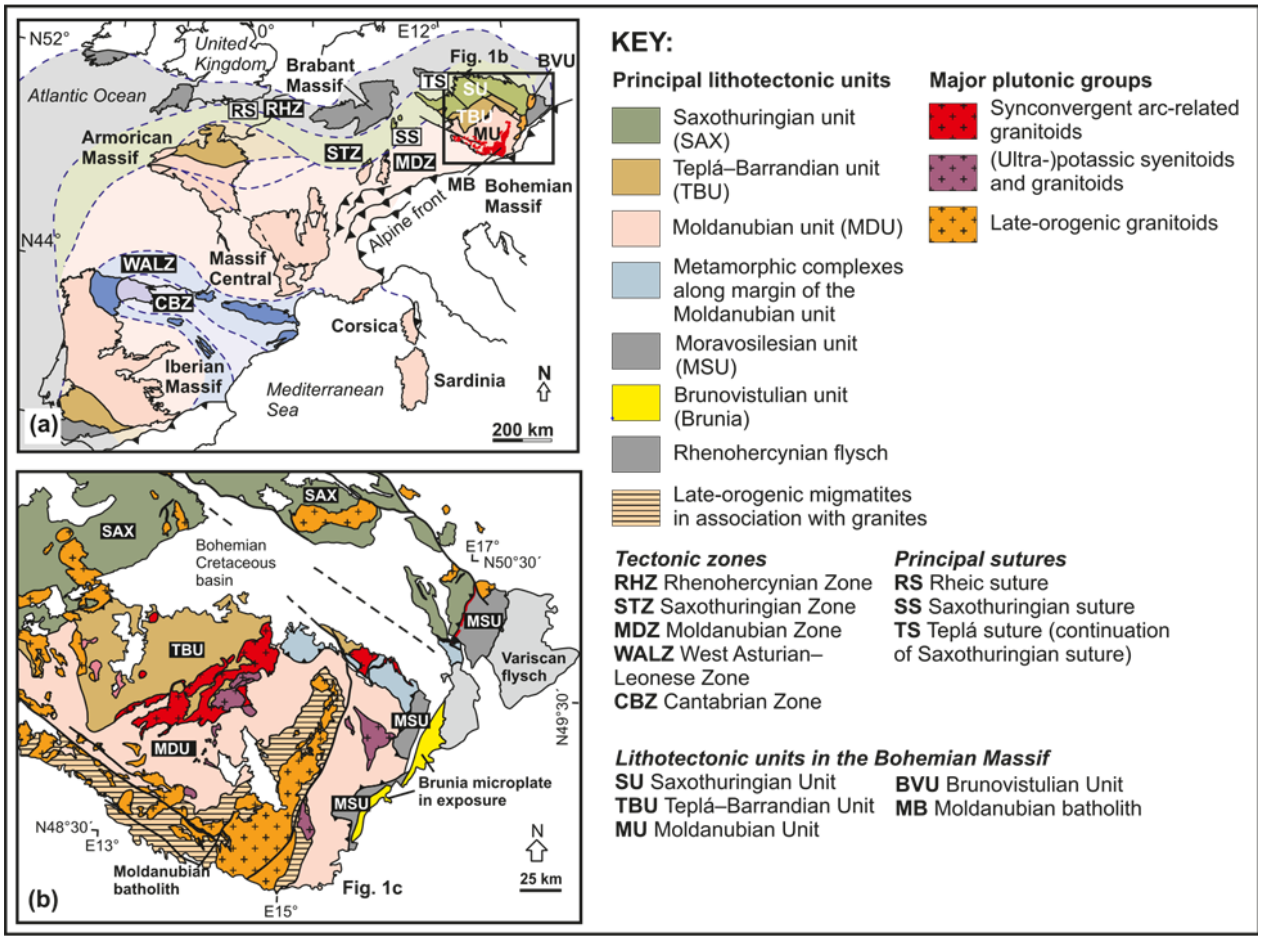

Fig. 1: (a) *Geological map of subdivisions of European Variscides;* ***(b)*** *Variscan lithologies and units of the Bohemian Massif. Modified after (Verner et al., 2014).*

2.1.1 Magmatic activity and Granitoid groups

Intrusions of Variscan Granitoids are most aabundant in the Moldanubian Unit. The largest Moldanubian batholiths are the South Bohemian Batholith, the Central Bohemian Batholith and the Oberpfalz Batholith (Finger, 1997). Variscan intrusions occur in the northern and southern external zones aswell, for instance in the Saxothuringian (Odenwald, Erzgebirge) and Rhenohercyan (Harz) units, as well as in the Alpine basement. Finger (1997) proposed that the Variscan granitoids can be divided into five main groups based on the age distribution, mineralogy, geochemistry and structural relationships. Their geographical distribution is shown in Fig. 2.

1. *The early Variscan I-type plutons (370–340 Ma).* The *v*ast majority of rocks in this group are metaluminous Hbl-bearing diorites, granodiorites and tonalites with low K_2O and Sr-isotopic compositions between 0.703 and 0.705. Granitoids of the first group occure in the Odenwald pluton in the Saxothuringian Zone, northern Vosges and the northern Schwarzwald. Granitoids with similar characteristics have been mapped in the Central Bohemian Batholith. These include the Mirotice and Stare Sedlo orthogneisses (370 Ma) (Kosler and McFarrow, 1994) or the metaluminous tonalites and granodiorites of the Sázava suite (350 Ma) (Holub et al., 1996).

2. *Syn-orogenic S-type granites (340 Ma).* Granitoids of this second group are mostly deformed S-type granites of strictly crustal origin. Their A/CNK ratio is between 1.1 and 1.3. These rocks appear to be closely related to thrusting and are deformed with fabrics formed in the magmatic state. In Lower Austria they show transitions into syn-deformational migmatites (Finger, 1997).

3. *Syn-orogenic to post-collisional S-type and high-K I-type granitoids (340-310 Ma).* This group represents most voluminous Variscan granitoids. Unlike the second group, these rocks are mostly undeformed. They are very abundant in the South Bohemian Batholith where these granitoids makes up the majority of the pluton lithology. A further division into four subgroups is possible. **(a)** Moderately peraluminous S-type two-mica granites. This subgroup is, for instance represented by the Eisgarn Granite of the South Bohemian Batholith. The melts are derived from lower to mid crust level paragneisses (Finger, 1997; Žák et al., 2013). **(b)** Highly potassic, weakly peraluminous to metaluminous K-feldspar megacryst biotite granitoids. The most important rock in this subgroup is the Weinsberg Granite in the South Bohemian Batholith (Finger and Clemens, 1995). The SiO_2 contents of these granitoids ranges from 60 to 70 wt %. The A/CNK ratios are between 0.95 and 1.1. Sr-isotopic ranges are between 0.706 and 0.710 (Frasl and Finger, 1991; Finger, 1997). **(c)** This subgroup is formed by K-feldspar megacryst rocks with high K_2O and MgO content. The rocks can mostly be characterized as melagranites and syenites. Mingling phenomenona are frequently present. In the Bohemian Massif rocks of this composition are known as Durbachites. They formed by mixing of crustal partial melts and upper mantle mafic magmas (Holub, 1977). **(d)** Fine-grained leucocratic low peraluminous S-type granites.

These rocks are usually younger and intrude and cross-cut into other rocks of this group. They include the Altenberg Granite (320-310 Ma) of the South Bohemian Batholith (Frasl and Finger, 1991).

4. *Late-Variscan Calc-alkaline plutons (310-290 Ma).* The group comprises tonalites, granodiorites and granites, which can be characterized as I-type granitoids based on their high Na_2O contents and low to medium A/CNK ratios (Finger, 1997). Most of these granitoids are fine to medium grained high-K biotite-granodiorites. These granitoids are abundant in the Alpine-Carpathian area (Finger et al., 1993; Petrik et al., 1994), but also in the South Bohemian Batholith (Mauthausen and Freistadt granitoids; Frasl and Finger, 1991).

5. *Late post-collisional leucogranites (300-250 Ma).* Rocks of this group are metaluminous to weakly peraluminous A-type leucogranites with high contents of K_2O, Rb, Th and high FeO/MgO ratio. These granitoids represent the youngest Variscan intrusions which often penetrate all other lithologies (Finger et al., 1993; Petrik and Broska 1994; Finger, 1997). In the Moldanubian Zone, these A-type leucogranites seem to be quite rare.

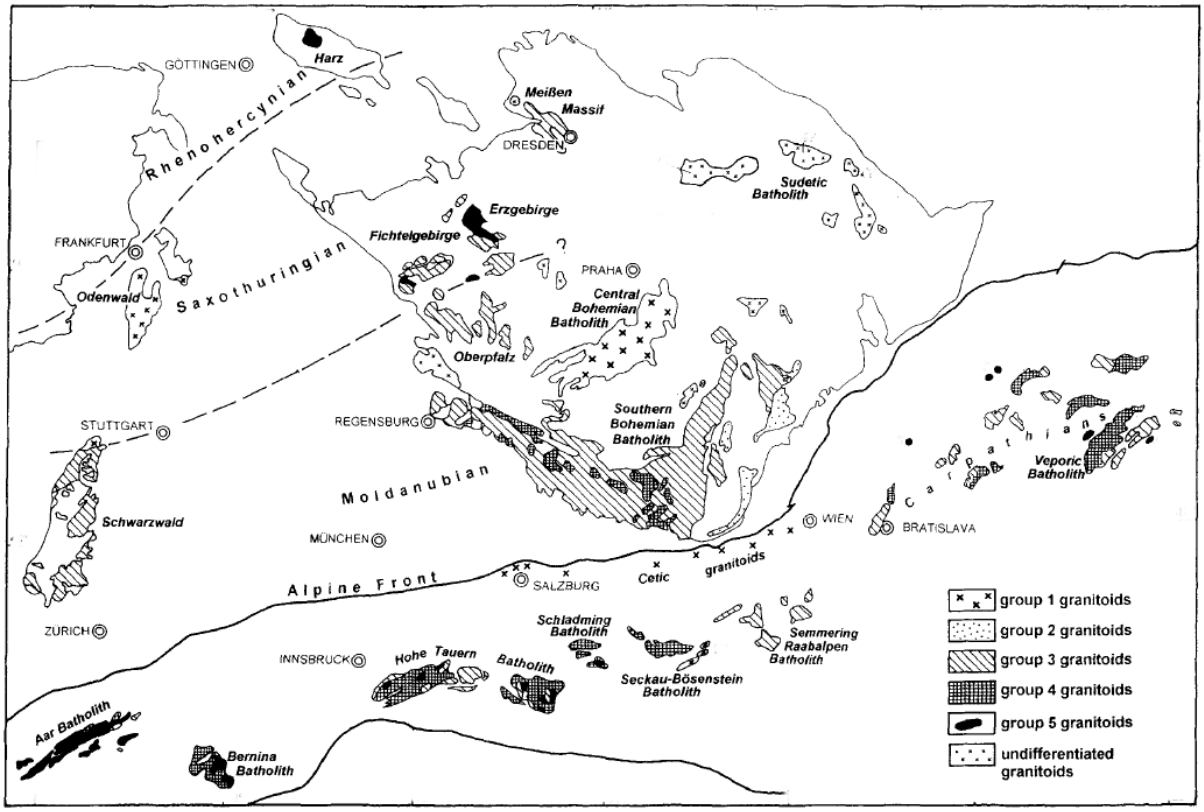

Fig. 2: *Geological sketch-map with locations of Variscan granitoid groups and intrusions within Central Europe. Modified after Finger (1997).*

2.2 Petrogenesis of the Moldanubian Batholith

2.2.1 General notes

Post-collisional magmatism connected with LP-HT metamorphism is a very common phenomenon in many orogenic zones worldwide. It usually occurs during late-orogenic crustal thinning. In the past many authors proposed their theories about numerous processes being responsible for the temperature increase in orogenic settings. The most widely accepted are: **(a)** thickening of the continental crust which cause accumulation of radiogenic elements producing heat (England and Thompson, 1984), **(b)** delamination of the thickened lithosphere and the thermal boundary layer (England, 1993), **(c)** gravitational collapse causing extension

of the lithosphere (Dewey, 1988), **(d)** slab breakoff (Davies and von Blackenburg, 1995) or **(e)** a mantle plume ascent (Watson and Mckenzie, 1991).

Regarding the Variscan Orogeny, some workers propose that there was little syn-collisional crustal thickening (< 50 km). Therefore crustal anatexis occurred mainly during post-collisional delamination and upwelling of the asthenosphere (Sylvester, 1998). The same author (Sylvester, 1998) also proposes that the coeval intruion of Variscan S-type granites and calc-alkaline granites may be and indication for the interaction of mantle-derived and crustal derived magmas. On the other hand Gerdes et al. (2000) stated that no geochemical evidence for a large contribution of mantle-derived magmas can be found in the Moldanubian Batholith. They corroborate the model of Finger and Clemens (1995) according to which the granitoids of the batholith formed mainly by fluid absent melting of metasedimentary and metaigneous crustal materials. Furthermore they claim that the heat generated by the decay of radiogenic elements in the thickened crust was sufficient for the partial melting of these rocks.

2.2.2 Structure of the Moldanubian Batholith

The Moldanubian Batholith is situated in the southern part of Bohemian Massif and its surface area is around 6 000–10 000 km^2. The Moldanubian Batholith can be divided into two segments oriented NNE – SSW and WNW – ESE (Fig. 4). Both segments are composed of a large number of smaller intrusions with different petrological and geochemical characteristics (Verner et al., 2009; Klomínský et al., 2010). Granitoids of the Moldanubian Batholith can be divided into **(a)** I- and I/S-type porphyric granitoids (type Weinsberg), **(b)** two-mica S-type peraluminous granitoids (type Eisgarn), **(c)** Calc-alkaline I-type granitoids (type Mauthausen). Besides these granites smaller leucocratic dikes of aplitic or pegmatitic composition are abundant. Major parts of these granitic rock intruded into the already exhumed Moldanubian crust in the interval from 329 to 323 Ma (Finger et al., 2009; Verner et al., 2014). The Weinsberg and Eisgarn suites make up more than 80 % of the

batholith area. Petrogenesis of these granites was caused by dehydration melting of psamitic or pelitic metasediments (mostly metagreywackes) (Finger, 1997).

Weinsberg Granite suite

This coarse-grained porphyritic biotite granite is the most abundant granite type in the Moldanubian Batholith. Newer work has shown that the Weinsberg granite involves at least two different intrusive batches, termed Weinsberg granite I and II (Stöbich, 1992; Finger and Clemens, 1995). By using the ID-TIMS dating method the following geochronological dates were acquired: Weinsberg granite (northern part, near Gmünd): 330.7 Ma, Weinsberg granite central part 326.0 Ma, Weinsberg granite west of Linz: 322.6 Ma (Gerdes et al., 2003). These different magma batches intruded into mid to upper-crustal levels of the South Bohemian Massif and created the Weinsberg Composite pluton. The total volume of Weinsberg type granites is over 30 000 km^3. The granite composition and thermal gradient in the country rocks imply that the Weinsberg granites were generated either by biotite-dehydratation melting of plagioclass-biotite gneisses at conditions of > 850 °C and < 1GPa (Finger and Clemens, 1995; Gerdes et al., 2000), or by partial melting of volcanosedimentary rocks and amphibolites and by mixing of mafic and felsic magmas. According to Gerdes et al., (2001) single Weinsberg granite subtypes have slightly different geochemical and isotopic composition. Also zircon morphologies are signiticantly different in Weinsberg granite types I and II (Stöbich, 1992).

The chemical distinction between different subtypes of Weinsberg granites is difficult. Overall, it can be stated that the Weinsberg granite is moderately peraluminous with SiO_2 between 64 and 74 wt%, K/(Ca + Na) between 0.3 – 1.2 and Mg/(Mg + Fe^{2+}) between 0.3 – 0.5 . On the bases of zircon morphology classification (Stöbich, 1992), the Weinsberg granites has been divided into two main types: WbG I and WbG II. The first type (WbG I) has further been subdivided into WbG Ia and WbG Ib on the basis of lower SiO_2 and lower A/CNK, $^{87}Rb/^{86}Sr$ and $^{87}Sr/^{86}Sr_i$ ratios (Fig. 3; Gerdes, 2001). WbG II is generally more silicic

than the WbG I, usually having higher Rb/Sr, K/(Ca + Na), but lower Zr and LREE contents and lower Nd_{init} (-5.1 to 5.8) in comparsion to WbG I (-4 to -5) (Gerdes, 2001).

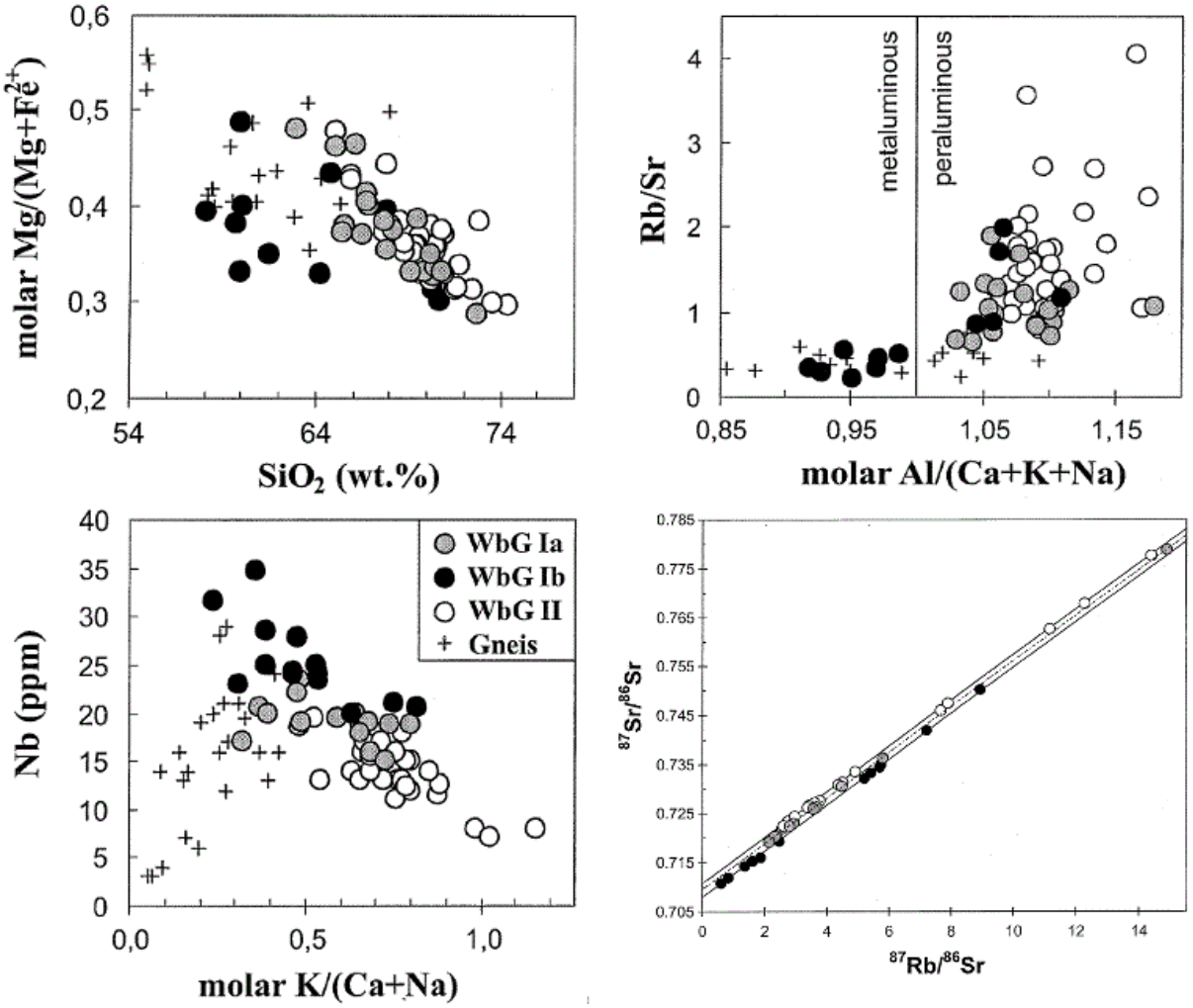

Fig. 3: *Sample of geochemical and isotopic compositions of three different types of Weinsberg granites (WbG Ia, WbG Ib and WbG II). 35 samples distributed over an 80 x 120 km area. Data from (Finger and Clemens, 1995; Gerdes, 2001). Modified after Gerdes (2001).*

Eisgarn granite suite

The Eisgarn Granite sensu stricto is a fine to medium-grained strongly peraluminous two-mica S-type granite. It intruded into the upper crust of the eastern and north-eastern part of the Moldanubian Batholith (N of Gmünd) where it creates Eisgarn Composite pluton. The intrusion age was determined to be between 329 and 327 Ma based on monazite (Gerdes et al., 2003). However granites similar to the Eisgarn type can be found in the western and southern parts of Moldanubian Batholith as well (Breiter, 1998, 2006; Matějka, 1998; René et al., 2003).

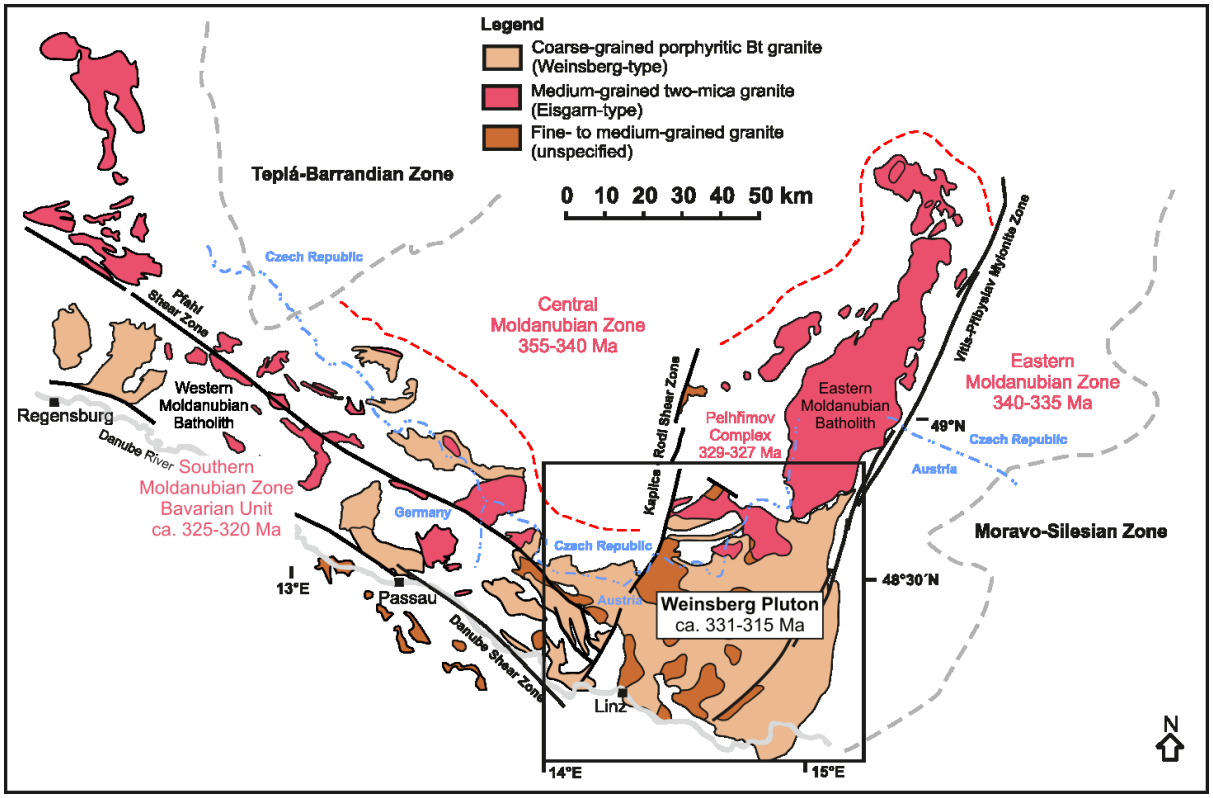

Fig. 4: *Geological sketch-map of spatial distribution of main intrusive rocks of Moldanubian Batholith. Modified after (Verner et al., 2009, Žák et al., 2014).*

2.3 Description of the studied area

The area of interest for this master thesis is located in the central-northern part of the Weinsberg Composite pluton of the Moldanubian Batholith. The investigated area is roughly located between the cities of Weitra (NW), Zwettl (NE), and villages Karlstift (SW) and Rappottenstein (SE). Dominating and the oldest lithology (331 – 323 Ma) in this area is the coarse-grained porphyric biotite Weinsberg Granite (predominantly WbG II variant) (Finger et al., 1997; Gerdes, 2001; Gerdes et al., 2003). But mostly on the western border around cities of Weitra and Karlstift outcrops of four geochemically different intrusive rocks which intruded into the older Weinsberg Granite can be found. However all of these lithologies are on almost every geological map marked as Eisgarn granite or Freidstat/Mauthausen type granitoids (Fig. 5). In newer work (Breiter 2006) they have been renamed as follows:

Žofín Granite. This fine grained two-mica granite has been discovered at the external parts of Weinsberg Composite pluton. Main occurrence is to the S, E and SW of the city of Weitra where it forms contacts with the biotite Weinsberg Granite (Breiter, 2006). The Žofín Granite is generally equigranular with higher content of biotite over muscovite. Contents of SiO_2 are between 69 and 72 %, MgO 0.4–0.9 wt% and Fe_2O_{3tot} 1.5–3 wt%. With alkali contents K_2O 5.2 5.5 wt% and Na_2O only 2.6–3.0 wt%. Isotopical ratios are very similar to the Eisgarn granite s. s. $^{87}Sr/^{86}Sr_i \sim 0.713$ (Breiter, 2006).

Mandelstein Granite. Generally a coarse-grained two-mica granite. Creates a lithology between cities of Weitra and Nové Hrady. Macroscopically this granite is very similar to the actual Eisgarn granite (Breiter, 2006). Content of both micas is approximately similar. Typical contents of SiO_2 is between 71 and 73 %. MgO 0.2–0.4 wt% and Fe_2O_{3tot} 1.0–2.2 wt%. Alkali contents are K_2O 4.5–5.0 wt% and Na_2O 2.8–3.3 wt%. This granite differs from typical Eisgarn Granite s. s. by lower $^{87}Sr/^{86}Sr_i \sim 0.706$ (Breiter, 2006).

Weitra Granite. This granite was newly defined by Humer et al. (2003). It is a fine-grained biotite granite and can be divided into macroscopically unrecognizable non-magnetic and magnetic varieties (Gnojek and Přichystal, 1997). The magnetic variety outcrops in the surroundings of the village of St. Martin. The non-magnetic variety can be found in the city

of Weitra and surroundings. Typical geochemical parameters are SiO_2 71–72 wt%, MgO 0.7–0.8 wt%, Fe_2O_{3tot} 2.0 – 3.0 wt%, K_2O 4.5–5.0 wt% and Na_2O 2.8–3.8 wt%. The $^{87}Sr/^{86}Sr$ initial ratios are the lowest and close to 0.705 (Humer et al. 2003; Breiter, 2006).

Karlstift Granite. Fine to medium-grained biotite granite that crops out SW of the city of Karlstift (Gnojek and Přichystal, 1997). Its origin is supposed to result from reaction of mixing of Freistadt and Weinsberg granites. For the Karlstift Granite zoned plagioclase is typical, orthoclase is less abundant and altered, high amounts of Sr (580-650 ppm), Th (25-28 ppm) and low concentrations of Rb (150-170 ppm). SiO_2 contents are between 67 and 69 wt%, MgO 0.8–1.3 wt%, K_2O 3.8–4.5 wt% and Na_2O 3.2–3.5 wt%. Initial Sr ratios are similar to those of Mandelstein Granite $^{87}Sr/^{86}Sr_i \sim 0.706$ (Breiter, 2006).

Between Zwettl and Rappottenstein the NNE–SSW trending Vitiz-Přibyslav mylonite zone is mapped. Several outcrops with mylonite or mylonitized Weinsberg granite can be found in this zone. The tectonic movements in the Vitiz-Přibyslav zone were probably caused by the Brunia microplate whose westernmost front edge coincides with the Vitiz-Přibyslav mylonite zone on the surface (Verner et al., 2006; Žák et al., 2011).

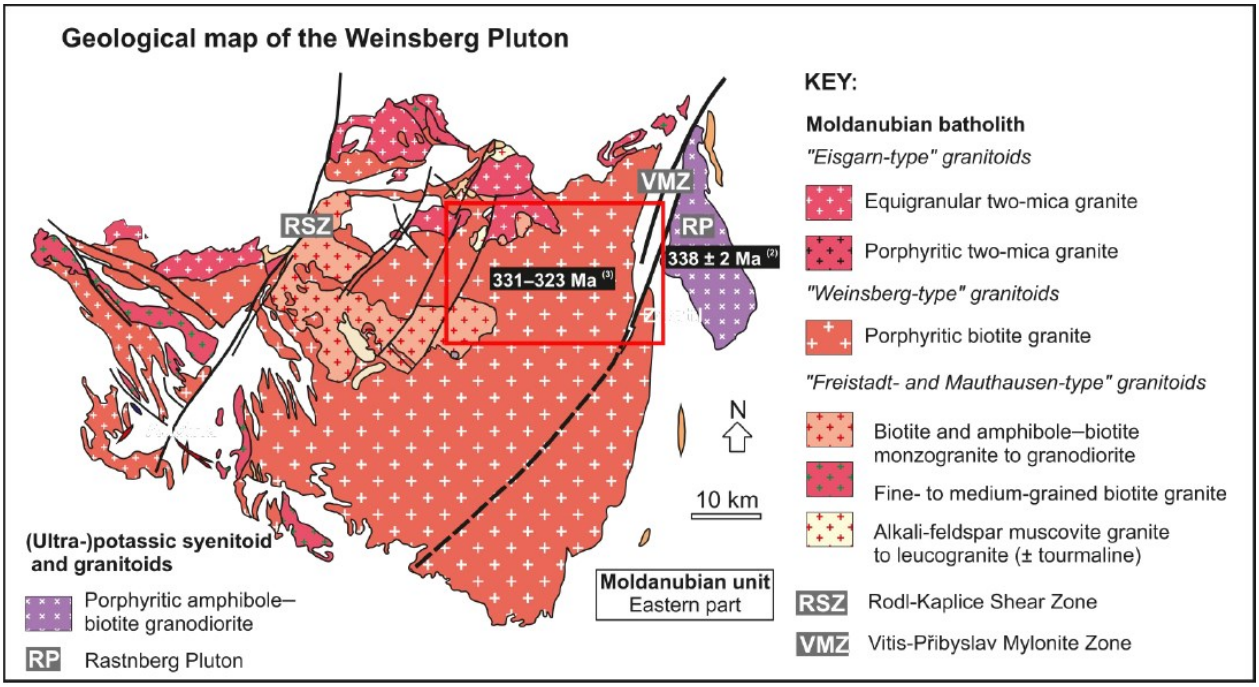

Fig. 5: *Geological map of the Weinsberg Pluton and dominating lithologies. Area of interest is highlighted by red rectangle. Modified after (Žák et al., 2014).*

3. Methodology

3.1 Optical microscopy

Fourteen thin-sections representing most important outcrops in the area of interest were thoroughly observed and many petrographical phenomenonons were described and documented in the optical polarization microscope at the Charles University of Prague.

3.2 Zircon morphology

Small (~ 0.5 kg) samples from 15 outcrops were broken to the prefered grain size (~ 1-5 mm) using the jaw crusher machine at the Department for Chemistry and Physics of Materials, University of Salzburg. The debris was then washed off by careful circular movement (panning) until only the requiered heavy mineral fraction remained. Residual heavy minerals were subsequently dried in the oven and the magnetic minerals were sorted out using a magnet. The remaining fraction contained many individual zircon crystals which were embedded in CONLOC-UV glue for further microscopic study. Using the optical polarization microscope the morphologies of between 50 to 100 single zircon crystals per sample were determined and plotted into the morphology classification diagram of Pupin (1980).

3.3 Whole-rock geochemistry

Twenty two large (2-5 kg) representative samples were collected from different outcrops. Weathered surfaces were removed and samples were ground to a fine powder in an Agate Ball Mill. Analyses were conducted by XRF methods on lithium tetraborate glass beads and pressed powder pellets using the Bruker Pioneer S4 crystal spectrometer at the Department for Chemistry and Physics of Materials, University of Salzburg. Obtained net count rates on single X-ray lines were recast into concentration data (wt% and ppm), based on an in-house calibration routine that involves measurements of ~ 30 international geostandards (USGS and GSJ). The calibration is based on the Bruker AXS software SPECTRAplus FQUANT (v1.7) and corrects absorption, fluorescence and line overlap effects. Results of a typical measurement, along with the analytical uncerntainties for single elements and the lower limits of detection are given in Lindner and Finger (2018).

3.4 Field work

In the course of this thesis 28 outcrops in the area of interest were documented. Apart from sampling and measuring for other geological, geophysical or geochemical properthies, structural measurement of direction and dip of magmatic fabrics, joints, faults and dike contacts were taken by using of standard geological compass. Complete field documentation can be found in the Appendix (Attachment 1 and 2).

3.5 Anisotropy of magnetic susceptibility

The AMS was measured at a low field of 200 Am^{-1} using the MFK1-A Kappabridge apparatus at the Laboratory of Rock Magnetism, Czech Geological Survey, Prague. A statistical analysis of the data was carried out using the ANISOFT 4.2 software

(www.agico.com). Three parameters are used to characterize the magnetic fabric (Jelínek 1981): (a) the mean susceptibility, $k_m = (k_1 + k_2 + k_3)/3$, reflecting the magnetic mineral species and their proportion in the measured rock volume; (b) the degree of anisotropy, $P = k_1/k_3$, which expresses the eccentricity of the AMS ellipsoid; and (c) the shape parameter, $T = 2\ln(k_2/k_3)/\ln(k_1/k_3) - 1$, which describes the shape of the AMS ellipsoid; for $-1 \leq T < 0$ the ellipsoid is prolate, for $T = 0$ it is triaxial, and for $1 \geq T > 0$ it is oblate. The maximum, intermediate, and minimum susceptibility axes are k_1, k_2, and k_3, respectively. The maximum principal susceptibility (k_1) represents magnetic lineation and the minimum principal susceptibility (k_3) represents a pole to magnetic foliation. The orientation of magnetic foliation and lineation are plotted in the lower hemisphere stereograms and as the station mean directions on the map (calculated according to Jelínek, 1978). In total samples were obtained from 10 localities across the northeastern Weinsberg Pluton.

4. Petrography

4.1 Coarse-grained porphyric biotite Granite, Granodiorite and Quartz monzonite (Weinsberg type)

This dominantly represented granite type often appears with preferential orientation of potassium feldspar (Kfs) phenocrysts of length about 2–7 cm. The matrix is formed mostly by quartz (26 to 40 Vol.%), potassium feldspar (18 to 35 Vol.%), plagioclase (20 to 40 Vol.%) and biotite (15 to 22 Vol.%). Low amounts of muscovite can be found in some samples (1 to 3 Vol.%). Matrix grain size is around 2–3 mm. Potassium feldspar phenocrysts are commonly perthitic with occasional small inclusions of biotite, muscovite and plagioclase and are predominantly xenomorphic or hypidiomorphic. Plagioclase is mostly hypidiomorphic and occasionally sericitized and rarely forms twins. Quartz is in the matrix allotriomorphic with oscillatory extinction of grains (Fig. 6a-f). Biotite can sometimes be afflicted by chloritization, which is perfectly visible at sample WPT06 (Fig. 6g-h). Most abundant accessoric minerals are zircon, monazite, apatite, ilmenite and titanite.

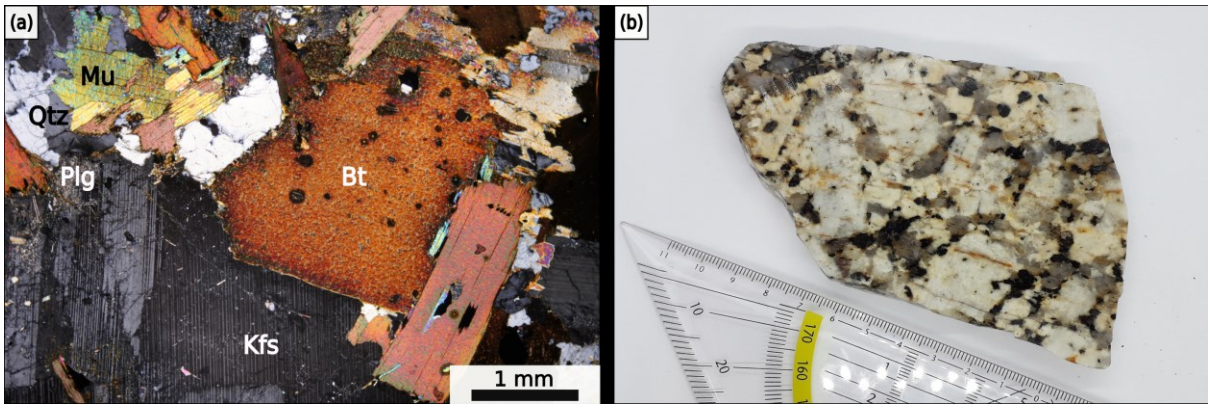

Fig. 6: *Micro and macroscopical pictures of coarse-grained porphyric biotite Weinsberg type granitoids from localities at the area of interest.* ***(a)*** *Micro-picture of sample WPT05A;* ***(b)*** *Macro-picture of sample WPT05A. Bt – Biotite, Qtz – Quartz, Kfs – Potassium feldspar, Plg – Plagioclase, Mu – Muscovite.*

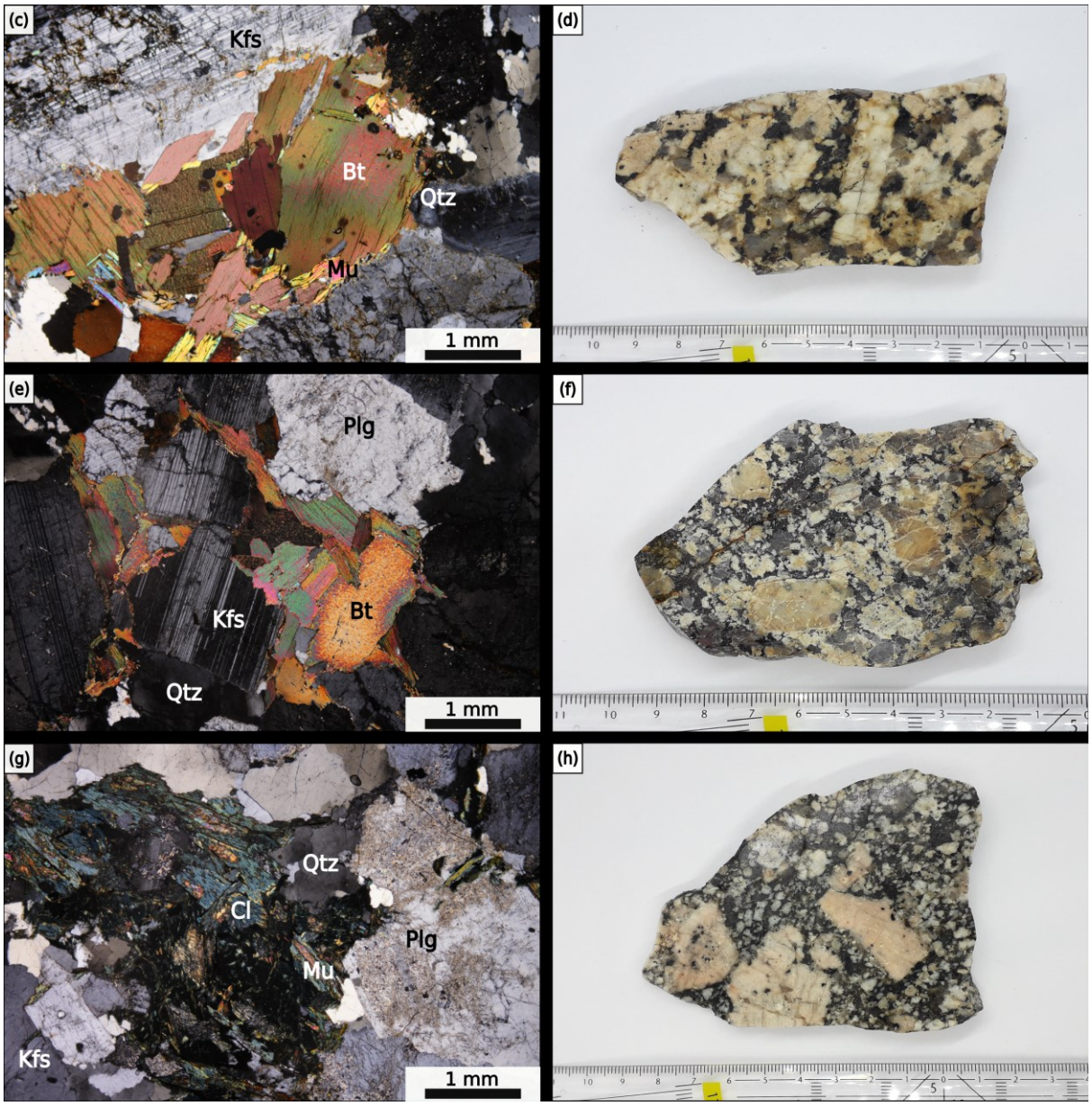

Fig. 6: *Micro and macroscopical pictures of coarse-grained porphyric biotite Weinsberg type granitoids from localities at the area of interest.* ***(c)*** *and* ***(d)*** *Micro and macro-picture of sample WPT13;* ***(e)*** *and* ***(f)*** *micro and macro-picture of sample WPT15;* ***(g)*** *and* ***(h)*** *micro and macro-picture of sample WPT06. Bt – Biotite, Qtz – Quartz, Kfs – Potassium feldspar, Plg – Plagioclase, Mu – Muscovite, Cl – Chlorite.*

4.2 Medium-grained two-mica Granite (Eisgarn sensu lato)

The Eisgarn Granite occurs as intrusive dikes at localities WPT05 (sample WPT05B) (Fig. 7a–b) and WPT15 (sample Fi-20-18). This rock can be distinguished from the typical Weinsberg granitoid by smaller phenocrysts (up to 2–3 cm) and smaller matrix grain size (~1 mm). Dominating minerals are plagioclase (25–35 Vol.%), quartz (~30 Vol.%), potassium feldspar (25–30 Vol.%), biotite (~7 Vol.%) and muscovite (~6 Vol.%). Hypidiomorphic plagioclase is commonly sericitized and forms twins. Quartz and potassium feldspar are mostly xenomorphic. Potassium feldspar is often perthitic and can contain microcline. Both micas are commonly merged into each other and occasionally afflicted by chloritization. Most abundant accessory minerals are apatite, monazite and zircon.

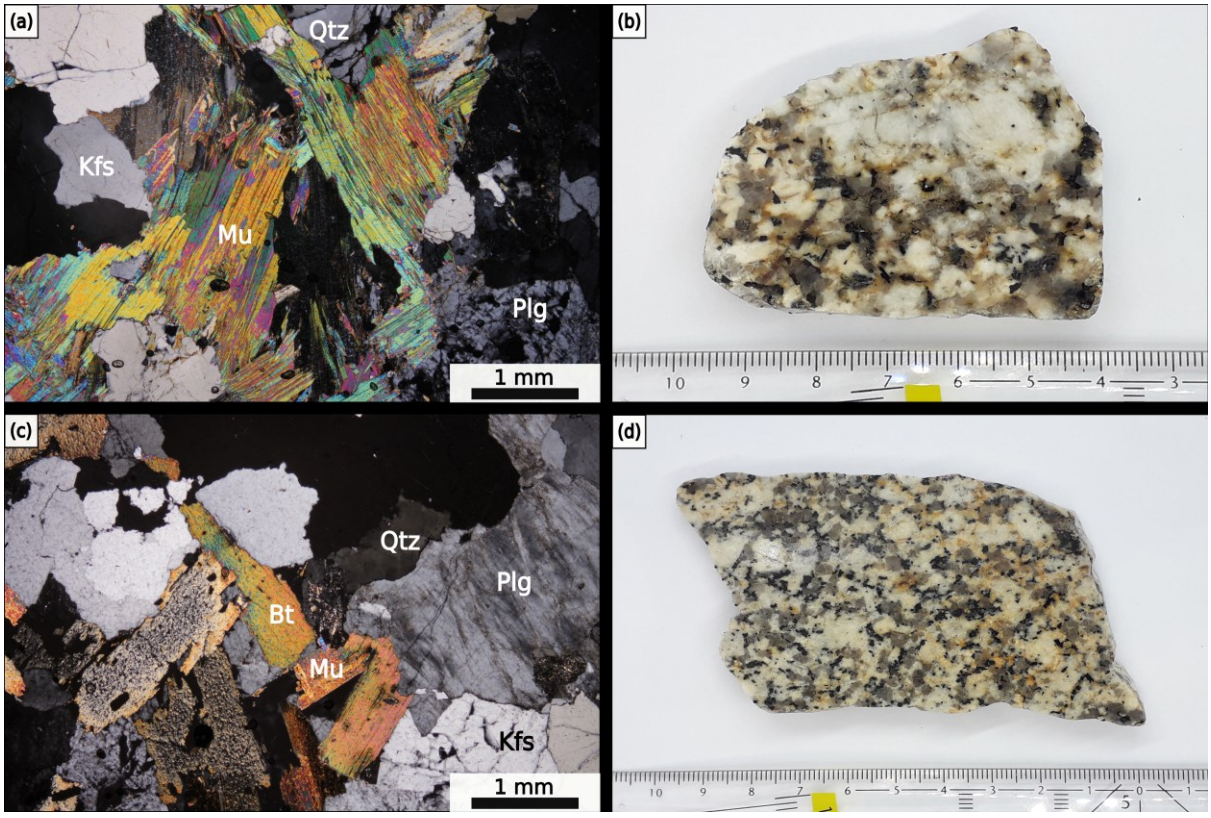

Fig. 7: *Micro and macroscopical pictures of medium-grained two-mica granites (Eisgarn sensu lato) from localities at the area of interest.* ***(a)*** *and* ***(b)*** *Micro and macro-picture of sample WPT05B;* ***(c)*** *and* ***(d)*** *micro and macro-picture of sample WPT16. Bt – Biotite, Qtz – Quartz, Kfs – Potassium feldspar, Plg – Plagioclase, Mu – Muscovite.*

The Weitra Granite type appears along with Weinsberg granitoids in the locality WPT16 (Fig. 7c–d). This granite is macro and microscopically very similar to the actual Eisgarn granites with same phenocrysts and grains size. The only examined difference was the lower amount of muscovite (~3 Vol.%).

4.3 Fine-grained and pegmatitic Leucogranite dikes

Leucogranite appears in the locality WPT19 (sample WPT19B) as a 30 cm dike and in the locality WPT17 as a ~100 cm dike. Visually it is a fine-grained massive rock with grey, white and yellow colours and hypautomorphic texture. Dominating minerals are quartz, potassium feldspar, albitic plagioclase, biotite and muscovite (Fig. 8a–b). Plagioclase is commonly sericitized and potassium feldspar is perthitic. Biotite can be localy chloritized. Pegmatitic sections of the dikes have zonal textures with fine to medium-grained parts and very coarse-grained parts with large crystals of potassium feldspar.

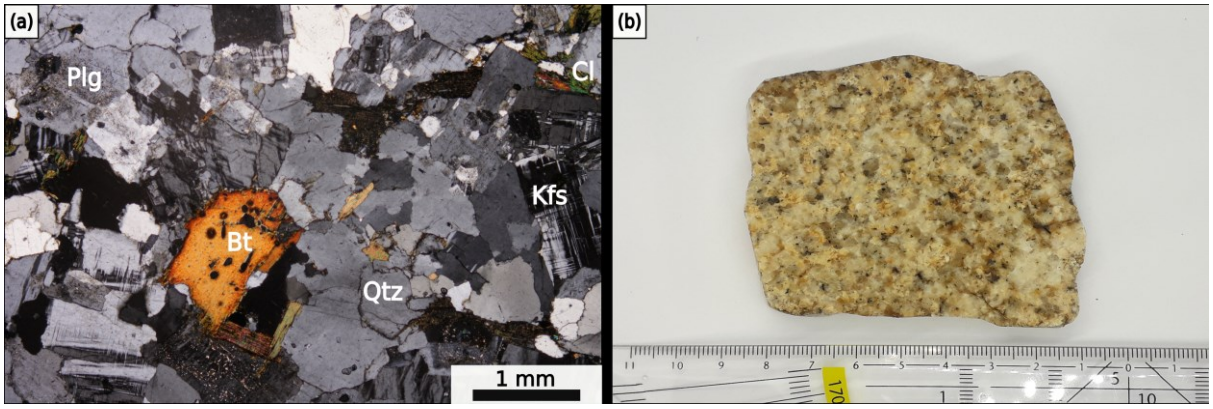

Fig. 8: *Micro and macroscopical pictures of fine-grained leucogranite from locality at the area of interest.* ***(a)*** *Micro-picture of sample WPT19B;* ***(b)*** *Macro-picture of sample WPT19B. Bt – Biotite, Qtz – Quartz, Kfs – Potassium feldspar, Plg – Plagioclase, Mu – Muscovite, Cl – Chlorite.*

4.4 Mylonitized Granite and Quartz mylonite

Mylonites appear in two localities directly in the Vitiz-Přibyslav Zone (WPT25 and WPT28). Visually it is a very fine-grained rock with completely deformed and compact texture, grey color and blue or green tinge. The internal fabric resembles a cataclastic flow pattern. Main minerals forming the matrix are quartz (~35 Vol.%), potassium feldspar (20–30 Vol.%), plagioclase (25–35 Vol.%), biotite (10–5 Vol.%) and muscovite (2–5 Vol.%). Biotite is partially chloritized (Fig. 9a–d).

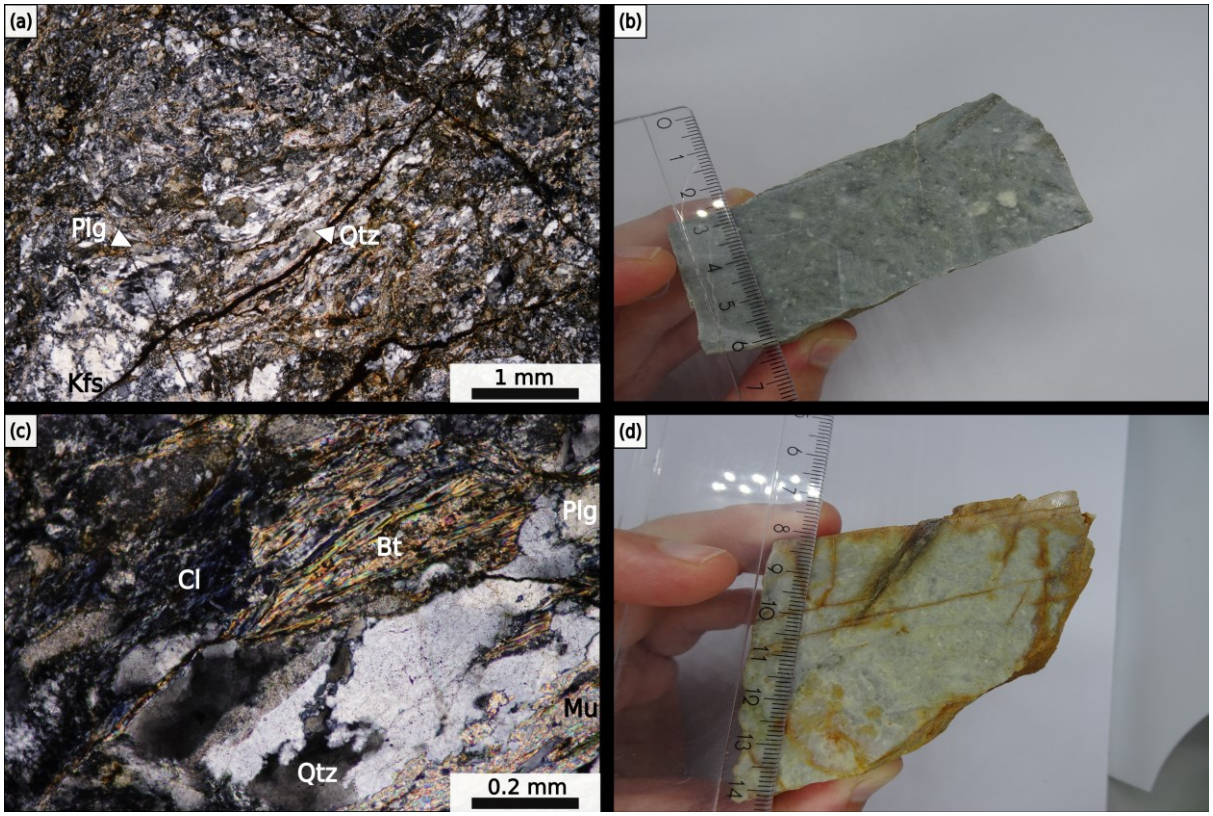

Fig. 9: *Micro and macroscopical pictures of mylonitized granites and quartz mylonite from localities at the area of interest.* ***(a)****,* ***(b)*** *and* ***(c)*** *micro and macro-pictures with different magnitudes of sample WPT25 (Fi-24-18);* ***(d)*** *macro-picture of sample WPT28 (Fi-23-18). Bt–Biotite, Qtz – Quartz, Kfs – Potassium feldspar, Plg – Plagioclase, Mu – Muscovite, Cl – Chlorite.*

4.5 Sillimanit-Biotite Paragneiss

This lithology appears in the locality WPT10 close to the Vitiz-Přibyslav mylonite zone. Texture of the paragneiss is formed by two visually distinguishable phenomenons. Firstly the bends of very fine-grained deformed material with high amount of quartz (~30 Vol.%), plagioclase (~20 Vol.%), commonly chloritized biotite (15–25 Vol.%), potassium feldspar (~20 Vol.%), muscovite (~5 Vol.%) and sillimanite (~3 Vol.%). Secondly the medium to coarse-grained parts formed predominantly by restitic quartz, commonly sericitized plagioclase and potassium feldspar with small inclusions of both micas (Fig. 10a-b).

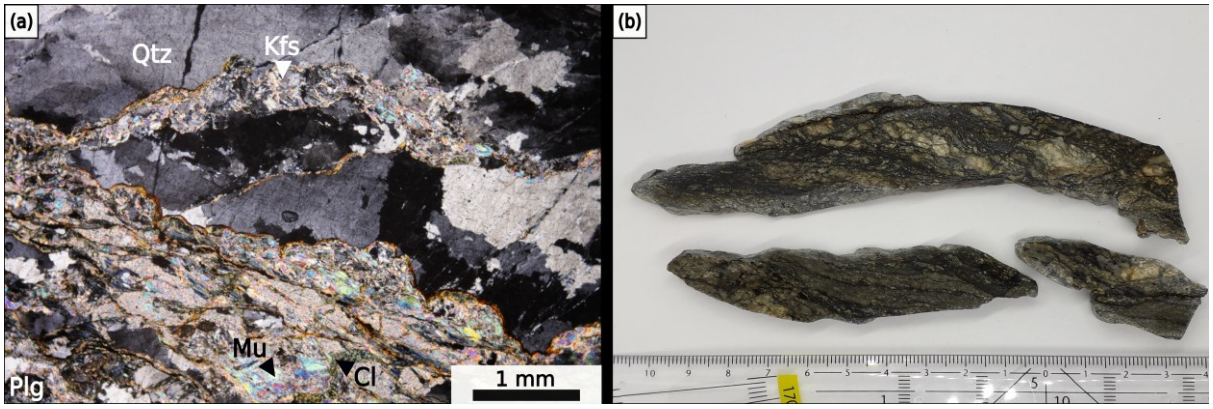

Fig. 10: *Micro and macroscopical pictures of Sillimanit-Biotite paragneiss from locality at the area of interest.* ***(a)*** *Micro-picture of sample WPT10;* ***(b)*** *macro-picture of sample WPT10. Qtz – Quartz, Kfs – Potassium feldspar, Plg – Plagioclase, Mu – Muscovite, Cl – Chlorite.*

5. Zircon Morphology

5.1 General aspects

5.1.1 The Typology Method

The first idea of using zircon morphology as an indicator of granite origin was proposed by Poldervaart; (Poldervaart, 1956; Larsen and Poldervaart, 1957). But the methods and differentiations of zircon crystals which have been used in recent days was proposed by Pupin; (Pupin and Turcon, 1972a; Pupin, 1980).

The method of typology of zircon crystals is based on the arrangement of given pyramidal and prismatic crystal faces which together create a population type. Certain zircon crystal faces have lower abundances than others which lead to less or more numerous subtypes (Pupin, 1980). This can help distinguish rocks with similar abundances of the same zircon type. However their subtypes distribution must be known. The subtypes and secondary types differentiation can be found in the Table 1. The main types can show between 0 and 2 prisms. That means {100} or {110} in combination with either one of these pyramids {101}, {211}, {301} or composition of {101} + {211}. All of the main types and subtypes can be found in the typology of zircon crystals classification diagram (Fig. 11). This diagram is based on relative development of crystal faces and is used for classification of zircon crystal populations in rocks. Elongation of crystals is not taken into account in this zircon typology (Pupin, 1980).

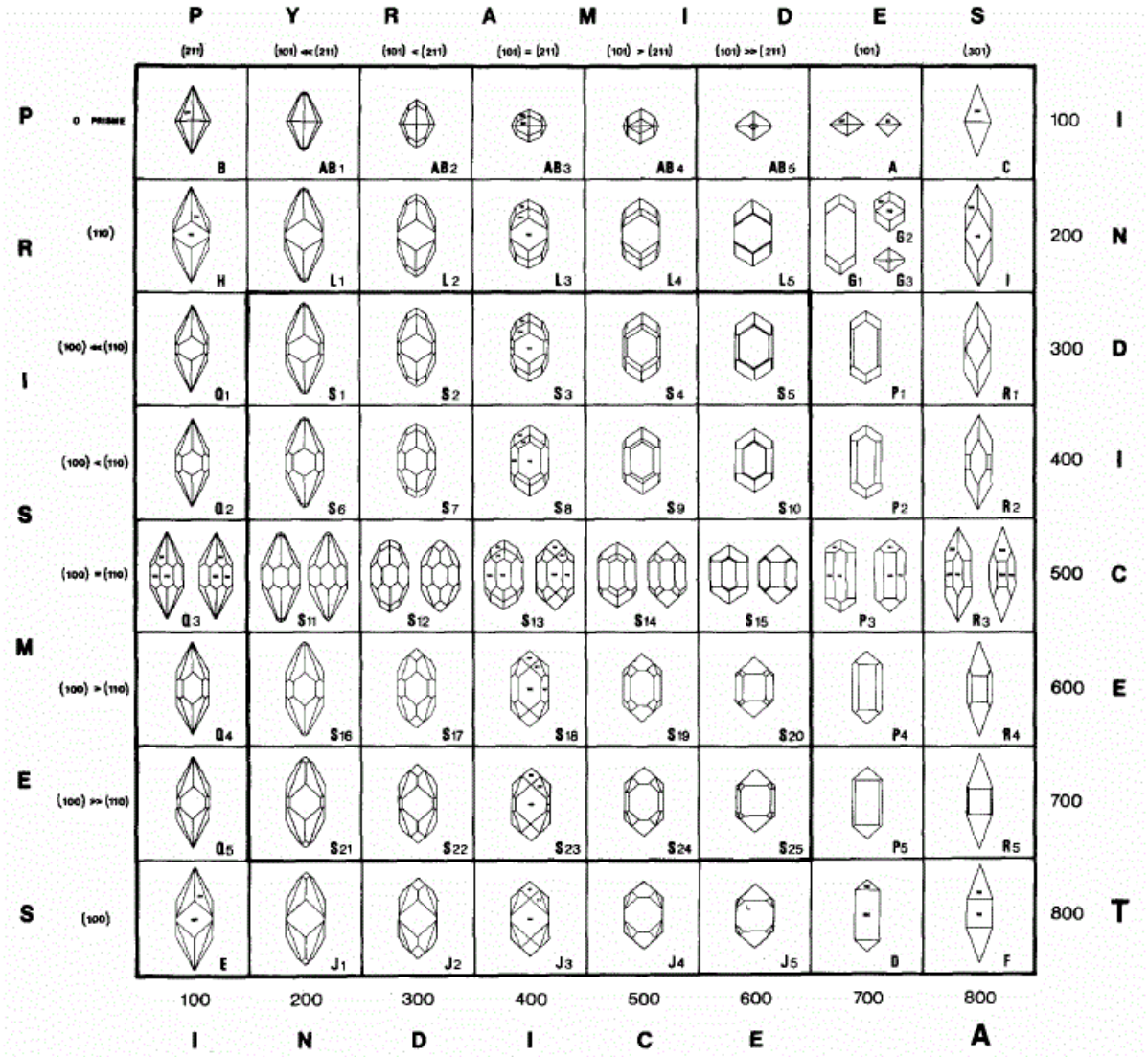

Fig 11: *Diagram of zircon typology classification. Based on the relative natural abundancies of zircon types and subtypes. In the middle of the diagram is placed S type habitus, which is the most abundant type in the rocks. The other main types are placed around this point. The top right column contain main types (C, I, R, F) which are purely theoretical. The A index reflects the Al / (Na + K) ratio. Taken from (Pupin, 1980).*

The major and most important factor in origin and relative growth of zircon pyramids is the geochemical composition of the crystallizing melt. Zircons crystallizing from the melt of hyperaluminous or hypoalkaline composition have well developed {211} pyramids, whereas zircons crystallizing from hyperalkaline melts show well developed {101} pyramids. Therefore the one factor for influencing the zircon morphology seems to be the Al/alkali ratio (Pupin, 1980).

The leading factor for development of zircon prisms seems to be more unclear. In the decades after zircon typology classification introduction many different theories were presented. According to (Pupin and Turco, 1972) the leading factor governing the relative development of zircon prisms is the temperature of the crystallization medium. (Vavra, 1990) proposed that the morphology of the prism form is mainly determined by the degree of $ZrSiO_4$ supersaturation. Stages of low degree of $ZrSiO_4$ supersaturation favors development of {110} crystal faces and vice versa. Lastly (Benisek and Finger, 1993) stated that the size relations of the two zircon prisms {100} and {110} are strongly dependent on the geochemistry of the growth medium. High abundance of U element in the granite melt favors development of {110} by producing a growth-blocking effect on {110} crystal surfaces of zircons.

Table 1: *Diferenciation of main, secondary and subtypes of zircon populations (Pupin, 1980).*

Prisms	Pyramids	Main types	Subtypes	Supplementary pyramids: secondary types and subtypes					Pinacoïd
				+{301}	+{112}	+{321}	+{311}	+{511}	+{001}
0	1 {101}	A	–	AC	Add	Add	Add	Add	Add
	{211}	B	–	BC					
	{301}	C	–	–	Z	Y	W	X	an
0	2 {101} – {211}	AB	5 (AB_1 à AB_5)	$ABC_{1\,à\,5}$	to the	to the	to the	to the	asterisk
1 {100}	1 {101}	D	–	K	main	main	main	main	to the
	{211}	E	–	EC					
	{301}	F	–	–	type:	type:	type:	type:	type:
1 {110}	1 {101}	G	3 (G_1 à G_3)	$M_{1\,à\,3}$	AZ, BZ, ...	AY, BY, ..	AW, BW, ...	AX, BX, ...	A*, B*, ...
	{211}	H	–	HC					
	{301}	I	–	–					
1 {100}	2 {101} – {211}	J	5 (J_1 à J_5)	$N_{1\,à\,5}$					
1 {110}	2 {101} – {211}	L	5 (L_1 à L_5)	$O_{1\,à\,5}$					
2 {100} – {110}	1 {101}	P	5 (P_1 à P_5)	$T_{1\,à\,l_5}$					
	{211}	Q	5 (Q_1 à Q_5)	$OC_{1\,à\,5}$					
	{301}	R	5 (R_1 à R_5)	–					
2 {100} – {110}	2 {101} – {211}	S	25 (S_1 à S_{25})	$V_{1\,à\,25}$		SY = V			

Decreasing frequency of Pyramids in nature

5.1.2 Petrogenetic Classification

On the basis of distribution of zircon typological populations the following petrogenetic classification was developed (Pupin, 1980):

1. *Granites of Crustal or Mainly Crustal Origin (orogenic)*. This group can be further divided into **(a)** Autochthonous and Intrusive Aluminous Leucogranites; **(b)** (Sub)autochthonous Monzogranites and Granodiorites; **(c)** Intrusive Aluminous Monzogranites and Granodiorites.

2. *Granites of Crustal and Mantle Origin, Hybrid Granites (orogenic),* can be divided into **(a)** Calc-Alkaline Series Granites; **(b)** Sub-Alkaline Series granites.

3. *Granites of Mantle or Mainly Mantle Origin (anorogenic),* can be divided into **(a)** Alkaline Series Granites; **(b)** Tholeiitic Series Granites. Typology distribution of zircon population of every petrogenetic group is presented on example granitic rocks on Figures 12 and 13.

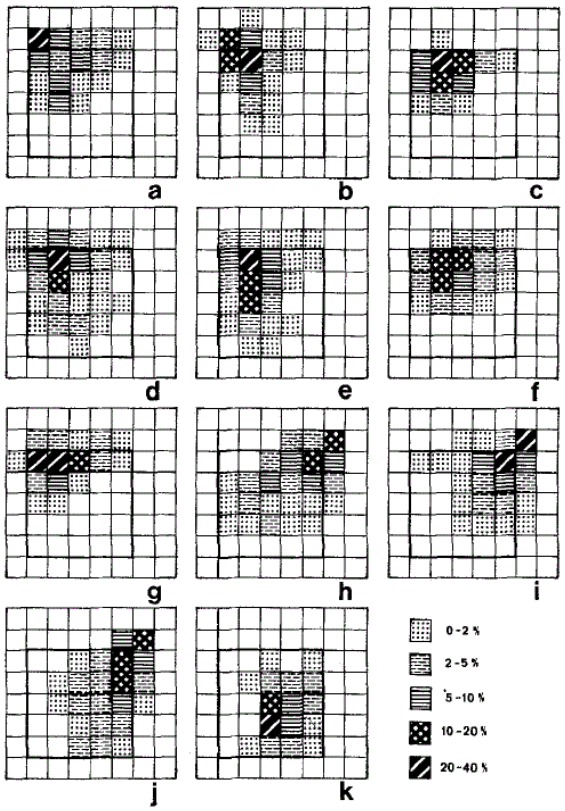

Fig. 12: *Typologic distribution of zircon population from granites;* ***a***, ***b*** *Aluminous Leucogranites;* ***c***, ***d*** *(Sub)autochthonous Monzogranites;* ***e***, ***f***, ***g*** *Intrusive Aluminous Monzogranites;* ***h***, ***i***, ***j***, ***k*** *Calc-Alkaline Series. Taken from (Pupin, 1980).*

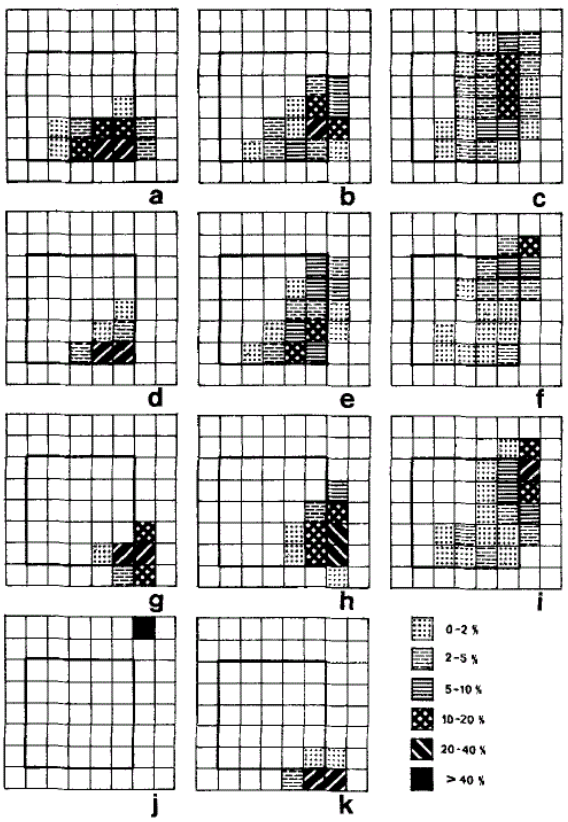

Fig. 13: *Typologic distribution of zircon population from granites;* ***a***, ***b***, ***c*** *Calc-Alkaline Series;* ***d***, ***e***, ***f*** *Sub-Alkaline Series;* ***g***, ***h***, ***i***, ***j*** *Alkaline Series;* ***k*** *Tholeiitic Series. Taken from (Pupin, 1980).*

5.2 Zircon Morphology results

5.2.1 Coarse-grained porphyric biotite Granite, Granodiorite and Quartz monzonite (Weinsberg type)

For this granitoid type zircon morphology classification was made from 12 localities. Total zircon population statistics for this granitoid type can be found in Fig. 14. Significantly dominating is the S type habitus into which over 97% of all zircon crystals examined fall. Most abundant subtype is the S_7 in which can be found for over 24% of all crystals. Other significant subtypes are S_{13}, S_{12}, S_2 and S_8 respectively. Around 1.5% zircons belong to the L type habitus (L_1, L_2 and L_3) and similar amount into P type habitus (P_2 and P_4). Zircon classification diagrams for every sample in this granitoid group is attached as Fig. 15.

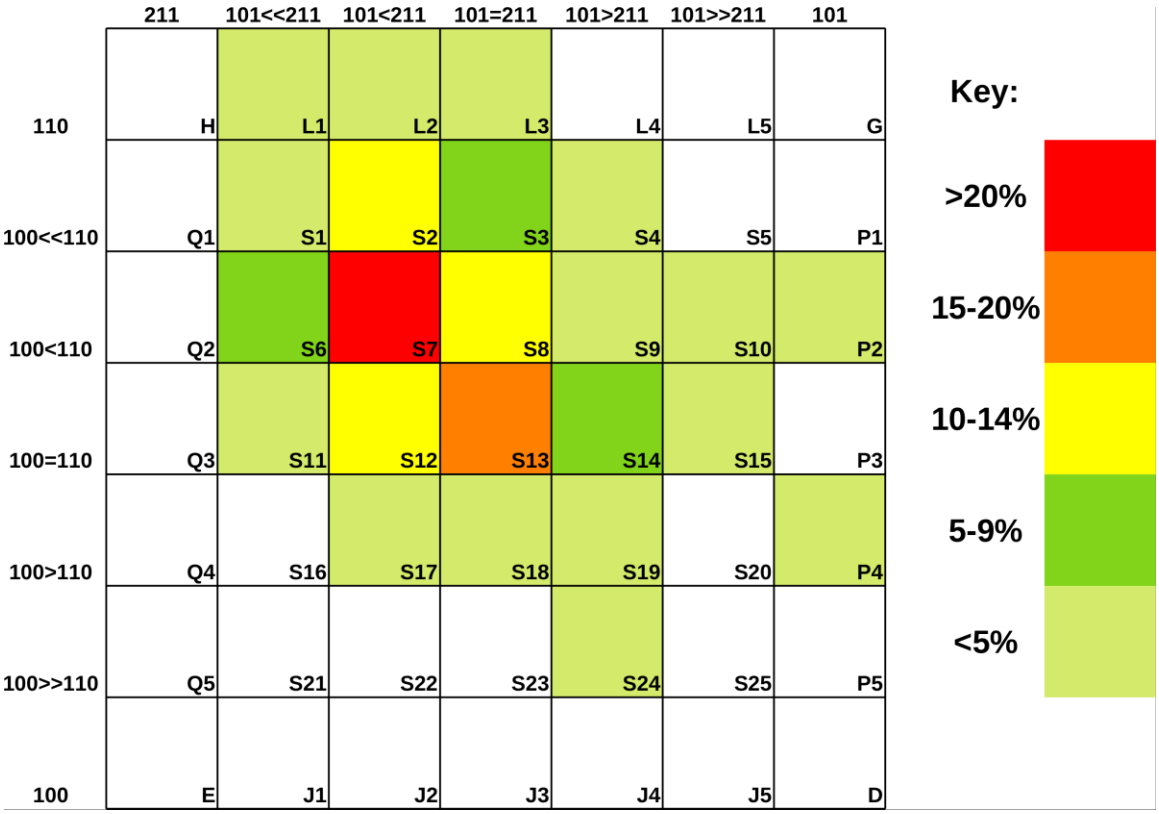

Fig. 14: *Mean zircon morphology classification diagram made for Weinsberg type granitoids. Data collected from 12 localities.*

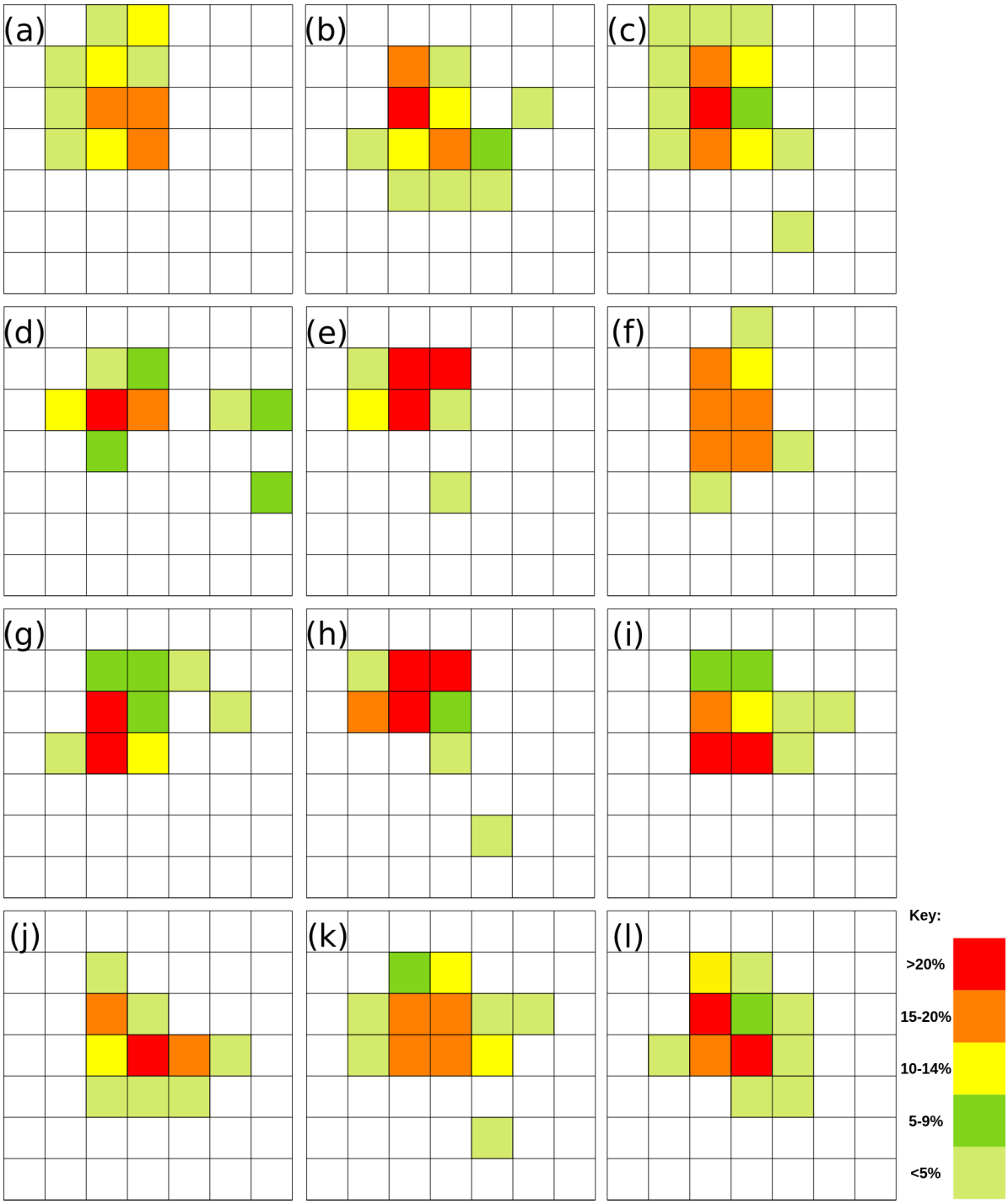

Fig. 15: *Zircon morphology classification diagrams for every separate Weinsberg type granitoid sample.* ***(a)*** *WPT15 (Fi-21-18);* ***(b)*** *WPT27 (Fi-22-18);* ***(c)*** *WPT05A;* ***(d)*** *WPT06;* ***(e)*** *WPT09;* ***(f)*** *WPT11;* ***(g)*** *WPT13;* ***(h)*** *WPT14;* ***(i)*** *WPT18;* ***(j)*** *WPT19A;* ***(k)*** *WPT20;* ***(l)*** *WPT21.*

5.2.2 Medium-grained two-mica Granite (Eisgarn sensu lato)

Zircon crystals from Eisgarn granite body from the locality WPT15 (Fi-20-18) are placed distinctly on the left hand side of the classification diagram. Here they create two dominating habitus: Q_1 which contains almost 25% of all zircons and S_6 in which around 21% of the zircons fall. Other significant habitus are Q_2 and S_1 which contain around 15% of all zircons each (Fig. 16a).

The two-mica granite from the locality WPT05 (sample WPT05B) has a more diverse zircon population. No habitus has over 20% of all zircons in this case. The most abundant habitus is S_2 with 18 %, followed by L2, S1, S4 and S13, which all have around 10% of zircons. In the interval between 5 and 10% of zircon crystals, S_6, S_8 and S_{12} habitus can be found ,(Fig. 16b).

Weitra type granite the from locality WPT16 has even more heterogenous zircon population with two clusters of significant habitus not so close to each other. One cluster is formed by S_{13} and S_8 habitus which have 13% and 12% of all crystals respectively. Other one is formed by P_1 habitus with 12% of crystals and G and P_2 habitus which have little bit than 10% each. Other more important habitus are L_3, S_3, S_2 and S_7 with amount of crystals between 5 and 7% (Fig. 16c).

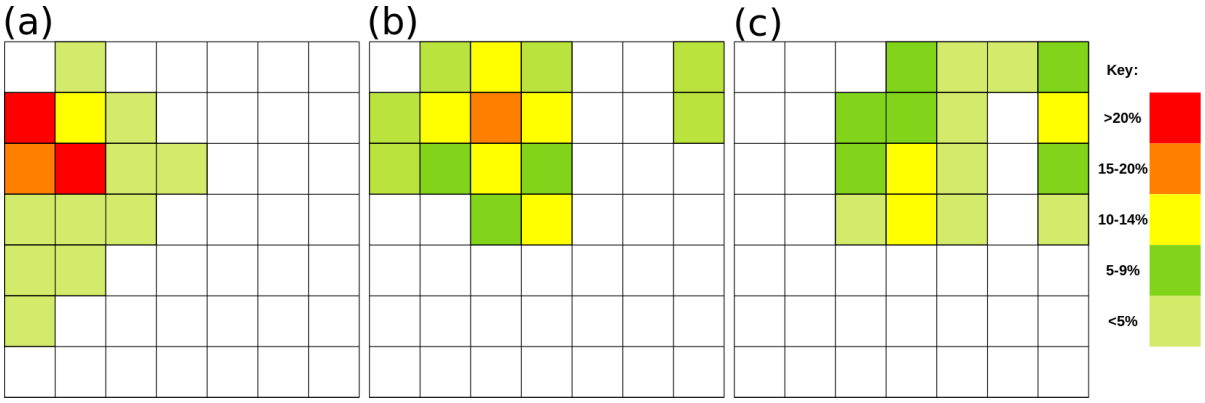

Fig. 16: *Zircon morphology classification diagram for medium-grained two-mica granites (Eisgarn sensu lato).* ***(a)*** *sample WPT15 (Fi-20-18);* ***(b)*** *sample WPT05B;* ***(c)*** *sample WPT16*

5.2.3 Fine-grained and pegmatitic Leucogranite dikes

The leucogranites are overall very unrewarding rocks for zircon morphology classification, which is caused by their extremely low Zr content. This is the case of our sample WPT17, where the zircon separation methods were unsuccessful and no representative zircon populations were obtained. However regarding the locality WPT19 and specifically leucogranitic sample WPT19B, the classification diagram was created and can be found in Fig. 17a. For this zircon population the habitus S_{13} is extremely dominating and contains around 40% of all zircon crystals examined. Other important habitus are the surrounding S_{14} and S_{12} in which around 16 and 10% of zircons fall ,respectively. Another interesting fact is that this sample has remarkably similar zircon population as surrounding Weinsberg lithology in the locality WPT19 (sample WPT19A) but the zircons of the leucogranite are distinctly more damaged (Fig. 15j).

5.2.4 Mylonitized Granite and Quartz mylonite

Regarding Mylonites in the area of interest, only zircons from the sample WPT25 (Fi-24-18) were successfuly separated. Their classification diagram and zircon population is very similar to the mean classification diagram of all Weinsberg granitoids in the area of interest (Fig. 15). Significantly dominating habitus is S_7 with almost 31% of all zircons. Other important habitus are S_2, S_{12} and S_8 with 18, 14 and 12% of zircons (Fig. 17b). A classification diagram for Quartz mylonite sample WPT28 (Fi-23-18) unfortunately could not be made due to the low amount of zircon crystals and their high level of corrosion.

5.2.5 Sillimanit-Biotite Paragneiss

Zircons of this paragneiss are very small, short and rounded, often have dark brown colour and are generally damaged. Most abundant zircon habitus are S_{12} and S_{13}, both having over 20% of total zircon crystals. The are followed by S_7 with 10% of crystals. All other habitus contain 8% or lower amount of zircons. The total population of this sample is quite spread around the diagram (Fig. 17c). It has the second highest amount of zircon crystals placed in the P habitus (14% at total).

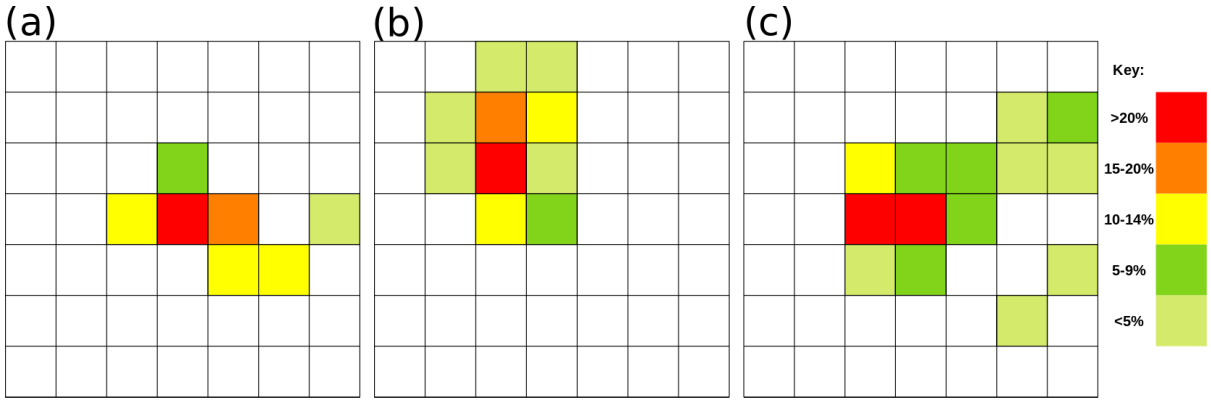

Fig. 17: *Zircon morphology classification diagram of Leucogranite, Mylonite and Sillimanit-Biotite Paragneiss from localities in the area of interest.* ***(a)*** *sample WPT19;* ***(b)*** *sample WPT25 (Fi-24-18);* ***(c)*** *sample WPT10.*

6. Whole-rock geochemistry

6.1 Coarse-grained porphyric biotite Granite, Granodiorite and Quartz monzonite (Weinsberg type)

This group is in the area of interest characterized by 13 samples (WPT05A; WPT06; WPT09; WPT11; WPT13; WPT14; WPT15; WPT15 Fi-21-18; WPT18; WPT19A; WPT20; WPT21; WPT27 Fi-22-18).

From the studied samples the following data was obtained: SiO_2 63–72.1 wt%, Al_2O_3 14.3–17.0 wt%, MgO 0.8–2.0 wt%, CaO 1.1–2.9 wt%, Na_2O 2.7–3.3 wt%, K_2O 3.8–6.7 wt% and Fe_2O_3 2.4–6.2 wt%. On the SiO_2 – K_2O plot (Peccerillo and Taylor, 1976) we can observe that the majority of the samples fall into the Shoshonite area and only two samples (WPT14 and WPT21) into the High-K calc-alkaline area (Fig. 18b; Fig. 19b). Particular attention should be given to the TAS diagram (Middlemost, 1994) (Fig. 18c; Fig. 19c) which shows that on the basis of SiO_2 – Na_2O+K2O most of the Weinsberg samples should be classified as Quartz monzonites, two as granodiorites and only three as granites (WPT09, WPT14 and WPT27 Fi-22-18). The A/CNK ratio (Shand, 1943) is between 1.0 and 1.2 so these granitoids can be marked as peraluminous (Fig. 18a; Fig. 19a). On the ternary AFM diagram (Irvine and Baragar, 1971) where A=Al_2O_3, F=FeO_{tot} and M=MgO it can be observed that the Weinsberg type granitoids have the highest amount of mafic contents considering the amount of Al_2O_3 (Fig. 19d). On the other hand after examination of SiO2 – FeOtot/MgO plot (Miyashiro, 1974) (Fig. 19e) we can see that the FeO_{tot}/MgO ratio is very similar to those of the Eisgarn type granites and much lower than the Leucogranite ones. The important trace element contents are the following: Ba 405–1450 ppm, Nd 28–82 ppm, Nb 9–20 ppm, Rb 130–299 ppm, Sr 131–242 ppm, Zr 183–405 ppm. Multielemental plot of the selected trace elements normalized on the Upper Continental Crust (Taylor and McLennan, 1995) is attached in Fig. 18d and Fig. 20 (please take into account that the U and Cs element contents can be inaccurate due to XRF measuring method).

Regarding the geotectonic classification, two types of diagrams were plotted: Granite tectonic discrimination diagrams (Frost et al., 2001), which shows that all Weinsberg type granitoids are magnesian (Fig. 21a) but that SiO2 / (K2O + Na2O - CaO) calc-alkalic classification is not so clear (Fig. 21b), and several Geotectonic classification of potassic rocks diagrams (Muller et al., 1992) (Fig. 21b–d).

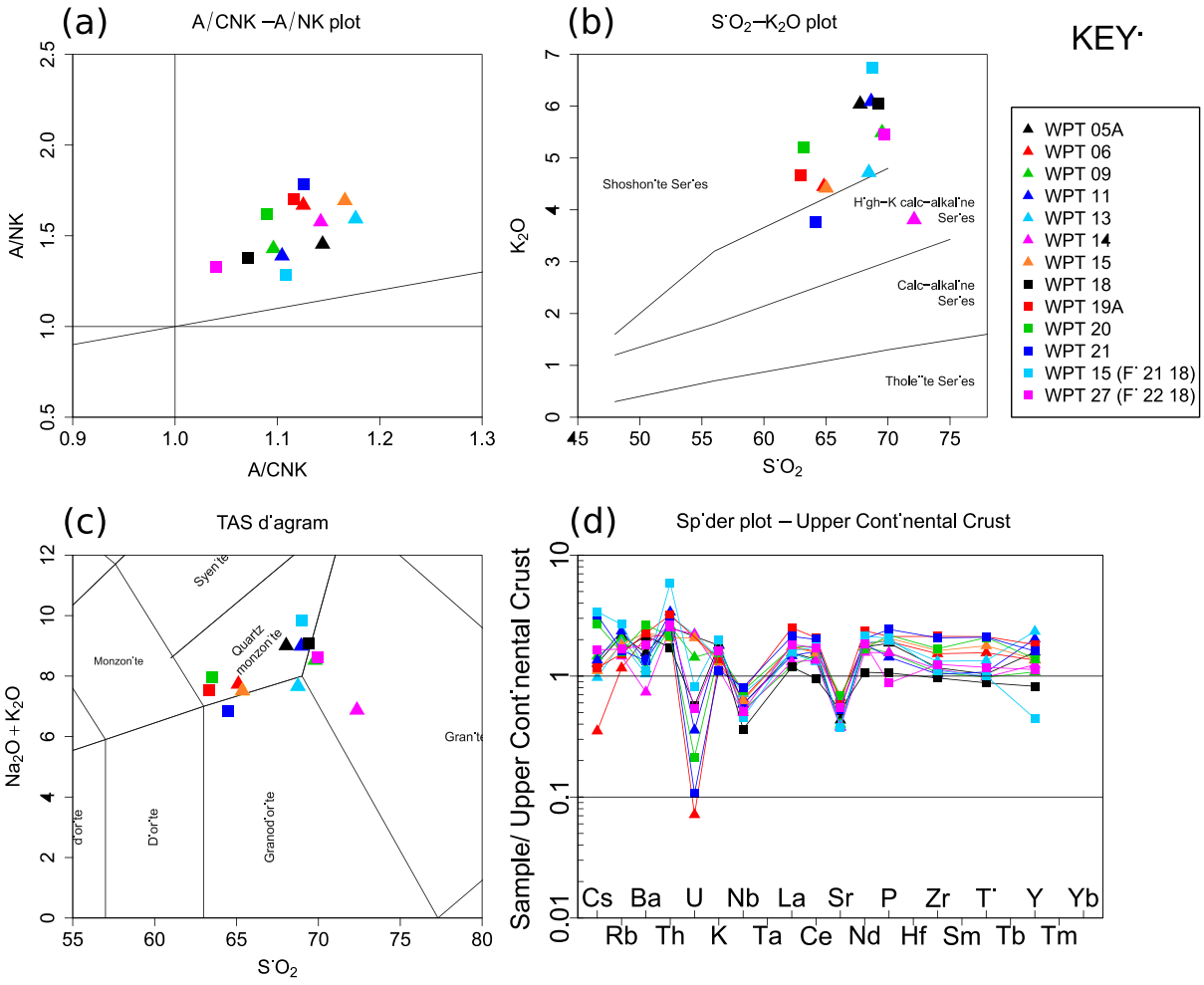

Fig. 18: *Selected classification diagrams for 13 samples of Weinsberg type granitoids from the area of interest.* ***(a)*** *A/CNK – A/NK plot (Shand, 1943) with scaled axes for better clarity of individual samples;* ***(b)*** *SiO_2 – K_2O plot (Peccerillo and Taylor, 1976);* ***(c)*** *TAS diagram (Middlemost, 1994) with scaled axes for improved readibility of individual samples;* ***(d)*** *Spider plot – Upper Continental Crust (Taylor and McLennan 1995). Diagrams plotted using the Geochemical Data Toolkit software (Janoušek et al., 2006).*

6.2 Medium-grained two-mica Granites (Eisgarn sensu lato)

This granite type is represented by three samples (WPT05B, WPT15 Fi-20-18 and WPT16).

Sample WPT05B is clearly peraluminous (A/CNK 1.2) with SiO_2 72.9 wt%. Other major and trace element characteristics: Al_2O_3 14.3 wt%, MgO 0.6 wt%, CaO 1.0 wt%, Na_2O 2.4 wt%, K_2O 5.8 wt%, Fe_2O_3 2.3 wt%, Ba 508 ppm, Nd 29 ppm, Rb 221 ppm, Sr 108 ppm and Zr 166 ppm.

Sample WPT16 representing the Weitra granite is peraluminous (A/CNK 1.1) with SiO_2 70.8 wt%, Al_2O_3 15.1 wt%, MgO 0.8 wt%, CaO 1.5 wt%, Na_2O 3.2 wt%, K_2O 5.2 wt% and Fe_2O_3 2.4 wt%. Contents of trace elements: Ba 826 ppm, Nd 43 ppm, Rb 233 ppm, Sr 298 ppm and Zr 183 ppm.

Sample WPT15 Fi-20-18 has very similar composition as WPT16. It is peraluminous with similar A/CNK ratio (1.1) and slightly lower SiO_2 content (69.1 wt%). Other major and trace element data: Al2O3 15.5 wt%, MgO 0.9 wt%, CaO 1.2 wt%, Na2O 3.2 wt%, K2O 6.3 wt%, Fe2O3 2.6 wt%, Ba 237 ppm, higher amount of Nd (82 ppm), Rb 248 ppm, Sr 142 ppm, higher amount of Th (72 ppm), Zr 235 ppm.

On the A/CNK – A/NK diagram (Shand, 1943) (Fig. 19a) it is clearly visible that in comparsion with the Weinsberg type granitoids, this granites have somewhat similar A/CNK ratios, but slightly lower A/NK ratio. On the TAS diagram (Middlemost, 1994) (Fig. 19c) samples WPT05B and WPT16 are classified as granites, however sample WPT15 (Fi-20-18) with lower amount of SiO_2 belongs to the Quartz monzonite. Regarding the Granite tectonic discrimination diagrams (Frost et al., 2001) these samples have magnesian alkali-calcic or magnesian alcalic characters (Fig. 21a-b).

Complete table of all the measurements can be found in the Appendix in Attachment 3.

6.3 Fine-grained and pegmatitic Leucogranite dikes

Three samples (WPT17A, WPT17B and WPT19B) from two outcrops characterize this group. Samples WPT17A (fine-grained) and WPT17B (pegmatitic) represent different parts of the same dike on the outcrop.

All samples are peraluminous with A/CNK ranging from a little more than 1.0 (WPT19B) to 1.3 (WPT17A) and A/NK between 1.0 and 1.5 (Fig. 19a). Contents of major and trace elements: SiO2 74.8–76.9 wt%, Al2O3 14.1–14.6 wt%, MgO < 0.1 wt%, CaO 0.5–0.6 wt.%, Na2O 3.4–4.6 wt%, K2O 3.6–6.5 wt%, Fe2O3 0.5–0.7 wt%, very low Ba (43–215 ppm) and Nd (7–18 ppm) contents, Rb 210–239 ppm, low Sr (16–73 ppm) and Th (1–10 ppm), and very low Zr (23–42 ppm) (Fig. 20). On the AFM ternary plot (Fig. 19d) all three samples are located exclusively almost in the pure Al_2O_3 area, which is caused by very low amount of mafic elements in the rocks. However in the SiO_2 – FeO_{tot}/MgO diagram the Leucogranites are placed in the Tholeiite Series with FeO_{tot}/MgO ratio between 8 and 10 (Fig. 19e). Regarding the Granite tectonic discrimination diagrams (Frost et al., 2001) the leucogranite samples have character from ferroan alcali-calcic to ferroan calc-alcalic (Fig. 21a).

6.4 Mylonitized Granite and Quartz mylonite

Mylonitized granite (WPT25 Fi-24-18) and Quartz mylonite (WPT28 Fi-23-18) represents the Vitiz-Přibyslav Mylonite zone in the area of interest.

Sample WPT25 Fi-24-18 is metaluminous with A/CNK ~ 0.9. SiO_2 69.8 wt%, Al_2O_3 15.3 wt%, MgO 0.3 wt%, CaO 1.0 wt%, Na_2O 4.3 wt%, K_2O 7.1 wt% and Fe_2O_3 1.7 wt%, Ba 244 ppm, Nd 22 ppm, high Rb (388 ppm), Sr 89 ppm and Zr 113 ppm.

Sample WPT28 Fi-23-18 is peraluminous (A/CNK 1.2) with extremely high content of SiO_2 (89 wt%) and SO_3 (0.44 wt%). Other elements are characterized by very low contents: Al_2O_3 5.8 wt%, MgO 0.2 wt%, CaO 0.1 wt%, Na_2O 1.5 wt%, K_2O 2.0 wt% and Fe_2O_3 0.8 wt%. Ba 207 ppm, Nd 15 ppm, Rb 108 ppm, Sr 33 ppm and Zr 64 ppm.

Both samples can be found on the SiO_2 – K_2O diagram (Fig. 19b), where WPT25 (Fi-24-18) has highest amount of K_2O, the WPT28 (Fi-23-18) is clearly recognizable by the extreme amount of SiO_2. On the ternary AFM plot (Fig. 19d) the mylonites are located between the Leucogranitic and Weinsberg/Eisgarn granitoid composition. Regarding the trace element spider-plot, contents of most selected trace elements are lower than Weinsberg/Eisgarn granitoids but higher than the Leucogranite ones (Fig. 20).

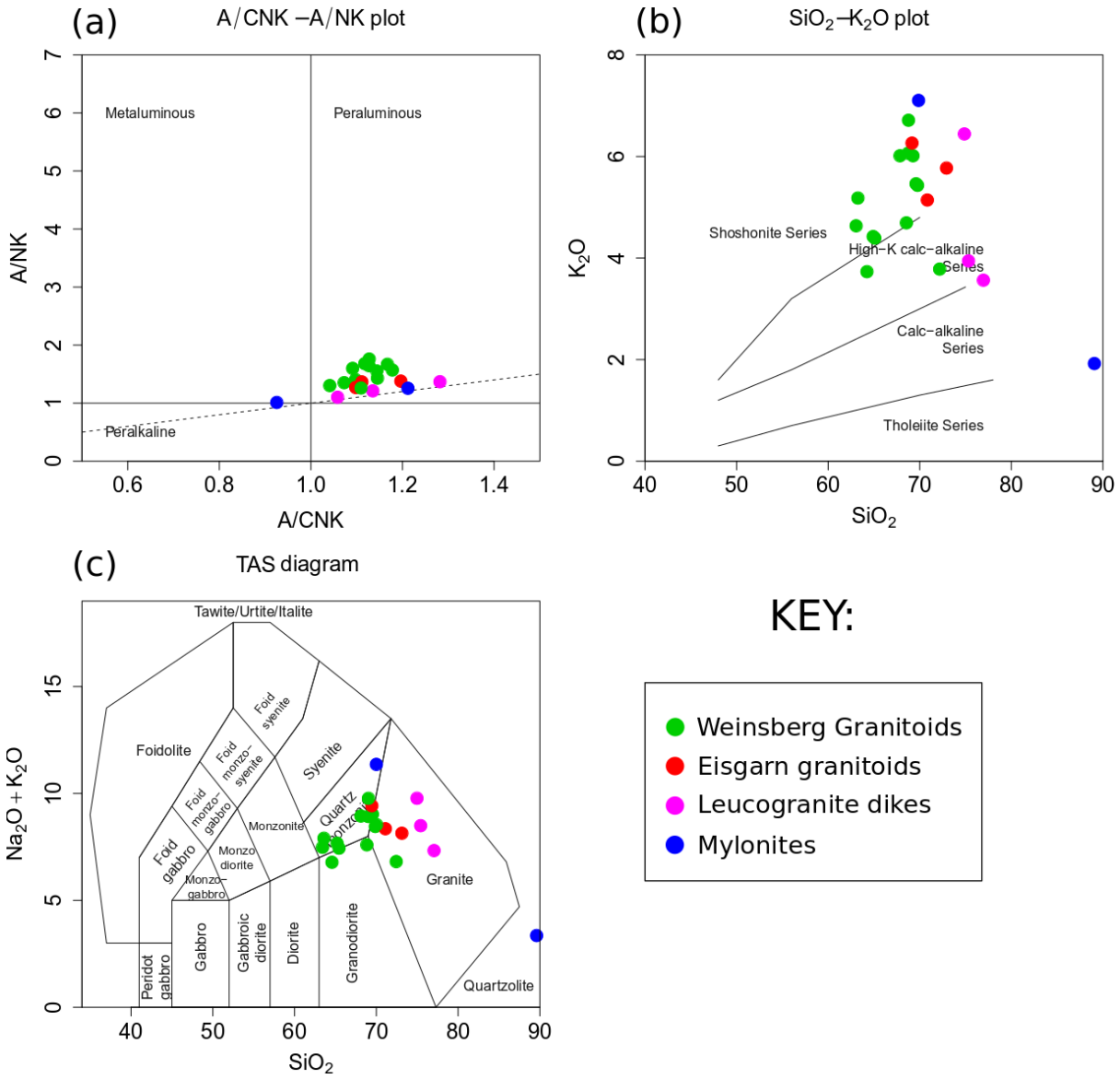

Fig. 19: *Selected classification diagrams for all main lithologies examined in the area of interest.* ***(a)*** *A/CNK – A/NK plot (Shand, 1943);* ***(b)*** *SiO2 – K2O plot (Peccerillo and Taylor, 1976);* ***(c)*** *TAS diagram (Middlemost, 1994).*

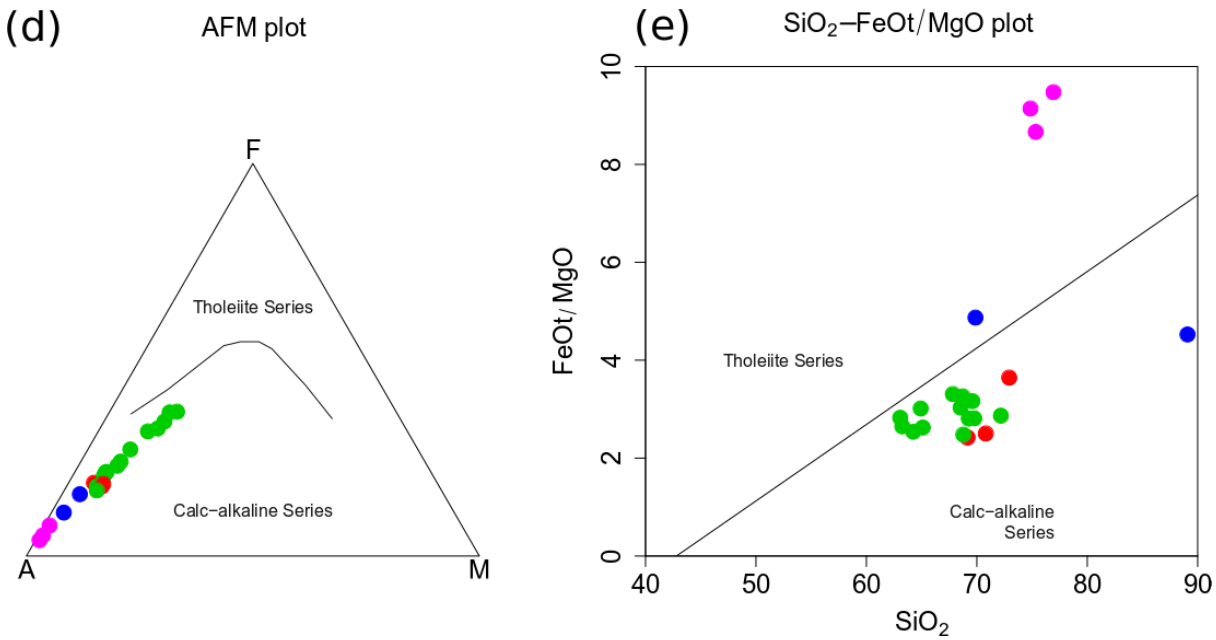

Fig. 19: *Selected classification diagrams for all main lithologies examined in the area of interest.* ***(d)*** *AFM plot (Irvine and Baragar, 1971);* ***(e)*** *SiO2 – FeO_{tot}/MgO plot (Miyashiro, 1974). Diagrams plotted using Geochemical Data Toolkit software (Janoušek et al., 2006).*

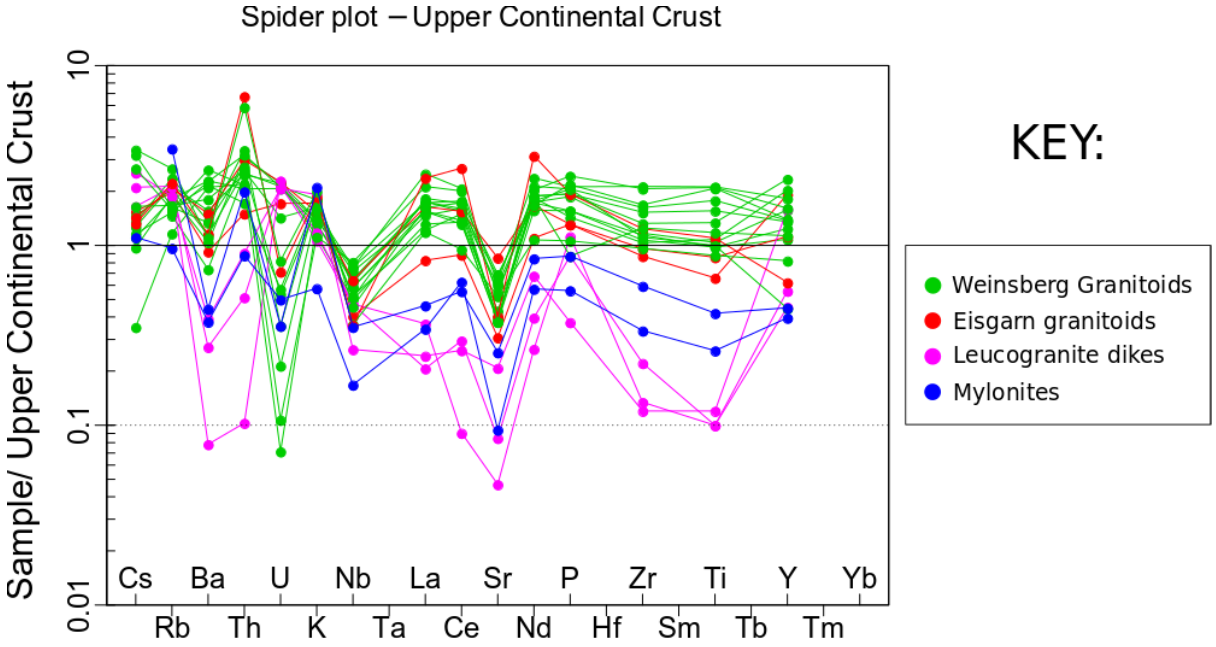

Fig. 20: *Spider-plot diagram (Taylor and McLennan, 1995) of selected trace elements normalized on the Upper Continental Crust for all main litholigies in the area of interest.*

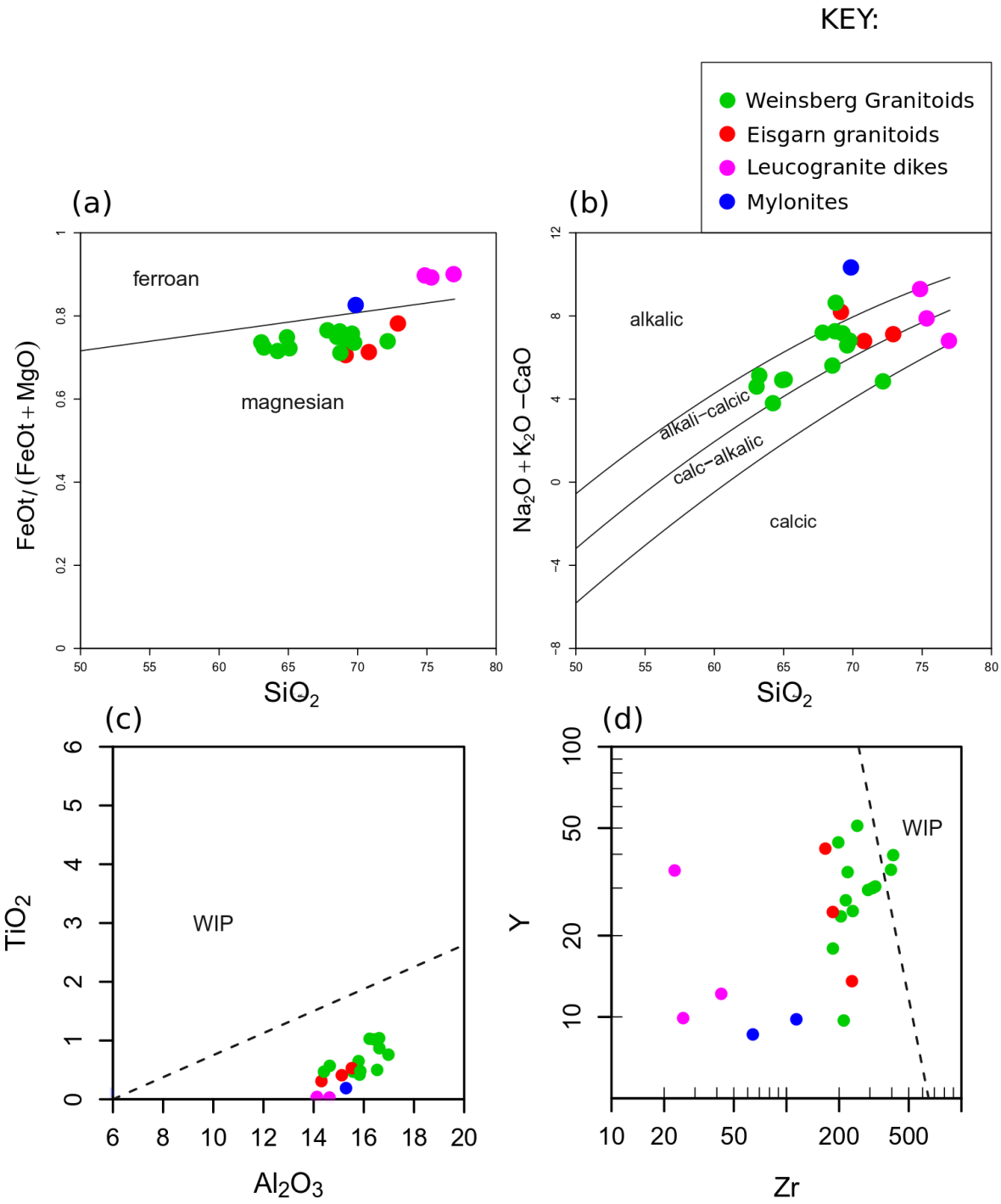

Fig. 21: *Selected geotectonic diagrams for all main lithologies examined in the area of interest.* ***(a)*** *and* ***(b)*** *ferroan-magnesian and calc-alkaline diagrams (Frost et al., 2001);* ***(c)*** *and* ***(d)*** *are different diagrams of Geotectonic classification of potassic rocks (Muller et al., 1992). Diagrams plotted using the Geochemical Data Toolkit software (Janoušek et al., 2006).*

6.5 Sillimanit-Biotite Paragneiss

This group is represented here only with single peraluminous sample (WPT 10), with extremely high A/CNK (2.5) and A/NK (2.8) ratios. Other characteristics are low SiO_2 (62.9 wt%), very high Al_2O_3 (20.0 wt%) and MgO (2.9 wt%), low Na_2O (1.6 wt%) and CaO (0.4 wt%), K_2O (4.1 wt%) and high Fe_2O_3 (6.7 wt%). Data from trace elements: Ba 739 ppm, Cr 238 ppm, low La/Th ratio (2.9), Nd 37 ppm, Rb 240 ppm, Sr 140 ppm and Zr 201 ppm.

7. Fabric pattern and Tectonics

7.1 Introduction and basic description

The field structural data have been collected from all localities described in the Attachment 2, where all the documented measurements and field data can be found. The taken structural data can be divided into ductile deformation structures which include magmatic and mylonite foliations and intrusive contacts of dikes, and the structures of brittle deformation as faults and joints.

7.2 Structures of Ductile deformation

The majority of the documented outcrops were not affected later after their origin by metamorphic nor oriented stress event, so their original fabric patter defined by preferred spatial orientation of mineral agregates (Fig. 24a) should be preserved. Stereographic projection of all measurements are displayed in the Fig. 22a.

In the northeastern Weinsberg Pluton two different pluton-wide magmatic foliations defined based on orientation, relationships and intensity (defined using criteria of Paterson et al. 1998; Paterson et al. 1989; Vernon 2000) have been identified. Each of the foliations are defined by planar and linear shape preferred orientation of K-feldspar and plagioclase phenocrysts (2 to 5 cm in length) and alignment of biotite aggregates. A relatively earlier margin-parallel magmatic foliation defined by the shape-preferred orientation of K-feldspar phenocrysts is dominant at most outcrops. These magmatic foliations have steep dip striking ~NNW–SSE to ~WNW–ESE and are associated with a weak magmatic lineations plunging from ~ENE to NE. This early magmatic fabric was heterogeneously overprinted by a transitional magmatic to sub-solidus fabrics, characterized by sub-horizontal foliation and ~WSW–ESE trending lineation. Intrusive contacts of the Weinsberg Composite Pluton are

steep, NNE–SSW trending and, are mostly parallel to the regional metamorphic fabrics in the host migmatites.

Accumulations of phenocrysts of potassium feldspars (Fig. 24b) and partially assimilated xenoliths of surrounding rocks (mostly migmatites and paragneisses) with size up to 30 cm (Fig. 24c) can be locally found in the Weinsberg granitoids. The xenoliths have thinly tabular shape with high aspect ratio in most cases. Remnant of the occurence of the mingling phenomenon can be found in the locality WPT05 (Fig. 24d). In the close surrounding of the Vitiz-Přibyslav Zone several mylonitized rocks was documented with very steep dip and W–E direction of the subsolidus foliation (Fig. 22b). Structural map of the area of interest with representing measurements from each locality can be found in the Fig. 23.

In addition, the Weinsberg granitoids contains abundant mafic microgranular enclaves mostly of dioritic composition. The enclaves are typically ellipsoidal with variable aspect ratios and their size varies from centimetres to a few decimetres at most.

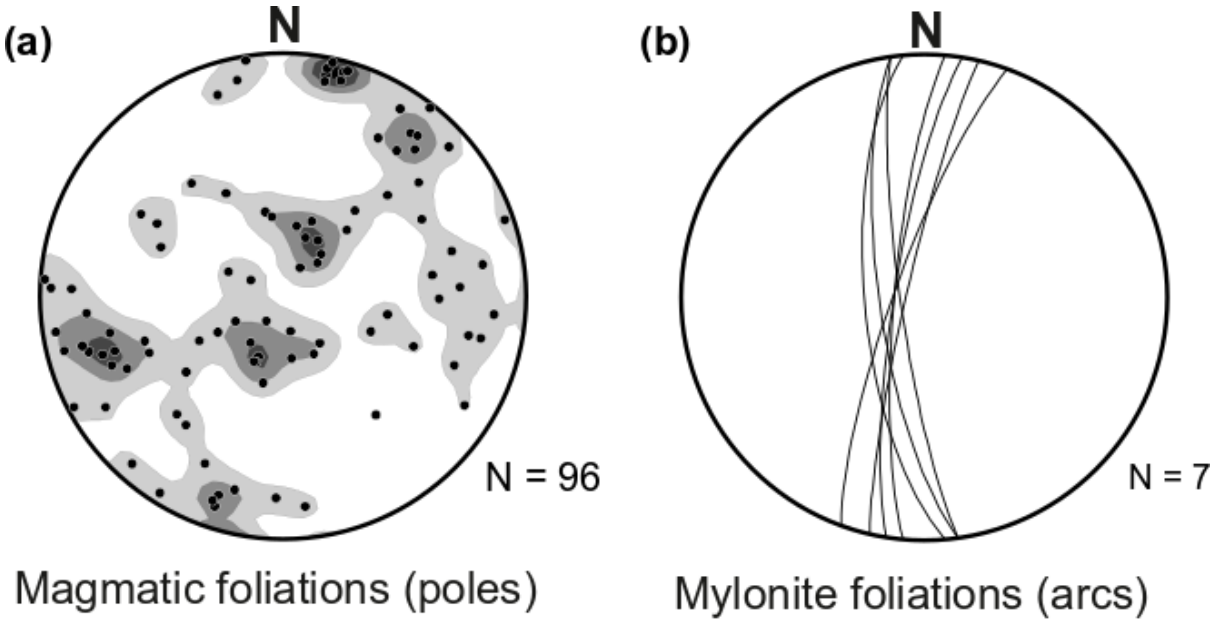

Fig. 22: *Stereographic projections of ductile structural data from Weinsberg type granitoids and Mylonites in the area of interest.* ***(a)*** *Magmatic foliations of Weinsberg pluton granitoids;* ***(b)*** *mylonite subsolidus foliations from Vitiz-Přibyslav Zone. N – number of measurements.*

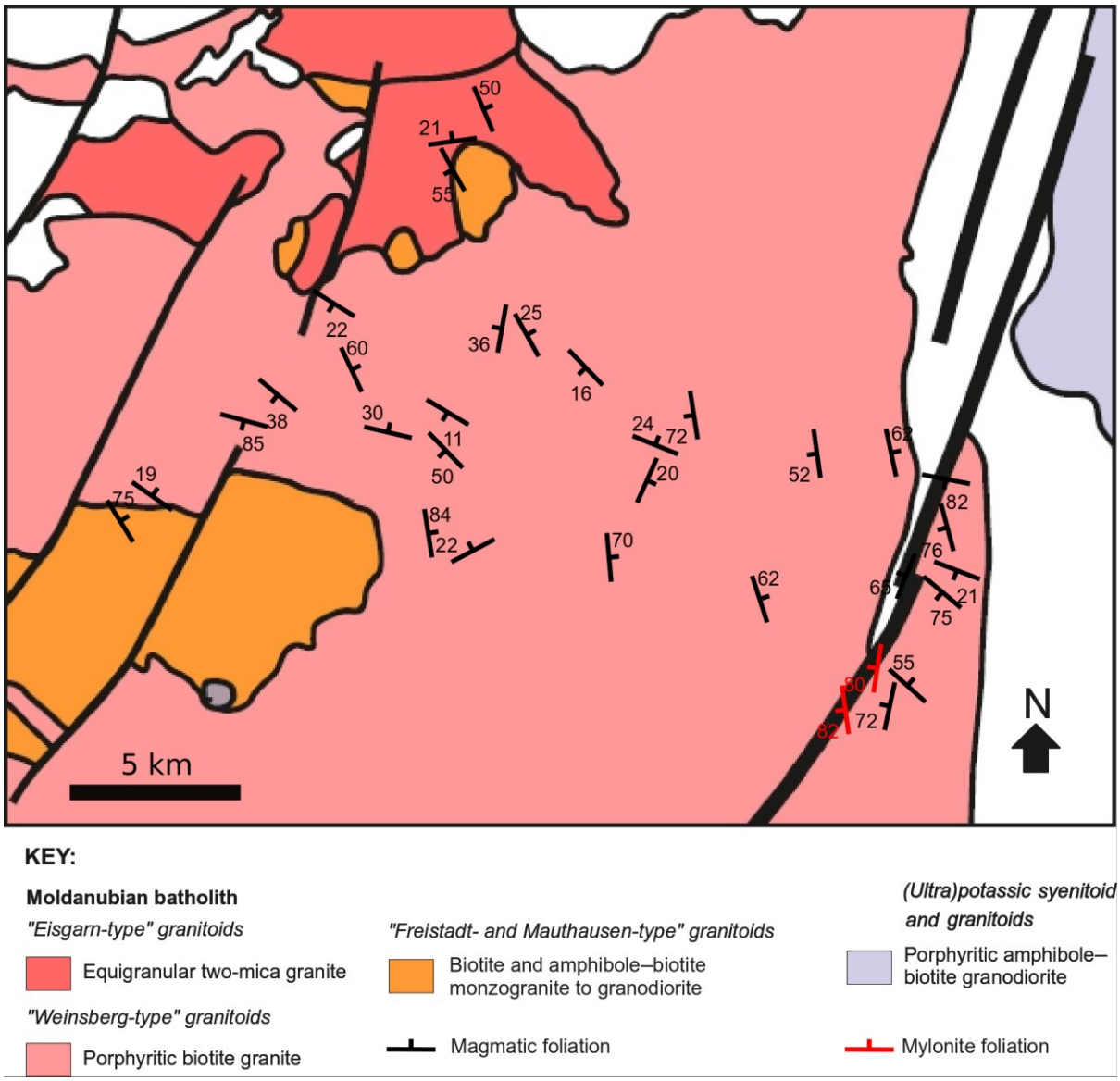

Fig. 23: *Geological map of the area of interest in the Weinsberg Composite Pluton with structural marks of magmatic and mylonite foliations representing structural measurements in each locality. Structural marks are oriented in the dominating direction of foliation and attached number characterizes the dip.*

Minor medium-grained two-mica Eisgarn type granitoids (Fig. 24e) and fine-grained leucogranites (Fig. 24f) appear on several outcrops (WPT05, WPT15, WPT16, WPT17 and WPT19). These two-mica Eisgarn granitoids form the dikes up to 70 cm in thickness with sharp contacts. This intrusive contacts have mostly WNW–ESE direction, but the angle of the dip varies.

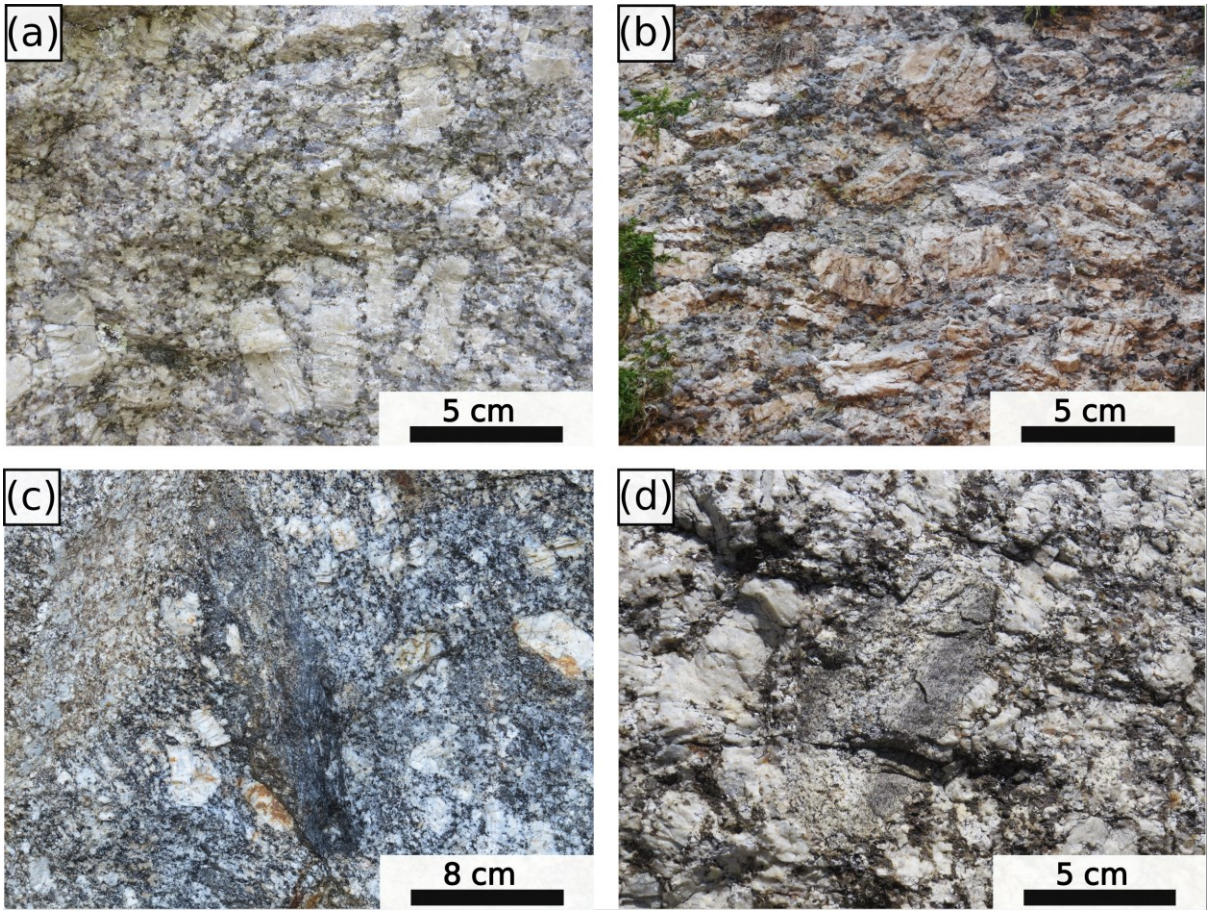

Fig. 24: *Structural phenomenons of ductile processes and fabric patterns in the localities in the area of interest.* ***(a)*** *Preferred spatial orientation of mineral agregates in the Weinsberg type granitoids (WPT14);* ***(b)*** *accumulation of potassium feldspars in the Weinsberg granitoids (WPT13);* ***(c)*** *partially assimilated xenolith (WPT05);* ***(d)*** *remnant after mingling event of Weinsberg lithology and fine to medium-grained melt (WPT05).*

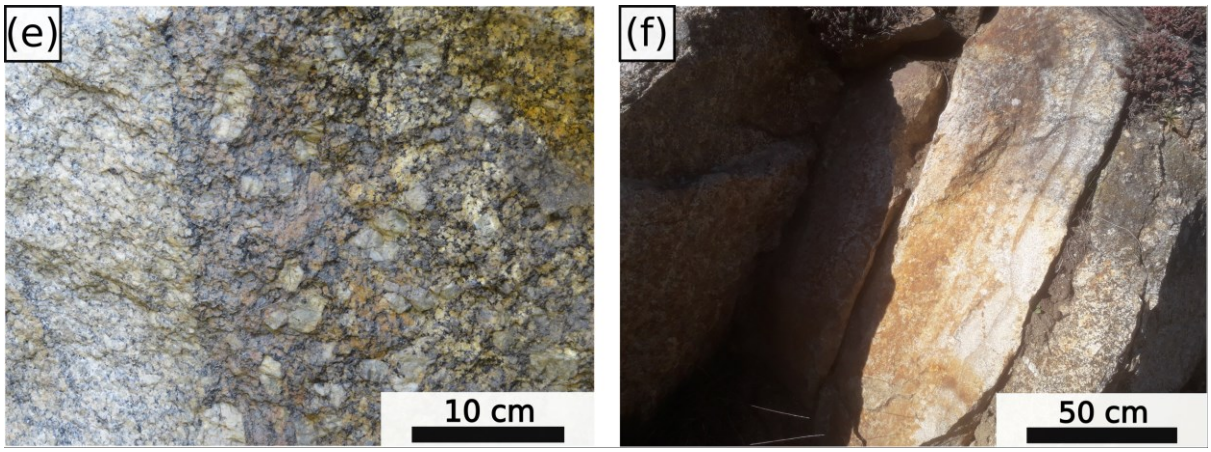

Fig. 24: *Structural phenomenons of ductile processes and fabric patterns in the localities in the area of interest.* ***(e)*** *Intrusive contact of older Weinsberg lithology (right hand side) and younger intruding two-mica medium-grained Eisgarn type granitoid (WPT15);* ***(f)*** *intrusive Leucogranite dike surrounded by older Weinsberg granitoids (WPT17).*

7.3 Structures of Brittle deformation

Brittle deformation is in the area of interest represented by faults and extensional joints (Fig. 25). Three types of faults were found in the studied area. Dextral faults dip steeply having NW–SE trend bearing slickensides dipping gently to NW. Subordinate dextral faults trend to N(NNE)–S(SSW) with slickensides plunging gently to N(NNE). Sinistral faults have predominantly N–S trend with slickensides plunging gently to the south (Fig. 25b). Minor normal faults dip steeply to SW or WNW including subvertical slickensides (Fig. 25c). Extensional joints have mostly subvertical orientation (Fig. 25e). Two significant trends of extensional joints - W(WNW) to E(ESE) and NNE to SSW were identified (Fig. 25f).

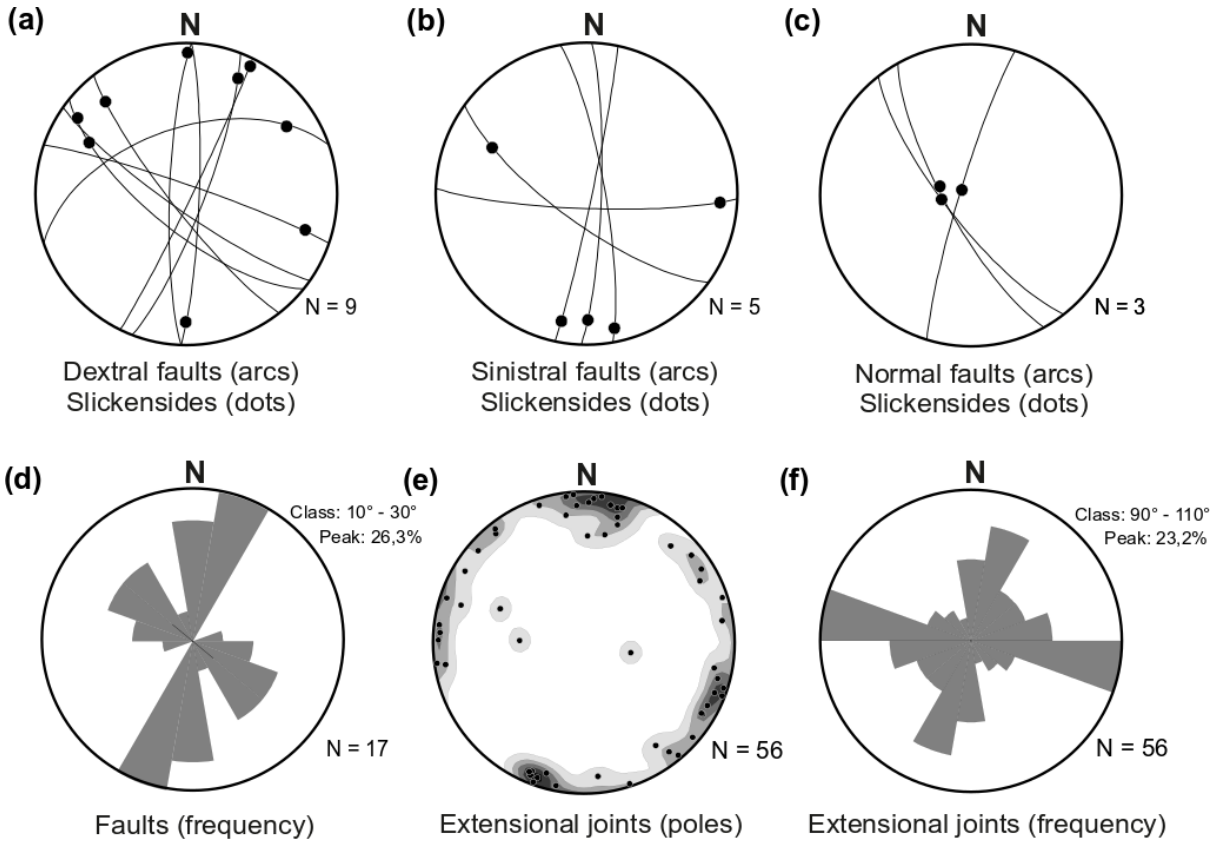

Fig. 25: *Stereographic projections and frequency histograms of brittle structural deformations in the area of interest.* ***(a)*** *Directions and angles of faults with dextral kinematics and their slickensides;* ***(b)*** *directions and angles of sinistral faults and their slickensides;* ***(c)*** *directions and angles of normal faults and their slickensides;* ***(d)*** *frequency histogram of occurence of fault directions of individual planes presented in Fig. 25a-c;* ***(e)*** *poles of planes of extensional joints;* ***(f)*** *frequency histogram of planes of extensional joints presented in Fig. 25e. N – number of measurements.*

8. Anisotropy of Magnetic Susceptibility

In total, the drilled cores were cut to 124 standard cylindrical specimens from Weinsberg granitoids (localities WPT05, WPT13, WPT14, WPT15A, WPT15B, WPT16, WPT17, WPT23 and WPT24) and mylonites of the Vitiz-Přibyslav Mylonite Zone (WPT25), each approximately 10 cm^3 in volume, which corresponds to an average of ~12 specimens per locality. The specimens were measured using a MFK1-A Kappabridge apparatus equipped with a 3D rotator in the Laboratory of Rock Magnetism, Czech Geological Survey in Prague. A statistical analysis of the data was treated using the ANISOFT 3.2 software (www.agico.com; Jelínek, 1978; Hrouda et al., 1990; Chadima and Jelínek, 2008). The basic parameters of AMS method are shown in Table 2.

Table 2: *Short description of most important terms and functions for AMS.*

Term	Shortcut	Function	Description
Principal susceptibilities	K1, K2, K3	K1 > K2 > K3	Characterize the Anisotropy ellipsoid; K1–magnetic lineation, K3–mag. foliation
Mean susceptibility	Km	(K1+K2+K3) / 3	Characterize the mean susceptibilty per each sample
Degree of anisotropy	P	K1 / K3	Characterize the difference between max. and min. principal susceptibilities
Shape parameter	T	(2*n2-n1-n3) - (n1-n3) n = ln(K)	Characterize the shape of the ellipsoid; 1>T>0 = planar fabric; -1<T<0 = linear fabric

Specimens from the Weinsberg granitoids and mylonites of the Vitiz-Přibyslav Mylonite Zone (VPMZ) are characterized by relatively low bulk susceptibility (k_b) ranging between 2.15×10^{-5} and 3.21×10^{-4} (SI) and 5.73×10^{-5} and 2.11×10^{-4} (SI), respectively.

In this diploma thesis I consider the values of degree of anisotropy as relatively low and high for $P < 1.060$ and $P > 1.060$, respectively, and for shape parameter $-1 \leq T < -0.010$ as prolate, $-0.010 \leq T < 0.010$ as neutral and $1 \geq T > 0.010$ as oblate shape of AMS ellipsoid.

In the Weinsberg granitoids the degree of anisotropy (P) of all individual specimens ranges from 1.011 to 1.226, however most stations lie in the interval 1.015 – 1.065 with

average and median value of 1.036 (Fig. 26a). The P – parameter in mylonites from the VPMZ ranges between 1.091 and 1.323 with average value 1.069. The shape parameter reveal interval –0.79 – 0.98, is evenly distributed with respect to degree of anisotropy, and all data average is slightly oblate ($T = 0.14$) having 27 % prolate, 32 % neutral and 41 % oblate shape of AMS ellipsoids (Fig. 26b). The mylonites of the VPMZ have mostly neutral shape parameter with average value $T = 0.083$.

Most of the magnetic foliations in the Weinsberg granitoids are oriented ~WNW–ESE dipping steeply to moderately, both towards ~NNE or ~SSW (Fig. 27). Magnetic lineations reveal several orientational maxima with prevailing ~NW–SE gently to moderately plunging fabrics. Magnetic foliation in mylonites of the VPMZ dips moderately to the W, magnetic lineation plunges gently to moderately to the SW. For orientation of all magnetic fabrics see Fig. 27 and Fig. 28 and maps (Fig. 29 and Fig. 30). Complete table of measurements for each specimen can be found in the Appendix as Attachment 4.

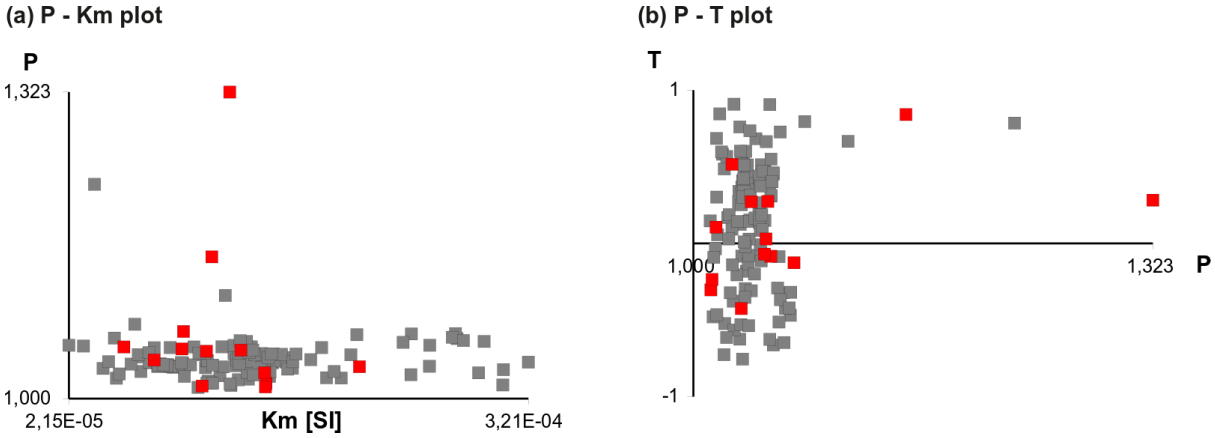

Fig. 26: *Selected AMS plots representing several magnetic properties of studied samples.* ***(a)*** *Degree of anisotropy – mean magnetic susceptibility plot;* ***(b)*** *degree of anisotropy – shape parameter plot. Grey squares represents samples from Weinsberg pluton, red squares mylonites from Vitiz-Přibyslav Zone.*

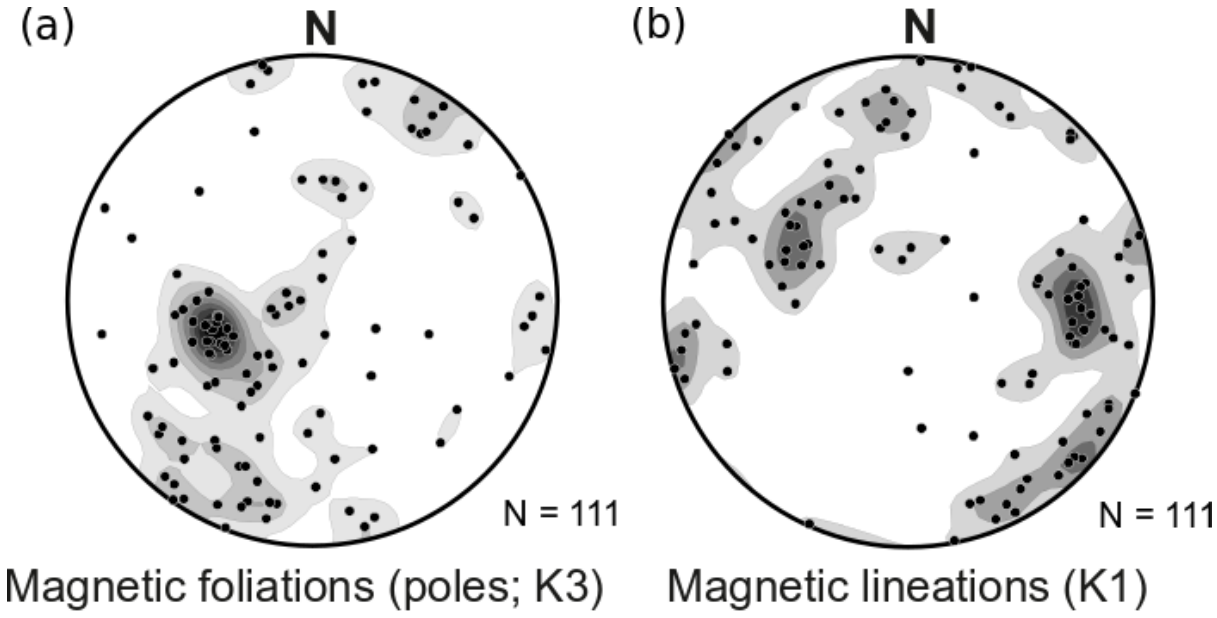

Fig. 27: *Stereographic projections of magnetic fabrics in the Weinsberg granitoids in the area of interest measured by AMS. (a) Poles of magnetic foliations (K3); magnetic lineations (K1). N – Number of measurements.*

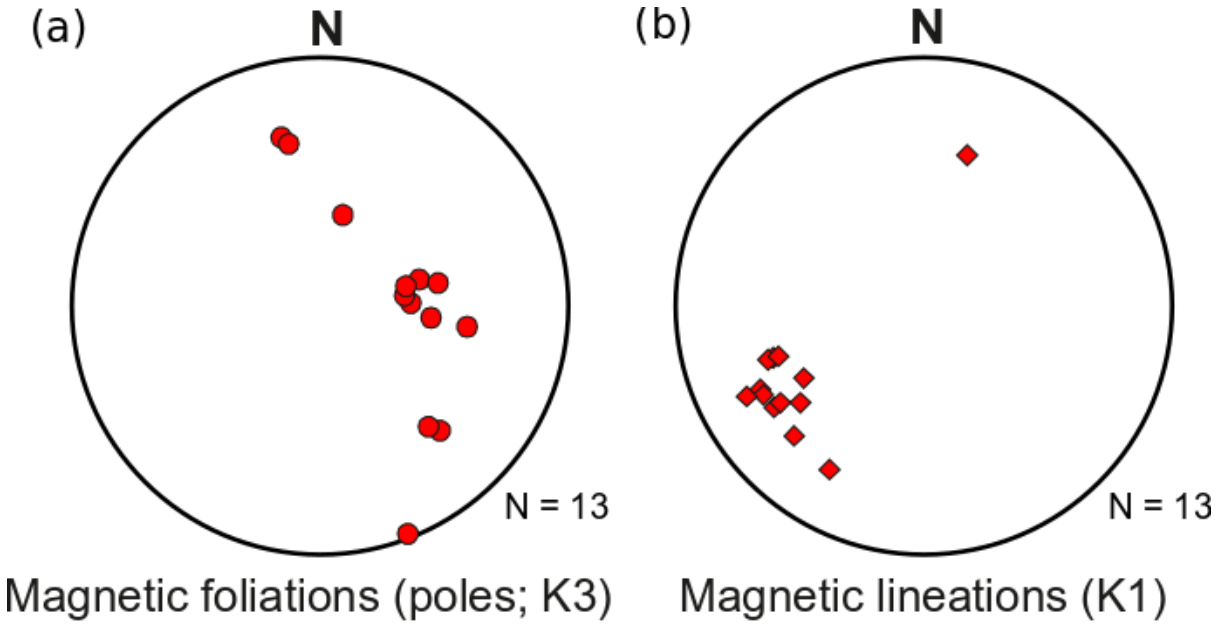

Fig. 28: *Stereographic projections of magnetic fabrics in the Vitiz-Přibyslav Mylonite Zone in the area of interest measured by AMS. (a) Poles of magnetic foliations (K3); magnetic lineations (K1). N – Number of measurements.*

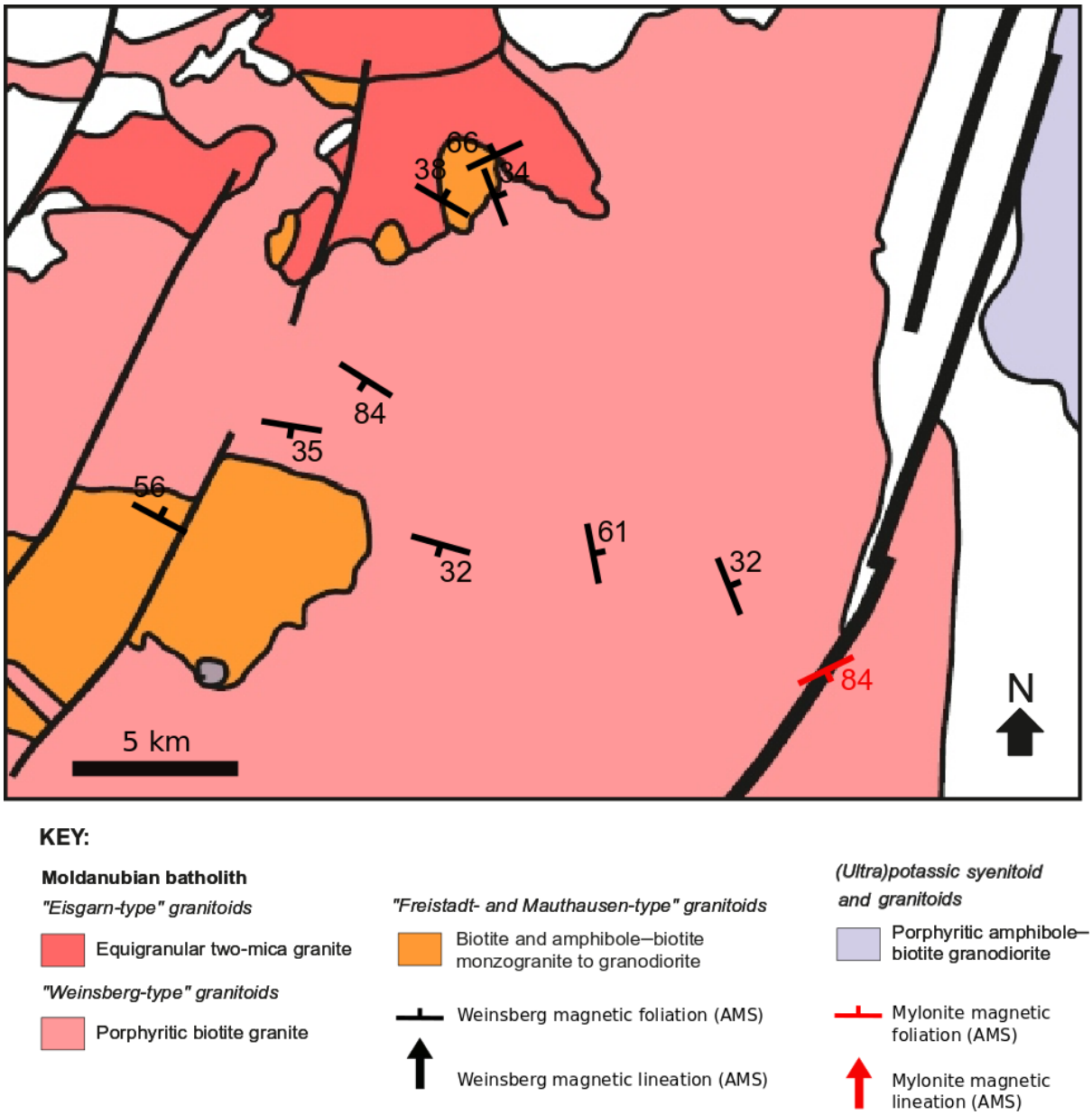

Fig. 29: *Geological map of the area of interest with structural marks of magnetic foliations of Weinsberg pluton and mylonites from the Vitiz-Přibyslav Zone. Each structural mark represents each measured locality with orientation and dip calculated by the Jelinek statistics (Jelínek, 1978).*

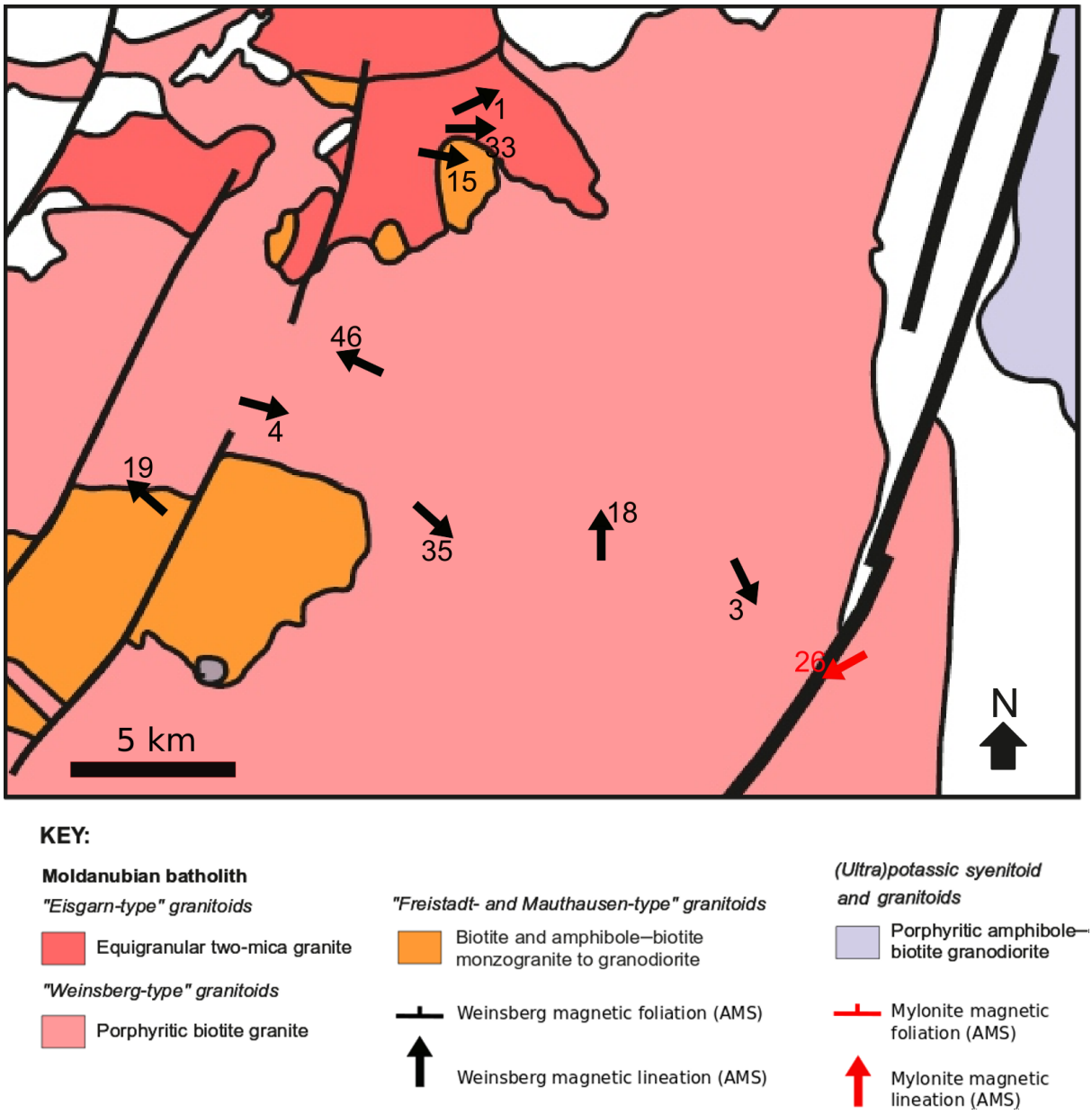

Fig. 30: *Geological map of the area of interest with structural marks of magnetic lineations of Weinsberg pluton and mylonites from the Vitiz-Přibyslav Zone. Each structural mark represents each measured locality with orientation and dip calculated by the Jelínek statistics (Jelínek, 1978).*

9. Discussion and Conclusions

On the basis of the geochemical composition of the studied Weinsberg granitoids, these rocks can be classified as mixed I/S-type quartz monzonites, granodiorites and granites depending on SiO_2 and alkali components (Fig. 19c). In agreement with Gerdes (2001) is possible to propose that the Weinsberg type granitoids were generated by partial melting of metavolcanosedimentary rocks as for example greywackes and amphibolites. Low Al_2O_3/TiO_2, Rb/Sr, Rb/Ba and high CaO/Na_2O ratios can also apoint to simple mixing between peraluminous crustal melts with mafic magmas or to partial melting of older metaigneous sources (Finger and Clemens, 1995; Büttner and Kruhl, 1997; Gerdes et al., 2000). These granitoids have also relatively high content of K_2O (Fig. 18b, Fig. 19b). On the basis of the A/CNK index (Fig. 18a; Fig. 19a) and trace elements distribution (e.g. Nb, Sr, Rb) it is possible to conclude that the prevailing studied Weinsberg granitoids can be classified as Weinsberg II type (WbG II). However, few samples reveal the geochemical composition typical for WbG II and WbG Ia (Gerdes 2001). For further consideration, geochemical composition of Weinsberg granitoids was corellated with the results of the zircon morphology analysis. As presented on the zircon morphology classification diagram (Fig. 14) as dominating zircon habitus for studied Weinsberg type granitoids the habitus S (subtype S7) was identified. In agreement with Stöbich (1992) we can conclude that the studied zircon populations are similar to those of the WbG II granitoids. For the two-mica Eisgarn-type granitoids forming minor intrusions in the prevailing Weinsberg-type granitoids is proposed a different petrogenetic model. Two-mica granites (Eisgarn suite) display distinctly higher Al_2O_3 / ($FeOt+MgO+TiO_2$), Rb/Ba, Rb/Sr and relatively lower CaO/Na_2O ratios as well as zircon morphology analyses are typical for melts generated by extensive anatexis of metapelites or metapsamites with varying amount of clay minerals and feldspars (e. g. Sylvester 1998).

Presence of xenoliths surrounding metamorphic rocks in the Weinsberg granitoids can be explained by the magmatic stopping that may have operated during the magma emplacement. Mingling between Weinsberg and Eisgarn-type granitoids have been identified on the locality WPT05 (sample WPT05B) could imply that in the area of interest the

Weinsberg and Eisgarn granitoids could have synchronnous occurence and their ages of emplacement is similar.

Their field relations show a mutliple magmatic to solid-state fabrics defined by the shape-preferred orientation of K-feldspar phenocrysts. Relics pluton margin-parallel magmatic foliation reveal strong re-orientation (overprint) to steeply dipping ~E-W to ~WNW–ESE trending magmatic foliation bearing ~NW ‑ SE gently plunging lineation. In addition, heterogeneous later overprint to gently dipping transitional magmatic to solid-state fabrics was found on several localities and next sharp superimposition of low-temperature mylonites belonging to NNE–SSW trending Vitiz-Přibyslav Mylonite Zone (VPMZ). Prevailing steeply dipping foliation reveal a neutral to oblate shape of AMS ellipsoid with relatively lower values of degree of anisotropy ranging from 1.011 to 1.226. However most of samples lie in the interval 1.015 to 1.065 with average and median value of 1.036. Magnetic fabrics in the Weinsberg granitoids (~WNW–ESE trending magnetic foliations and ~NW–SE gently to moderately plunging magnetic lineations) reveal significant similarity in orientation with mezoscopic fabrics identified based on the field structural mapping.

These contrasting fabrics preserved in studied Weinsberg granitoids (northeastern part of the Weinsberg Pluton) can be interpreted in terms of an earlier intrusive strain during magma emplacement followed by regional tectonic deformation (e.g. Finger, et al., 2010). The origin of prevailing ~E–W to ~WNW–ESE trending magmatic foliation deformation was perhaps related to the regional strain field reflecting N–S oriented compression (N–S compression) continuously changing to the dextral strike-slip shearing along the regional shear zones (Pfahl and Danube shear zones) which were mapped in southwestern flank of the Moldanubian Zone, westward of studied area (Brandmayr et al., 1995). The latter transitional magmatic to solid-state fabrics may have assisted unroofing and minor vertical shortening of the pluton-host rock complexes during latter stages of magma crystallization (Paterson et al. 1998).

Based on the integration of the structural, petrological and geochemical data set the interpretation of geodynamic evolution and emplacement of eastern part of the Weinsberg Pluton (southern Moldanubian Batholith) could be proposed. This interpretation invokes: (a) indentation and underthrusting of a continental microplate (Brunia) in the east at around ~340–330 Ma, driving mantle delamination and subsequent heating and anatexis in the

metapelitic lower crust as the heterogeneous source for Weinsberg- and Eisgarn-types of granitoids; (b) subsequent growth of a large metamorphic dome along the edge of the Brunia indentor followed by polyphase emplacement of entire eastern part of Moldanubian Batholith around ~330–325 Ma including the Weinsberg Composite Pluton in the south; (c) increasing role of N–S shortening and associated NW–SE dextral shearing along localized shear zones which caused the prevailing WNW–ESE trending magmatic fabrics in Weinsberg Pluton; (d) minor subvertical shortening as the result of later stages of domal exhumation and subsequent low-temperature localized deformation and mylonitization along the eastern edge of NNE–SSW trending domal structure (polyphase Vitiz-Přibyslav Mylonite Zone).

References

Benisek, A., & Finger, F. (1993). Factors controlling the development of prism faces in granite zircons: a microprobe study. *Contributions to Mineralogy and Petrology*, *114*(4), 441–451. doi: 10.1007/BF00321749

Brandmayr, M., Dallmeyer, R. D., Handler, R., & Wallbrecher, E. (1995). Conjugate shear zones in the Southern Bohemian Massif (Austria): implications for Variscan and Alpine tectonothermal activity. *Tectonophysics*, *248*(1-2), 97-116.

Breiter, K.., & Scharbert, S. (1998). Latest intrusions of the Eisgarn Pluton (South Bohemia–Northern Waldviertel). *Jb Geol BA*, *141*, 25-37.

Breiter, K., & Scharbert, S. (2006). Two-mica and biotite granites in the Weitra-Nové Hrady area, Austria - Czech Republic. *Journal of the Czech Geological Society*, *51*(3–4), 217–230.

Büttner, S., & Kruhl, J. H. (1997). The evolution of a late-Variscan high-T/low-P region: The southeastern margin of the Bohemian massif. *Geologische Rundschau*, *86*(1), 21–38. doi: 10.1007/s005310050119

Chadima, M., & Jelínek, V. (2008). Anisoft 4.2.–Anisotropy data browser. *Contributions to Geophysics and Geodesy*, *38*(Special Issue), 38-41.

Chlupác, I., Havlicek, V., & Kriz, J. (1998). *Palaeozoic of the Barrandian (Cambrian to Devonian)*. Prague: Czech geol. survey.

Dallmeyer, R. D., & Urban, M. (1998). Variscan vs Cadomian tectonothermal activity in northwestern sectors of the Teplá-Barrandian zone, Czech Republic: Constraints from 40Ar/39Ar ages. *International Journal of Earth Sciences*, *87*(1), 94–106.

Davies, J. H., & Blanckenburg, F. von. (1995). Slab breakoff: A model of lithosphere detachment and its test in the magmatism and deformation of collisional orogens. *Earth and Planetary Science Letters*, *129*, 85–102.

Dewey, J. F. (1988). Extensional collapse of orogens. *Tectonics*, *7*(6), 1123–1139. doi: 10.1029/TC007i006p01123

Dörr, W., Fiala, J., Vejnar, Z., & Zulauf, G. (1998). U-Pb zircon ages and structural development of metagranitoids of the Teplá crystalline complex: Evidence for pervasive Cambrian plutonism within the Bohemian massif (Czech Republic). *International Journal of Earth Sciences*, *87*(1), 135–149.

England, P. (1993). Convective removal of thermal boundary layer of thickened continental lithosphere: A brief summary of causes and consequences with special reference to the Cenozoic tectonics of the Tibetan Plateau and surrounding regions. *Tectonophysics*, *223*(1–2), 67–73. doi: 10.1016/0040-1951(93)90158-G

England, P. C., & Thompson, A. B. (1984). PTt paths of regional metamorphism. I. heat transfer during the evolution of regions of tectonically thickened continental crust. *Journal of Petrology*, *25*, 894–928.

Finger, F., & Clemens, J. D. (1995). Migmatization and "secondary" granitic magmas: effects of emplacement and crystallization of "primary" granitoids in Southern Bohemia, Austria. *Contributions to Mineralogy and Petrology*, *120*(3–4), 311–326. doi: 10.1007/BF00306510

Finger, F., Roberts, M. P., Haunschmid, B., Schermaier, A., & Steyrer, H. P. (1997). Variscan granitoids of central Europe: their typology, potential sources and tectonothermal relations. *Mineralogy and Petrology*, *61*(1–4), 67–96. doi: 10.1007/BF01172478.

Finger, F., Gerdes, A., Janoušek, V., René, M., & Riegler, G. (2007). Resolving the Variscan evolution of the Moldanubian sector of the Bohemian Massif: The significance of the Bavarian and the Moravo-Moldanubian tectonometamorphic phases. *Journal of Geosciences*, *52*(1–2), 9–28. doi: 10.3190/jgeosci.005

Finger, F., Gerdes, A., René, M., & Riegler, G. (2009). The Saxo-Danubian Granite Belt: magmatic response to post-collisional delamination of mantle lithosphere below the southwestern sector of the Bohemian Massif (Variscan orogen). *Geologica Carpathica*, *60*(3), 205–212. doi: 10.2478/v10096-009-0014-3

Franke, W. (1989). Variscan plate tectonics in Central Europe-current ideas and open questions. *Tectonophysics*, *169*(4), 221–228. doi: 10.1016/0040-1951(89)90088-7.

Franke, W. (2000). The mid-European segment of the Variscides: Tectonostratigraphic units, terrane boundaries and plate tectonic evolution. *Geological Society Special Publication*, *179*, 35–56. doi: 10.1144/GSL.SP.2000.179.01.05

Franke, W. (2006). The Variscan orogen in Central Europe: Construction and collapse. *Geological Society Memoir*, *32*, 333–343. doi: 10.1144/GSL.MEM.2006.032.01.20

Franke, W., Dallmeyer, R. D., & Weber, K. (1995). Geodynamic evolution. In *Pre-Permian geology of central and eastern Europe* (pp. 579-593). Springer, Berlin, Heidelberg.

Frasl, G., & Finger, F. (1991). Geologisch-petrographische Exkursion in den österreichischen Teil des Südböhmischen Batholiths. *European Journal of Mineralogy*, *3*(2), 23-40.

Frost, B. R., Barnes, C. G., Collins, W. J., Arculus, R. J., Ellis, D. J., & Frost, C. D. (2001). A geochemical classification for granitic rocks. *Journal of petrology*, *42*(11), 2033-2048.

Gerdes, A. (2001). Magma homogenization during anatexis, ascent and/or emplacement? Constraints from the Variscan Weinsberg Granites. *Terra Nova*, *13*(4), 305–312. doi: 10.1046/j.1365-3121.2001.00365.x

Gerdes, A., Worner, G., & Henk, A. (2000). Post-collisional granite generation and HT-LP metamorphism by radiogenic heating: the Variscan South Bohemian Batholith. *Journal of the Geological Society*, *157*(3), 577–587. doi: 10.1144/jgs.157.3.577

Gerdes, A., Friedl, G., Parrish, R. R., & Finger, F. (2003). High-resolution geochronology of Variscan granite emplacement the South Bohemian Batholith. *Journal of the Czech Geological Society*, *48*(1–2), 53–54.

Gnojek, I., & Přichystal, A. (1997). Ground geophysical and geological mapping in the central part of the Moldanubian pluton. *Jahrbuch der Geologischen Bundesanstalt, Wien*, *140*, 193-250.

Holub, F. V. (1977). Petrology of inclusions as a key to petrogenesis of the durbachitic rocks from CzechoslovakiaDie Petrologie der Einschlsse in durbachitischen Gesteinen aus der Tschechoslowakei als Schlssel zu ihrer Petrogenese. *TMPM Tschermaks Mineralogische Und Petrographische Mitteilungen*, *24*(3), 133–150. doi: 10.1007/bf01158191

Holub, F.V., Rossi, P. and Cocherie, A.: 1996, New results of the dating of Central Bohernian complex and their implication, Tektonický vývoj orogennich pásem - termální, mechanické a sedimentární záznamy, 15-16. (in Czech)

Humer, B. (2003). *Der Weitraer Pluton im nordwestlichen Waldviertel (Niederösterreich)*. Master Thesis, University of Salzburg, 157 p

Hrouda, F., Jelínek, V., & Hruskova, L. (1990). A package of programs for statistical evaluation of magnetic data using IBM-PC computers. *Eos Trans. AGU*, *71*(43), 1289.

Irvine, T. N. J., & Baragar, W. R. A. (1971). A guide to the chemical classification of the common volcanic rocks. *Canadian journal of earth sciences*, *8*(5), 523-548.

Janoušek, V., Farrow, C. M., & Erban, V. (2006). Interpretation of whole-rock geochemical data in igneous geochemistry: introducing Geochemical Data Toolkit (GCDkit). *Journal of Petrology*, *47*(6), 1255-1259.

Jelínek, V., & Kropáček, V. (1978). Statistical processing of anisotropy of magnetic susceptibility measured on groups of specimens. *Studia Geophysica et Geodaetica*, *22*(1), 50–62. doi: 10.1007/BF01613632

Klomínský, J., Jarchovský, T., Rajpoot, G.S. (2010). Atlas of Plutonic Rocks and Orthogneisses in the Bohemian Massif: Technical Report TR-01-2010. Czech Geological Survey, Prague.

Košler, J., & Farrow, C. M. (1994). Mid-late Devonian arc-type magmatism in the Bohemian Massif: Sr and Nd isotope and trace element evidence from the Staré Sedlo and Mirotice gneiss complexes, Czech Republic. *Journal of the Czech Geological Society*, *39*(1), 56-58.

Larsen, L. H., & Poldervaart, A. (1957). Measurement and distribution of zircons in some granitic rocks of magmatic origin. *Mineralogical Magazine and Journal of the Mineralogical Society*, *31*(238), 544-564

Lindner, M., Finger, F., Lindner, M., & Finger, F. (2018). Geochemical characteristics of the Late Proterozoic Spitz granodiorite gneiss in the Drosendorf Unit (Southern Bohemian Massif, Austria) and implications for regional tectonic interpretations. *Journal of Geosciences*, *63*(4), 345–362. doi: 10.3190/jgeosci.271

Matejka, D., & Janousek, V. (1998). Whole-rock geochemistry and petrogenesis of granites from the northern part of the Moldanubian Batholith (Czech Republic). *ACTA-UNIVERSITATIS CAROLINAE GEOLOGICA*, 75-79.

Middlemost, E. A. K. (1994). Naming materials in the magma/igneous rock system. *Earth Science Reviews*, *37*(3–4), 215–224. doi: 10.1016/0012-8252(94)90029-9

Miyashiro, A. (1974). Volcanic rock series in island arcs and active continental margins. *American journal of science*, *274*(4), 321-355.

Müller, D., Rock, N. M. S., & Groves, D. I. (1992). Geochemical discrimination between shoshonitic and potassic volcanic rocks in different tectonic settings: a pilot study. *Mineralogy and Petrology*, *46*(4), 259-289.

O'Brien, P. J., & Vrána, S. (1995). Eclogites with a short-lived granulite facies overprint in the Moldanubian Zone, Czech Republic: petrology, geochemistry and diffusion modelling of garnet zoning. *Geologische Rundschau*, *84*(3), 473–488. doi: 10.1007/BF00284515

Paterson, S. R., Vernon, R. H., & Tobisch, O. T. (1989). A review of criteria for the identification of magmatic and tectonic foliations in granitoids. *Journal of structural geology*, *11*(3), 349-363.

Paterson, S. R., Fowler Jr, T. K., Schmidt, K. L., Yoshinobu, A. S., Yuan, E. S., & Miller, R. B. (1998). Interpreting magmatic fabric patterns in plutons. *Lithos*, *44*(1-2), 53-82.

Peccerillo, A., & Taylor, S. R. (1976). Geochemistry of eocene calc-alkaline volcanic rocks from the Kastamonu area, Northern Turkey. *Contributions to Mineralogy and Petrology*, *58*(1), 63–81. doi: 10.1007/BF00384745

Petrik, I., & Broska, I. (1994). Petrology of two granite types from Tribec Mts, Western Carpathian: an example of allanite-magnetite versus monazite-ilmenite dichotomy. *Geological Journal*, *29*(May 1992), 59–78.

Petrik, I., Broska, I., & Uher, P. (1994). Evolution of the western Carpathian granite magmatism: age, source rock, geotectonic setting and relation to the Variscan structure. *Geologica Carpathica*, *45*(5), 283–291.

Poldervaart, A. (1956). Zircon in rocks; 2, Igneous rocks. *American Journal of Science*, *254*(9), 521-554.

Pupin, J. P. (1980). Zircon and granite petrology. *Contributions to Mineralogy and Petrology*, *73*(3), 207–220. doi: 10.1007/BF00381441

Pupin, J. P., & Turco, G. (1972). Une typologie originale du zircon accessoire. *Bulletin de Minéralogie*, *95*(3), 348-359.

Racek, M., Štípská, P., Pitra, P., Schulmann, K., & Lexa, O. (2006). Metamorphic record of burial and exhumation of orogenic lower and middle crust: A new tectonothermal model for the Drosendorf window (Bohemian Massif, Austria). *Mineralogy and Petrology*, *86*(3–4), 221–251. doi: 10.1007/s00710-005-0111-7

Rene, M., Matejka, D., & Nosek, T. (2003). Geochemical constraints on the origin of a distinct type of two-mica granites (Destna--Lasenice type) in the Moldanubian batholith (Czech Republic). *Acta Montana. Serie A: Geodynamics*, *23*(130), 59-77.

Schulmann, K., Štípská, P., & Powell, R. (2008). Contrasting metamorphic histories of lenses of high-pressure rocks and host migmatites with a flat orogenic fabric (Bohemian Massif, Czech Republic): A result of tectonic mixing within horizontal crustal flow? *Journal of Metamorphic Geology*, *26*(6), 623–646. doi: 10.1111/j.1525-1314.2008.00781.x

Shand, S. J. (1943). *Eruptive rocks: their genesis, composition, and classification, with a chapter on meteorites*. J. Wiley & sons, Incorporated.

Siebel, W. (1995). Anticorrelated Rb-Sr and K-Ar age discordances, Leuchtenberg granite, NE Bavaria, Germany. *Contributions to Mineralogy and Petrology*, *120*(2), 197–211. doi: 10.1007/BF00287117

Stöbich, D. M. (1992). *Trachtstudien an den akzessorischen Zirkonen des Weinsberger Granits im östlichen Mühlviertel und westlichen Waldviertel*. na.

Sylvester, P. J. (1998). Post-collisional strongly peraluminous granites. *Lithos*, *45*(1–4), 29–44. doi: 10.1016/S0024-4937(98)00024-3

Taylor, S. R., & McLennan, S. M. (1995). The geochemical evolution of the continental crust. *Reviews of Geophysics*, *33*(2), 241-265.

Vavra, G. (1990). On the kinematics of zircon growth and its petrogenetic significance: a cathodoluminescence study. *Contributions to Mineralogy and Petrology*, *106*(1), 90–99. doi: 10.1007/BF00306410

Verner, K., Jiří Žák, Hrouda, F., & Holub, F. V. (2006). Magma emplacement during exhumation of the lower- to mid-crustal orogenic root: The Jihlava syenitoid pluton, Moldanubian Unit, Bohemian Massif. *Journal of Structural Geology*, *28*(8), 1553–1567. doi: 10.1016/j.jsg.2006.03.037

Verner, K., Žák, J., Pertoldová, J., Šrámek, J., Sedlák, J., Trubač, J., & Týcová, P. (2009). Magmatic history and geophysical signature of a post-collisional intrusive center emplaced near a crustal-scale shear zone: The Plechý granite pluton (Moldanubian batholith, Bohemian Massif). *International Journal of Earth Sciences*, *98*(3), 517–532. doi: 10.1007/s00531-007-0285-9

Verner, K., Žák, J., Šrámek, J., Paclíková, J., Zavřelová, A., Machek, M., … Johnson, K. (2014). Formation of elongated granite-migmatite domes as isostatic accommodation structures in collisional orogens. *Journal of Geodynamics*, *73*, 100–117. doi: 10.1016/j.jog.2013.10.002

Vernon, R. H. (2000). Review of Microstructural Evidence of Magmatic and Solid-State Flow. *Visual Geosciences*, *5*(2), 1–23. doi: 10.1007/s10069-000-0002-3

Von Raumer, J. F., Janoušek, V., & Stampfli, G. M. (2012). Durbachites-vaugnerites—A time-marker across the European Variscan basement. *Géologie de la France*, *2012*, 178-180.

Watson, S., & McKenzie, D. (1991). Melt Generation by Plumes: A Study of Hawaiian Volcanism. *Journal of Petrology*, *32*(3), 501–537. doi: 10.1093/petrology/32.3.501

Zulauf, G., Schitter, F., Riegler, G., Finger, F., Fiala, J., & Vejnar, Z. (1999). Age constraints on the Cadomian evolution of the Teplá Barrandian unit (Bohemian Massif) through electron microprobe dating of metamorphic monazite. *Zeitschrift Der Deutschen Geologischen Gesellschaft*, *150*(4), 627–639.

Žák, J., Verner, K., Finger, F., Faryad, S. W., Chlupácová, M., & Veselovskỳ, F. (2011). The generation of voluminous S-type granites in the Moldanubian unit, Bohemian Massif, by rapid isothermal exhumation of the metapelitic middle crust. *Lithos*, *121*(1–4), 25–40. doi: 10.1016/j.lithos.2010.10.002

Žák, J., Verner, K., Sláma, J., Kachlík, V., & Chlupáčová, M. (2013). Multistage magma emplacement and progressive strain accumulation in the shallow-level Krkonoše-Jizera plutonic complex, Bohemian Massif. *Tectonics*, *32*(5), 1493-1512.

Žák, J., Verner, K., Janoušek, V., Holub, F. V., Kachlík, V., Finger, F., … Trubač, J. (2014). A plate-kinematic model for the assembly of the Bohemian Massif constrained by structural relationships around granitoid plutons. *Geological Society, London, Special Publications*, *405*(1), 169–196. doi: 10.1144/SP405.9

Appendix

Attachment 1: Topographical map of the area of interest with all documented localities.

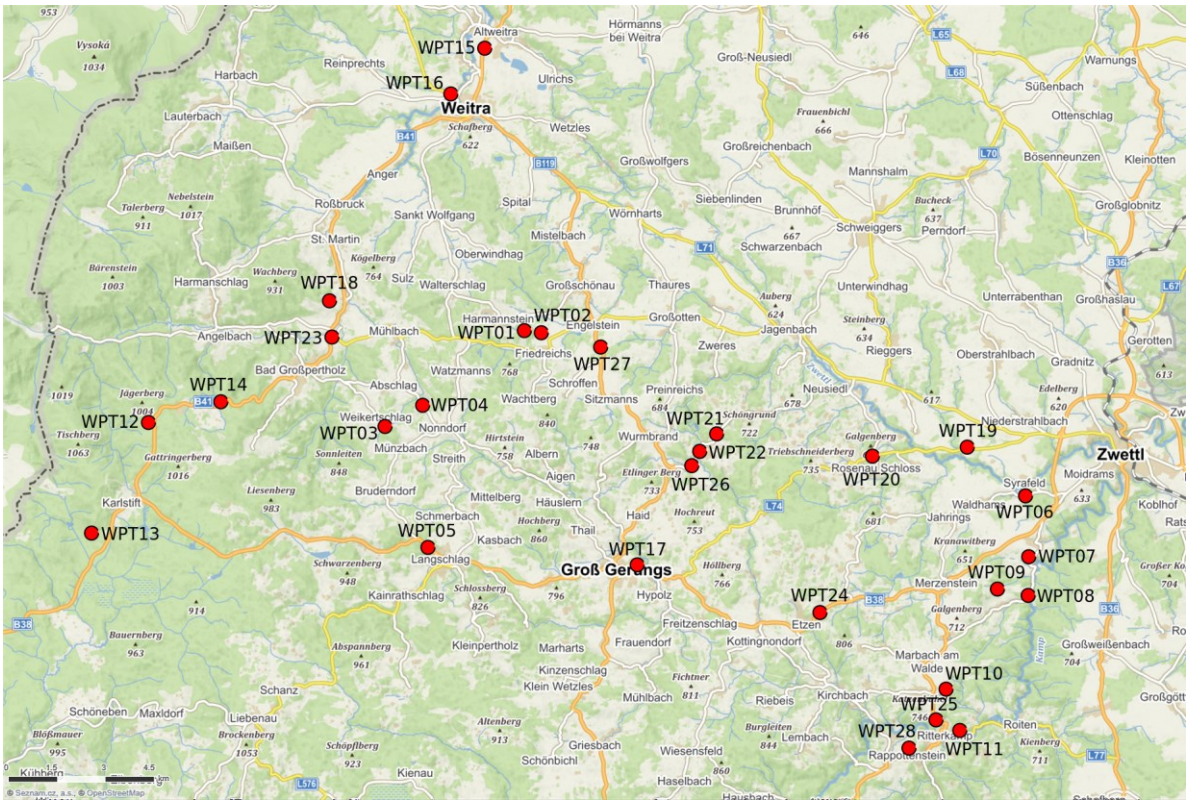

Attachment 2: Complete field documentation (W g. - Weinsberg type granitoids, E g. - Eisgarn type granitoids, L g. - Leucogranites, Mylo - Mylonites, Para - Paragneiss, Weitra - Weitra granite))

STATION			**FAULTS**				
Station	**GPS**	**Litho**	**Fault**		**Fault lineation**		**Fault**
			direction	dip	direction	dip	Kinematics
WPT01	N48° 38.260' E14° 55.360'	W g.					
WPT02	N48° 38.310' E14° 55.620'	W g.					
WPT03	N48° 36.820' E14° 51.670'	W g.					
WPT04	N48° 37.010' E14° 52.740'	W g.					
WPT05	N48° 34.770' E14° 52.680'	W g. +	219	70	294	26	dextral
		E g.	241	76	286	76	normal
			341	54	56	21	dextral
			232	81	312	17	dextral
			220	80			
			232	76	262	74	normal
			215	81	308	16	dextral
WPT06	N48° 35.810' E15° 07.630'	W g.					
WPT07	N48° 34.540' E15° 07.810'	W g.					
WPT08	N48° 33.890' E15° 07.770'	W g.	216	74	292	30	sinistral
			182	82	92	12	sinistral
WPT09	N48° 34.040' E15° 07.050'	W g.					
WPT10	N48° 32.300' E15° 05.510'	Para					

WPT11	N48° 31.670' E15° 06.000'	W g.					
WPT12	N48° 36.960' E14° 45.800'	W g.					
WPT13	N48° 35.110' E14° 44.440'	W g.	102	87	185	5	
WPT14	N48° 37.180' E14° 47.610'	W g.	287	84	301	81	normal
			292	86	205	5	
			116	87	21	21	dextral
			111	80	22	4	dextral
WPT15 (Fi-20-18)	N48° 43.182' E14° 54.159'	W g. +	92	83	172	15	dextral
(Fi-21-18)		E g.					
WPT16	N48° 42.130' E14° 53.350'	W g. +	80	80	164	10	sinistral
		Weitra	92	82	167	12	sinistral
			19	85	105	19	dextral
			272	81	352	5	dextral
WPT17	N48° 34.340' E14° 57.970'	W g. + L g.					
WPT18	N48° 38.820' E14° 50.440'	W g.	46	75	135	21	
WPT19	N48° 36.360' E15° 06.060'	W g. + L g.					
WPT20	N48° 36.190' E15° 03.510'	W g.					
WPT21	N48° 36.480' E14° 59.740'	W g.					
WPT22	N48° 36.260' E14° 59.420'	W g.					
WPT23	N48° 38.150' E14° 50.230'	W g.					
WPT24	N48° 33.690' E15° 02.600'	W g.					
WPT25 (Fi-24-18)	N48° 31.840' E15° 05.450'	Mylo					

WPT26	N48° 36.140' E14° 59.200'	W g.					
WPT27 (Fi-22-18)	N48° 38.090' E14° 57.020'	W g.					
WPT28 (Fi-23-18)	N48° 31.356' E15° 04.972'	Mylo					
NP498		W g.					
NP499		W g.					
NP500		W g.					
NP501 (558)		W g.					
NP502 (559)		W g.					
Kobyli vrch		W g.					

STATION	**JOINTS**		**PLUTON**				**Dikes**		
Station	**Joint**		**Magmatic foliation**		**Subsolidus foliation**		**Dikes**		
	direction	dip	direction	dip	direction	dip	Litho	direction	dip
WPT01	252	86	280	36					
WPT02			61	25					
			62	18					
WPT03			13	30					
WPT04	20	88	211	11					
			226	50					
WPT05	222	75	322	52					
	11	86	92	85					
	291	82	94	88					
	261	82	76	82					
			81	84					
			74	72					
			76	74					
			301	76					
			251	86					

			62	87					
			332	22					
			22	22					
			218	74					
WPT06	162	85	25	65					
	22	81	191	82					
			212	80					
WPT07	177	80	255	61					
	92	35	271	54					
	297	81	275	76					
	281	77	291	48					
	172	74	267	62					
WPT08	142	85	220	75					
	320	87	218	65					
	238	81	222	70					
	131	82	32	85					
	311	85	192	88					
	182	82	201	21					
			292	32					
			230	62					
WPT09	354	78	292	65					
WPT10									
WPT11	282	26	282	67					
	342	88	218	88					
	173	87	228	81					
	141	82	42	82					
			282	72					
			62	32					
			37	56					
			42	55					
WPT12									

WPT13	191	62	35	19					
	195	75	34	10					
	291	88	195	81					
			191	24					
			117	12					
			58	75					
			322	20					
WPT14	196	82	195	85					
			201	27					
			220	38					
			151	40					
WPT15(Fi-20-18)			2	72			E g.	102	27
(Fi-21-18)			67	50				348	76
			72	50					
			354	76					
			112	45					
WPT16	184	85	241	55			Weitra	7	22
			352	21					
			141	50					
WPT17			85	70			L g.	305	70
WPT18	301	81	172	27					
	81	82	212	22					
			222	19					
WPT19	196	70	72	67			L. g	280	30
	112	50	78	62					
			120	50					
			120	57					
WPT20	325	72	262	52					
	182	60							
WPT21	322	81	52	42					

	94	85	261	72					
WPT22	231	81	22	24					
	108	85							
WPT23			65	60					
WPT24	242	76	72	62					
	23	82	68	65					
WPT25(Fi-24-18)					290	80			
					262	75			
					275	80			
					279	80			
					283	84			
					265	70			
WPT26			114	20					
WPT27(Fi-22-18)			348	12					
			226	16					
WPT28(Fi-23-18)					262	82			
NP498	91	86	168	29					
	187	87	196	86					
NP499	285	81	18	80					
	22	84	191	85					
NP500	82	88	19	78					
	16	79	24	24					
NP501 (558)	288	87	18	75					
	194	81	171	88					
			191	79					
NP502 (559)	19	84	168	80					
	107	74	162	76					
Kobyli vrch	121	81	211	65					
	301	80	14	71					
	176	88	224	31					
	97	86	92	76					

	191	82							

Attachment 3: Table of complete XRF geochemistry results.

Sample	SiO2 (%)	Al2O3 (%)	MnO (%)	MgO (%)	CaO (%)	Na2O (%)
WPT 05A	67,76	16,51	0,03	0,81	1,69	2,93
WPT 05B	72,85	14,29	0,04	0,56	0,97	2,38
WPT 06	64,84	16,96	0,06	1,42	2,7	3,25
WPT 09	69,53	15,55	0,03	0,76	1,82	3
WPT 10	62,86	19,95	0,08	2,94	0,4	1,62
WPT 11	68,65	15,69	0,03	0,83	1,6	2,86
WPT 13	68,46	15,77	0,05	1,08	1,93	2,91
WPT 14	72,11	14,39	0,03	0,86	1,91	3,04
WPT 15	65,02	16,6	0,05	1,69	2,44	3,05
WPT 16	70,75	15,1	0,03	0,84	1,5	3,21
WPT 17A	76,87	14,1	0,03	0,07	0,49	3,79
WPT 17B	75,26	14,61	0,02	0,06	0,58	4,58
WPT 18	69,19	15,81	0,03	0,76	1,8	3,01
WPT 19A	62,99	16,59	0,07	1,94	2,82	2,85
WPT 19B	74,79	14,11	0,01	0,05	0,45	3,36
WPT 20	63,18	16,39	0,07	1,96	2,71	2,72
WPT 21	64,17	16,21	0,07	2,04	2,92	3,05
WPT 15 (Fi 20 18)	69,08	15,5	0,02	0,94	1,17	3,16
WPT 15 (Fi 21 18)	68,7	15,84	0,03	0,88	1,08	3,06
WPT 27 (Fi 22 18)	69,69	14,62	0,04	1,03	1,67	3,11
WPT 28 (Fi 23 18)	89	5,75	0	0,15	0,14	1,45
WPT 25 (Fi 24 18)	69,8	15,27	0,02	0,31	0,98	4,27

Sample	K2O (%)	TiO2 (%)	P2O5 (%)	Fe2O3 (%)	SO3 (%)	F (%)
WPT 05A	6,04	0,52	0,3	3,01	0	0,2
WPT 05B	5,8	0,33	0,21	2,29	0,01	0,14
WPT 06	4,45	0,78	0,31	4,81	0,01	0,16
WPT 09	5,49	0,49	0,25	2,7	0,02	0,2
WPT 10	4,06	0,78	0,17	6,67	0,01	0,23
WPT 11	6,09	0,54	0,23	3,04	0,01	0,22
WPT 13	4,72	0,67	0,31	3,68	0,01	0,24
WPT 14	3,81	0,49	0,25	2,77	0,01	0,18
WPT 15	4,42	0,89	0,33	4,99	0,01	0,25
WPT 16	5,17	0,43	0,21	2,37	0,01	0,17
WPT 17A	3,59	0,05	0,14	0,74	0	0,07
WPT 17B	3,97	0,05	0,18	0,58	0	0,06
WPT 18	6,04	0,44	0,17	2,4	0,01	0,13
WPT 19A	4,66	1,06	0,34	6,16	0,01	0,23
WPT 19B	6,47	0,06	0,06	0,51	0	0,03
WPT 20	5,21	1,04	0,35	5,84	0,01	0,24
WPT 21	3,76	1,05	0,39	5,83	0,01	0,27
WPT 15 (Fi 20 18)	6,29	0,55	0,31	2,56	0,04	0,18
WPT 15 (Fi 21 18)	6,74	0,5	0,33	2,46	0,01	0,18
WPT 27 (Fi 22 18)	5,46	0,59	0,14	3,26	0,01	0,16
WPT 28 (Fi 23 18)	1,95	0,13	0,09	0,76	0,44	0,07
WPT 25 (Fi 24 18)	7,13	0,21	0,14	1,69	0,01	0,06

Sample	As (PPM)	Ba (PPM)	Ce (PPM)	Cl (PPM)	Co (PPM)	Cr (PPM)
WPT 05A	1,3	856,9	88	76,7	5	33,1
WPT 05B	1,7	507,7	56,8	47,3	3,5	11,3
WPT 06	0	1157,2	102,4	64,1	6,7	50,7
WPT 09	3,8	627,6	95,8	61,3	3,4	23,3
WPT 10	3,6	739,4	89,7	54,8	17,5	238,4
WPT 11	-0,7	752,2	102,6	74,6	6,2	41
WPT 13	0	572,3	84,1	62,3	5,5	33,7
WPT 14	1,5	405	86,3	51,4	5,6	17,3

WPT 15	0,4	1257,7	99	149,4	11,1	32,7
WPT 16	1,6	825,9	99	68,1	3,6	11,5
WPT 17A	2,2	149,5	18,9	13	1,7	0
WPT 17B	1,4	43,1	5,8	12,2	2	14
WPT 18	6,1	1182,4	60,8	79,1	4,1	23,3
WPT 19A	0,6	1243,7	132,7	130,2	8,2	46,5
WPT 19B	0	215,3	16,7	10,7	3,6	15,5
WPT 20	2,2	1449,9	113	112,9	9,8	55,3
WPT 21	4,6	734,9	128,6	81,2	10,1	49,6
WPT 15 (Fi 20 18)	1,8	637,3	172,3	209,5	4,5	42,8
WPT 15 (Fi 21 18)	1,6	607,3	110,6	47,1	4,9	77,1
WPT 27 (Fi 22 18)	4,1	993,5	109,6	81,9	7,3	34,2
WPT 28 (Fi 23 18)	0	206,6	40,1	26,4	2,2	29,7
WPT 25 (Fi 24 18)	0	244,3	35,6	21,6	2,2	15,3

Sample	Cs (PPM)	Dy (PPM)	Ga (PPM)	Gd (PPM)	La (PPM)	Nb (PPM)
WPT 05A	4,7	1,5	21,9	7,9	46,6	14,6
WPT 05B	5,7	7	17,1	5,7	24,8	10,1
WPT 06	1,3	1,5	23	7,1	52,4	16,2
WPT 09	5,4	5,9	18,8	10,7	36,4	13,1
WPT 10	16,5	5,4	26	5,5	44,8	11,5
WPT 11	5	3,5	21,9	8,4	44,1	14,7
WPT 13	3,6	7,2	21	8,8	46,2	17,9
WPT 14	0	0	19,6	7,3	39,4	12,5
WPT 15	4,1	0	21	7,2	52,4	15,6
WPT 16	5,3	2,7	19,1	7,1	49,2	16
WPT 17A	7,8	1	20,6	3,5	6,2	11,7
WPT 17B	6,1	5,6	20,2	1,3	11	11,8
WPT 18	0	3	19	4,4	35,6	9,1
WPT 19A	4,3	0,1	23,3	8,1	75,2	18,9
WPT 19B	9,4	10,7	13,9	6	7,3	6,6
WPT 20	9,9	1	22,3	6,6	51,8	18,9
WPT 21	11,8	0	24	7,6	63,8	20,2

WPT 15 (Fi 20 18)	4,9	3,9	22,1	15,1	71,1	9
WPT 15 (Fi 21 18)	12,6	0	23,4	11,1	48,7	11,4
WPT 27 (Fi 22 18)	6,1	1,8	19,4	7,9	54,8	12,8
WPT 28 (Fi 23 18)	4,1	2,3	7,4	5,1	10,3	4,2
WPT 25 (Fi 24 18)	0	3,9	17	5,7	13,9	8,8

Sample	Nd (PPM)	Ni (PPM)	Pb (PPM)	Rb (PPM)	Sc (PPM)	Sn (PPM)
WPT 05A	45,2	12,5	38,2	241,2	6,7	2,9
WPT 05B	28,6	10,6	31,5	220,9	3,2	7,7
WPT 06	48,9	15,1	38,6	130,4	7,7	3,1
WPT 09	44,8	12,4	36,8	230,2	5,7	8,1
WPT 10	37	56,3	9,5	239,9	12,3	10
WPT 11	47,9	11,1	36,8	264,1	6,6	5,4
WPT 13	49,1	13,4	29,8	211,2	11,7	6,2
WPT 14	40,8	11,7	26,1	163,8	9,7	4,4
WPT 15	46	15,6	30,5	203,5	9,6	0,6
WPT 16	43,4	9,9	33,5	233,4	6,8	7,7
WPT 17A	10,3	7,6	19,3	238,9	7	10
WPT 17B	6,9	6,6	19,2	236,1	5,1	14,4
WPT 18	27,9	11	38,2	181	5,9	6,2
WPT 19A	61,6	19,1	35	171,2	9,1	3,4
WPT 19B	17,6	7,8	57,1	210,4	-1	10,4
WPT 20	43,6	18,2	33,4	177	18	4,5
WPT 21	52,9	19,8	26,2	182,5	14,6	6,2
WPT 15 (Fi 20 18)	81,9	13,2	45,9	248,2	5,2	4,4
WPT 15 (Fi 21 18)	55,5	12,5	46,6	299,3	4,7	4,8
WPT 27 (Fi 22 18)	48	14,7	46,2	187	10,3	6,8
WPT 28 (Fi 23 18)	14,9	8,9	17,6	108,1	0	7,6
WPT 25 (Fi 24 18)	22	10,4	37,5	387,6	1,6	3

Sample	Sr (PPM)	Th (PPM)	U (PPM)	V (PPM)	W (PPM)	Y (PPM)
WPT 05A	151,1	27	0	24,5	14	34,7
WPT 05B	107,5	16,1	4,8	24,1	11,2	42,4

WPT 06	233,7	23,5	0,2	52,4	10,2	29,8
WPT 09	139,9	27,8	4	27,9	12,8	23,8
WPT 10	140	15,3	3	124,9	16,4	30
WPT 11	134,2	36,2	1	30,1	11,8	44,7
WPT 13	134,3	33,1	6,2	34,2	11,3	51,5
WPT 14	131,3	26,5	6,2	31,7	10,2	27,3
WPT 15	209,5	22,1	5,8	56,9	11,5	30,3
WPT 16	298,3	31,9	6,3	30,1	15,4	24,7
WPT 17A	29,7	5,5	6	0,4	13,5	12,3
WPT 17B	16,4	1,1	6,4	3,1	16,7	10
WPT 18	182,5	18,4	1,6	25,6	12,6	18,1
WPT 19A	215,8	34,2	0	75,3	11,4	40,1
WPT 19B	72,9	9,7	5,8	0	12,9	35,2
WPT 20	241,9	23,1	0,6	68,8	17,8	30,7
WPT 21	184,9	29,4	0,3	65,1	12,1	35,4
WPT 15 (Fi 20 18)	141,6	72,1	2	23,2	12,5	13,7
WPT 15 (Fi 21 18)	132	62,8	2,3	25,9	22,5	9,8
WPT 27 (Fi 22 18)	192,7	28,4	1,5	36,2	11,4	24,9
WPT 28 (Fi 23 18)	33	9,4	1,4	12,7	13,9	8,7
WPT 25 (Fi 24 18)	89	21,3	1	6,9	12,4	9,9

Sample	**Zn (PPM)**	**Zr (PPM)**
WPT 05A	57,6	222,2
WPT 05B	44	165,6
WPT 06	79,3	290,6
WPT 09	52,2	203,3
WPT 10	150,4	200,7
WPT 11	62,3	196,5
WPT 13	71,3	252
WPT 14	53,9	216,8
WPT 15	114,6	308,3
WPT 16	67,9	182,7
WPT 17A	29,4	42,1

WPT 17B	19,3	25,5
WPT 18	40,5	183
WPT 19A	96,2	404,5
WPT 19B	12,9	22,8
WPT 20	85,3	319,8
WPT 21	94,9	393
WPT 15 (Fi 20 18)	100,6	235,1
WPT 15 (Fi 21 18)	80,5	211,1
WPT 27 (Fi 22 18)	59,9	237,6
WPT 28 (Fi 23 18)	17,4	63,8
WPT 25 (Fi 24 18)	30,8	113,1

Attachment 4: Table with complete AMS measurements. (Kd – declination, Ki – inclination of respected principal susceptibilities)

Sample	**Km**	**L**	**F**	**P**	**Pj**	**T**	**U**	**K1d**	**K1i**	**K2d**	**K2i**	**K3d**	**K3i**
WPT13/1/1	68,39	1,00	1,03	1,03	1,03	0,91	0,91	31	66	131	5	223	23
WPT13/1/2	123,40	1,02	1,09	1,11	1,12	0,67	0,65	158	5	249	5	23	82
WPT13/1/3	87,44	1,02	1,04	1,05	1,06	0,39	0,38	100	16	339	60	197	25
WPT13/1/4	130,13	1,01	1,04	1,05	1,05	0,50	0,49	82	46	295	39	190	17
WPT13/2/1	89,30	1,01	1,02	1,03	1,03	0,12	0,12	3	72	193	18	102	3
WPT13/2/2	140,32	1,02	1,04	1,06	1,06	0,31	0,30	331	70	205	12	111	16
WPT13/3/1	52,41	1,02	1,00	1,02	1,02	-0,73	-0,73	132	5	41	7	257	82
WPT13/3/2	154,17	1,01	1,03	1,04	1,04	0,34	0,33	330	35	95	40	215	31
WPT13/5/1	198,93	1,01	1,02	1,02	1,02	0,49	0,48	299	9	39	49	201	40
WPT13/5/2	156,80	1,02	1,02	1,04	1,04	0,15	0,14	333	51	100	26	204	27
WPT13/6/1	179,01	1,01	1,03	1,04	1,04	0,41	0,40	306	4	43	61	213	29
WPT13/6/2	69,90	1,01	1,04	1,04	1,05	0,68	0,68	112	0	22	62	202	28
WPT14/1/1	108,91	1,02	1,03	1,05	1,05	0,21	0,19	145	25	248	25	16	54
WPT14/1/2	205,17	1,01	1,03	1,05	1,05	0,38	0,37	139	7	232	23	33	66
WPT14/1/3	110,45	1,03	1,01	1,03	1,04	-0,63	-0,63	124	6	216	15	12	74
WPT14/1/4	189,35	1,02	1,01	1,02	1,02	-0,52	-0,53	280	12	180	40	24	48
WPT14/1/5	146,93	1,03	1,02	1,05	1,05	-0,06	-0,07	295	23	205	0	114	67
WPT14/1/6	96,48	1,00	1,03	1,03	1,04	0,76	0,76	84	10	334	63	179	25
WPT14/2/1	167,02	1,01	1,02	1,03	1,03	0,34	0,33	180	67	296	11	30	21
WPT14/3/1	95,65	1,02	1,02	1,04	1,04	-0,18	-0,19	94	26	312	58	192	17

WPT14/3/2	64,42	1,01	1,07	1,08	1,09	0,80	0,79	154	39	252	11	355	49
WPT14/3/3	77,10	1,00	1,05	1,05	1,06	0,91	0,90	15	1	105	4	271	86
WPT14/3/4	43,71	1,01	1,02	1,03	1,03	0,27	0,26	117	9	26	10	249	77
WPT14/3/5	111,25	1,01	1,03	1,04	1,04	0,74	0,73	257	25	90	64	349	5
WPT14/3/6	154,83	1,02	1,02	1,05	1,05	-0,01	-0,02	98	20	307	67	192	10
WPT15A/1/1	274,27	1,04	1,02	1,06	1,07	-0,32	-0,33	258	6	96	84	348	2
WPT15A/1/2	256,57	1,05	1,01	1,06	1,06	-0,66	-0,67	262	9	24	74	170	14
WPT15A/1/3	244,53	1,05	1,02	1,07	1,07	-0,47	-0,48	258	6	35	82	167	6
WPT15A/2/1	273,29	1,05	1,02	1,07	1,07	-0,32	-0,33	254	1	161	81	344	9
WPT15A/2/2	291,98	1,05	1,01	1,06	1,06	-0,51	-0,52	74	2	332	81	164	9
WPT15A/2/3	239,21	1,04	1,02	1,06	1,06	-0,29	-0,30	251	4	347	55	158	35
WPT15A/2/4	137,19	1,03	1,03	1,06	1,06	-0,09	-0,10	75	8	180	60	341	28
WPT15A/3/1	271,26	1,05	1,02	1,07	1,07	-0,42	-0,44	45	5	312	31	142	58
WPT15A/3/2	186,12	1,04	1,01	1,05	1,06	-0,63	-0,63	44	5	313	10	160	78
WPT15A/4/2	278,52	1,04	1,02	1,06	1,06	-0,37	-0,38	29	15	272	59	127	27
WPT15A/4/3	209,05	1,05	1,02	1,07	1,07	-0,42	-0,43	45	7	300	65	138	24
WPT15B/1/1	87,17	1,01	1,02	1,03	1,04	0,37	0,36	99	28	3	12	252	60
WPT15B/1/2	92,39	1,01	1,02	1,04	1,04	0,41	0,40	104	31	3	17	248	54
WPT15B/1/3	85,80	1,01	1,03	1,04	1,04	0,50	0,50	92	30	355	12	245	57
WPT15B/1/4	74,86	1,01	1,03	1,04	1,04	0,47	0,46	84	28	350	8	246	61
WPT15B/2/1	80,17	1,01	1,03	1,04	1,04	0,57	0,57	104	30	8	11	261	58
WPT15B/2/2	73,67	1,01	1,03	1,04	1,04	0,35	0,34	78	32	169	2	261	58
WPT15B/2/3	79,35	1,01	1,02	1,03	1,03	0,25	0,24	72	35	164	2	257	55
WPT15B/2/4	100,66	1,01	1,02	1,04	1,04	0,34	0,33	85	30	348	12	240	57
WPT15B/2/5	87,81	1,01	1,03	1,03	1,04	0,52	0,52	88	32	351	11	245	56
WPT15B/3/1	94,70	1,01	1,03	1,04	1,04	0,51	0,51	102	33	1	16	249	52
WPT15B/3/2	80,93	1,01	1,03	1,04	1,04	0,60	0,60	97	33	0	11	254	55
WPT15B/3/3	79,55	1,01	1,03	1,04	1,04	0,51	0,51	88	31	351	12	243	57
WPT15B/3/4	85,58	1,01	1,02	1,04	1,04	0,30	0,30	87	42	350	8	251	47
WPT15B/3/5	111,63	1,01	1,03	1,04	1,04	0,32	0,31	89	35	349	14	242	52
WPT16/1/1	114,28	1,01	1,01	1,02	1,02	0,30	0,30	312	6	46	33	213	56
WPT16/1/2	127,03	1,01	1,00	1,01	1,01	-0,48	-0,48	24	34	284	14	176	53
WPT16/1/3	119,90	1,01	1,01	1,02	1,02	0,17	0,16	133	8	42	4	286	81
WPT16/1/4	138,47	1,00	1,02	1,02	1,02	0,58	0,58	292	16	66	68	198	15
WPT16/2/1	113,45	1,01	1,01	1,02	1,02	0,06	0,05	80	45	181	11	281	43
WPT16/2/2	112,21	1,00	1,02	1,02	1,02	0,85	0,84	351	29	93	21	214	54
WPT16/2/3	111,34	1,01	1,00	1,02	1,02	-0,47	-0,47	65	22	310	47	172	35
WPT16/2/4	152,14	1,01	1,02	1,02	1,03	0,57	0,56	78	13	336	42	182	45
WPT16/2/5	115,17	1,00	1,01	1,02	1,02	0,69	0,68	124	40	338	45	229	18
WPT16/3/1	105,64	1,01	1,01	1,01	1,01	0,15	0,14	340	42	121	41	230	21
WPT16/3/2	131,80	1,00	1,02	1,02	1,02	0,60	0,59	340	19	73	10	189	69
WPT16/3/3	126,43	1,01	1,01	1,02	1,02	-0,04	-0,04	101	9	7	24	211	64
WPT17/1/1	256,31	1,02	1,02	1,03	1,03	-0,08	-0,09	359	33	110	29	231	44

WPT17/1/2	194,32	1,02	1,01	1,03	1,03	-0,57	-0,57	356	19	200	70	89	8
WPT17/1/3	130,24	1,03	1,00	1,04	1,04	-0,76	-0,76	12	3	279	41	106	49
WPT17/1/4	320,80	1,02	1,02	1,04	1,04	-0,13	-0,14	14	11	112	37	270	52
WPT17/1/5	304,57	1,02	1,01	1,03	1,03	-0,21	-0,21	1	24	216	62	97	14
WPT17/2/1	162,89	1,02	1,02	1,04	1,04	0,14	0,13	348	18	105	54	247	30
WPT17/2/2	244,24	1,01	1,02	1,03	1,03	0,19	0,18	353	27	100	31	230	47
WPT17/2/3	288,39	1,01	1,02	1,03	1,03	0,09	0,09	354	14	129	70	261	14
WPT17/2/4	304,12	1,01	1,01	1,01	1,01	-0,09	-0,10	3	2	262	79	94	11
WPT23/1/1	121,95	1,03	1,01	1,03	1,04	-0,53	-0,54	304	44	173	34	63	27
WPT23/1/2	152,50	1,02	1,01	1,03	1,03	-0,38	-0,38	300	51	143	36	45	11
WPT23/1/3	146,56	1,02	1,01	1,04	1,04	-0,30	-0,30	293	58	111	32	201	1
WPT23/2/1	129,02	1,02	1,03	1,05	1,05	0,27	0,26	298	50	129	40	34	5
WPT23/2/2	137,57	1,02	1,01	1,03	1,03	-0,14	-0,15	293	45	165	32	56	29
WPT23/2/3	163,93	1,01	1,02	1,03	1,03	0,14	0,14	277	47	113	42	16	8
WPT23/2/4	115,04	1,01	1,03	1,04	1,04	0,42	0,42	313	40	119	49	217	7
WPT23/3/1	166,94	1,02	1,03	1,04	1,04	0,17	0,16	285	41	143	43	33	20
WPT23/3/2	145,93	1,01	1,03	1,03	1,04	0,60	0,60	317	45	122	44	220	7
WPT23/3/3	137,65	1,02	1,02	1,04	1,04	0,03	0,02	289	52	131	36	33	11
WPT23/3/4	160,00	1,02	1,03	1,05	1,05	0,13	0,12	303	42	105	46	205	9
WPT23/4/1	131,07	1,03	1,01	1,04	1,04	-0,31	-0,32	269	52	110	36	13	10
WPT23/4/2	151,35	1,03	1,02	1,04	1,04	-0,20	-0,21	292	32	148	52	34	18
WPT23/4/3	167,28	1,02	1,02	1,04	1,04	-0,08	-0,09	288	46	126	43	27	9
WPT23/4/4	132,32	1,02	1,03	1,05	1,05	0,15	0,14	306	38	123	52	215	1
WPT24/1/1	132,47	1,02	1,02	1,04	1,04	-0,02	-0,03	149	12	51	31	257	57
WPT24/1/2	132,23	1,01	1,04	1,05	1,05	0,51	0,51	154	9	57	35	257	53
WPT24/1/3	141,75	1,01	1,01	1,03	1,03	0,03	0,02	135	8	44	11	259	77
WPT24/1/4	142,58	1,01	1,03	1,05	1,05	0,44	0,43	163	15	64	31	275	55
WPT24/1/5	51,11	1,05	1,01	1,06	1,07	-0,65	-0,66	204	1	106	82	294	8
WPT24/1/6	129,00	1,02	1,04	1,06	1,06	0,45	0,44	169	1	78	41	260	49
WPT24/2/1	138,83	1,01	1,04	1,05	1,05	0,47	0,46	317	11	57	40	214	47
WPT24/2/2	109,61	1,03	1,02	1,05	1,05	-0,11	-0,13	118	8	25	24	225	64
WPT24/2/3	133,08	1,01	1,05	1,06	1,07	0,73	0,72	313	0	43	33	222	58
WPT24/2/4	102,90	1,02	1,04	1,06	1,06	0,31	0,30	153	4	57	52	246	38
WPT24/3/1	153,43	1,02	1,03	1,05	1,05	0,37	0,36	146	14	49	28	260	58
WPT24/3/2	169,50	1,02	1,03	1,05	1,05	0,09	0,08	330	9	64	21	219	67
WPT24/3/3	121,15	1,01	1,04	1,06	1,06	0,55	0,54	132	16	31	34	243	51
WPT25/1/1	149,89	1,01	1,01	1,02	1,02	0,11	0,10	239	43	350	21	98	40
WPT25/1/2	77,03	1,02	1,03	1,04	1,04	0,27	0,26	251	36	17	39	136	31
WPT25/1/3	96,16	1,04	1,03	1,07	1,07	-0,13	-0,14	243	27	339	11	88	60
WPT25/1/4	149,45	1,01	1,00	1,01	1,01	-0,30	-0,31	251	34	350	12	96	53
WPT25/1/5	108,33	1,01	1,01	1,01	1,01	-0,24	-0,24	210	25	311	21	75	56
WPT25/2/1	57,33	1,03	1,03	1,06	1,06	-0,08	-0,10	241	27	336	9	83	62
WPT25/2/2	126,24	1,11	1,20	1,32	1,33	0,28	0,22	243	21	124	51	347	31

WPT25/2/3	210,79	1,02	1,01	1,03	1,04	-0,43	-0,43	236	28	331	9	77	61
WPT25/2/4	111,10	1,03	1,02	1,05	1,05	-0,07	-0,08	225	27	128	14	14	59
WPT25/2/5	95,08	1,02	1,03	1,05	1,05	0,27	0,26	236	31	115	41	349	34
WPT25/3/1	149,04	1,01	1,02	1,03	1,03	0,52	0,51	232	37	332	14	79	50
WPT25/3/2	133,57	1,02	1,03	1,05	1,05	0,03	0,02	251	38	66	52	159	2
WPT25/3/3	114,60	1,01	1,14	1,15	1,17	0,84	0,83	16	37	256	34	138	35
WPT5/1/1	21,49	1,02	1,04	1,06	1,06	0,46	0,45	120	41	12	19	264	43
WPT5/1/2	38,20	1,02	1,20	1,23	1,25	0,79	0,77	264	14	163	38	11	49
WPT5/1/3	54,33	1,02	1,01	1,03	1,03	-0,32	-0,33	249	22	144	33	5	49
WPT5/2/1	30,93	1,02	1,04	1,06	1,06	0,40	0,39	25	13	143	64	289	23
WPT5/2/2	62,01	1,02	1,01	1,04	1,04	-0,35	-0,36	328	49	151	41	59	2
WPT5/2/3	66,69	1,02	1,03	1,05	1,05	0,15	0,14	326	42	112	43	219	18
WPT5/3/1	82,90	1,02	1,02	1,04	1,04	0,01	0,00	122	15	317	74	213	4
WPT5/3/2	106,17	1,02	1,03	1,05	1,05	0,19	0,18	131	48	271	34	16	21
WPT5/3/3	96,69	1,02	1,00	1,02	1,03	-0,61	-0,62	160	15	57	40	266	46
WPT5/3/4	47,29	1,03	1,01	1,04	1,04	-0,54	-0,54	174	47	60	21	314	36
WPT5/4/1	141,25	1,01	1,04	1,05	1,06	0,66	0,66	352	76	108	6	199	12
WPT5/4/2	73,53	1,02	1,03	1,05	1,05	0,09	0,08	86	68	328	10	235	19